Variability of the Southern Hemisphere Westerly Winds during the Holocene: Insights from coupled climate modelling

Dissertation zur Erlangung des akademischen Grades eines Doktors der Naturwissenschaften

Dr. rer. nat.

im Fachbereich 5 (Geowissenschaften)
der Universität Bremen

vorgelegt von

Vidya Raghava Varma

Bremen, September 2011

Erklärung

Name: Vidya Raghava Varma

Anschrift: Leher Heerstraße 118, 28359 Bremen, Deutschland

Hiermit versichere ich, dass ich

1. die Arbeit ohne unerlaubte fremde Hilfe angefertigt habe,
2. keine anderen als die von mir angegebenen Quellen und Hilfsmittel benutzt habe und
3. die den benutzten Werken wörtlich oder inhaltlich entnommenen Stellen als solche kenntlich gemacht habe.

Bremen, September 2011

Gutachter

Prof. Dr. Michael Schulz

Prof. Dr. Dierk Hebbeln

Promotionskolloquium: 12.12.2011

Mitglieder der Kommission:

Herr Prof. Dr. Michael Schulz

Herr Prof. Dr. Dierk Hebbeln

Frau Prof. Dr. Gesine Mollenhauer

Herr Prof. Dr. Rüdiger Stein

Herr Dr. Henning Kuhnert

Frau Anne Seidenglanz

Acknowledgements

Three years of this PhD position was funded through the DFG (Deutsche Forschungsgemeinschaft, German Research Foundation) Priority Programme "INTERDYNAMIK" (Project: HOLOPARC) and through the DFG Research Center/Cluster of Excellence "The Ocean in the Earth System".

Firstly I would like to thank my supervisor Prof. Dr. Michael Schulz whose extremely sincere passion and enthusiasm for science, reflecting through his inspiring comments and suggestions, benefitted me in improving the quality of my work. I would like to equally thank Dr. Matthias Prange for his endless support and guidance along with his infectious cheerfulness which helped me a lot in completing this work. Special thanks to Dr. Ute Merkel who always patiently answered my queries, be it program codes or music notes. Obligations to Dr. Andreas Manschke for all the support provided. Thanking all the 'geomod' members for their support and valuable suggestions during the group seminars and also for the many entertaining coffee breaks, especially Heather, Thejna, Rima, Huadong, Axel, Dian etc. Special thanks to GLOMAR for providing the platform for many encouraging discussions as well as many informative courses. I am also deeply indebted to the members of the Institut Für Meteorologie, Freie Universität Berlin, especially Prof. Dr. Ulrich Cubasch, Dr. Thomas Spangehl, Semjon Schimanke, Dr. Kerstin Prömmel, Thomas Bergmann, Sourabh Bal et al., whose warm support made my research stay fruitful and memorable. Thanking all my co-authors for their inputs and suggestions in writing my research papers.

I am unexplainably obliged to Roschelle, Nisha, Joby and Bimiya for their warm and genuine friendship. Last but never the least, I would like to sincerely thank my family for their tremendous support and faith in me without which I wouldn't have been able to complete my research.

Summary

The Southern Hemisphere Westerly Winds (SWW) constitute an important zonal circulation that significantly influences the climate system. Understanding the variability and the impact of various forcings on the SWW remains a significant area of investigation.

As an important forcing which influences the climate on decadal to millennial time-scales, solar activity is considered to be a potential driver for SWW variability. Two ways of looking at the influence of solar activity on climate change are through the 'bottom-up' and 'top-down' mechanisms. In 'bottom-up' mechanism, the applied changes in total solar irradiance mostly affect the climate system through shortwave absorption by the surface, whereas less direct heating by solar radiation takes place at higher levels of the atmosphere. Under this mechanism, the strength and position of the SWW are strongly related to meridional surface temperature gradients. By contrast, a "top-down" mechanism influences the troposphere via stratospheric ozone responses to variations in ultraviolet radiation. These solar-induced changes in stratospheric ozone are also a postulated factor for shifting the SWW by influencing the tropospheric subtropical westerly jet through dynamical coupling between the atmospheric layers.

Another important forcing of global climate on longer time scales is accomplished by changes in the seasonal insolation caused by the varying Earth orbital parameters. This astronomical forcing is generally regarded as a dominant factor for glacial interglacial climate. A considerable variation in the seasonal and latitudinal distribution of insolation, especially a decrease in austral winter-spring insolation accompanied by an increase in austral summer-fall insolation, can be observed between 7 kyr BP and present-day. These changes in seasonal insolation can also be considered as a potential forcing that causes long-term variations in the structure, position and intensity of the SWW on multi-millennial timescales.

In order to study the response of the SWW during the Holocene under the above mentioned forcings, numerical modelling is applied. Numerical experiments were carried out with idealized solar forcing using the comprehensive global climate model CCSM3 (Community Climate System Model version 3) to study the response of SWW under solar variability. In

addition to these simulations, a high-resolution iron record from the Chilean continental slope (41°S), which is interpreted to reflect changes in the position of the SWW, is shown to be significantly correlated with reconstructed solar activity during the past 3000 years. Taken together, the proxy and model results suggest that centennial-scale periods of lower (higher) solar activity caused equatorward (southward) shifts of the annual mean SWW (based on a 'bottom-up' mechanism).

To study the influence of the stratosphere and its ozone content on SWW variability, two simulations (one with fixed and one with solar-induced varying stratospheric ozone) were analysed from the coupled Atmosphere-Ocean General Circulation Model, EGMAM (ECHO-G with Middle Atmosphere Model) covering the period from Late Maunder Minimum to Pre-Industrial (1675-1790 AD). The results from these analyses are in agreement with the findings from CCSM3 experiments, suggesting that for periods of lower solar activity, the annual mean SWW does exhibit an equatorward shift. The response in simulations with varying stratospheric ozone is more pronounced and robust compared to the one with fixed ozone suggesting an important contribution from the middle atmosphere through a 'top-down' mechanism.

To study the evolution of the SWW under orbital forcing from the mid-Holocene (7 kyr BP) to pre-industrial modern times (250 yr BP), transient experiments using CCSM3 were carried out. In addition, a model inter-comparison is also carried out using orbitally forced Holocene transient simulations from four other coupled global climate models. Analyses and comparison of the model results suggest that the annual and seasonal mean SWW are subjected to an overall strengthening and poleward shifting trend during the course of the mid-to-late Holocene under the influence of orbital forcing, except for the austral spring season, where the SWW exhibit an opposite trend of shifting towards the equator.

Zusammenfassung

Die südhemisphärischen Westwinde (SWW) stellen eine bedeutende zonale Zirkulation dar, die das Klimasystem der Erde signifikant beeinflusst. Das Verständnis ihrer Variabilität und der Einfluss unterschiedlicher Antriebsmechanismen sind daher ein wichtiges Forschungsgebiet.

Als ein wichtiger Antriebsmechanismus, der das Klima auf Zeitskalen von Jahrzehnten bis Jahrtausenden beeinflusst, wird die Aktivität der Sonne als potenzieller Motor für SWW-Variabilität betrachtet. Dabei gibt es grundsätzlich zwei mögliche Wege, über welche die Sonnenaktivität Klimaänderungen bewirken kann, nämlich „bottom-up“ und „top-down“. Beim „bottom-up“-Mechanismus beeinflussen Änderungen in der solaren Gesamtstrahlungsenergie das Klimasystem über die Absorption kurzwelliger Strahlung an der Oberfläche, während die direkte Erwärmung oberer Atmosphärenschichten durch Absorption solarer Strahlung nur gering ist. Bei diesem Mechanismus hängen Stärke und Lage der SWW eng mit meridionalen Temperaturgradienten an der Oberfläche zusammen. Im Gegensatz dazu beeinflusst der „top-down“-Mechanismus die Troposphäre durch Änderungen in der stratosphärischen Ozonkonzentration, die ihrerseits durch Variationen im ultravioletten Bereich des Solarspektrums hervorgerufen werden. Diese solarinduzierten Änderungen in der stratosphärischen Ozonchemie stellen ebenfalls einen möglicherweise wichtigen Faktor für SWW-Änderungen dar, wobei die dynamische Kopplung zwischen den Atmosphärenschichten entscheidend ist.

Ein weiterer wichtiger Antriebsmechanismus für Klimavariabilität auf längeren Zeitskalen hängt mit jahreszeitlichen Änderungen der Insolation aufgrund von variierenden Erdbahnparametern zusammen. Dieser astronomische Antriebsmechanismus wird im Allgemeinen als dominanter Faktor für Glazial-Interglazial-Klimaschwankungen betrachtet. Eine erhebliche Variation in der jahreszeitlichen und breitengradabhängigen Verteilung der Insolation – insbesondere eine Abnahme in der südhemisphärischen Winter-Frühlings-Einstrahlung sowie eine Zunahme in der südhemisphärischen Sommer-Herbst-Insolation – kann für den Zeitraum 7 ka vor heute bis heute beobachtet werden. Diese Änderungen in der jahreszeitlichen Einstrahlung können ebenfalls als potenzieller Antriebsmechanismus

betrachtet werden, welcher langfristige Veränderungen in der Struktur, Position und Stärke der SWW auf Zeitskalen von mehreren Jahrtausenden verursacht.

Das Verhalten der SWW im Holozän hinsichtlich der oben genannten Antriebsmechanismen sollte mit Hilfe numerischer Modelle studiert werden. Um den Einfluss variabler Sonnenaktivität auf die SWW zu untersuchen, wurden numerische Experimente mit dem komplexen globalen Klimamodell CCSM3 (Community Climate System Model Version 3) mit idealisiertem solaren Antrieb durchgeführt. Zudem wurde der Eisengehalt eines zeitlich hochaufgelösten marinen Sedimentkerns vom chilenischen Kontinentalrand (41°S) statistisch untersucht. Der Eisengehalt in diesem Sedimentkern spiegelt Änderungen in der SWW-Position wieder und zeigt signifikante Korrelation mit rekonstruierter Sonnenaktivität während der letzten 3000 Jahre. Zusammengenommen deuten Proxy- und Modellergebnisse stark darauf hin, dass – auf der Jahrhundertzeitskala – Perioden geringer (hoher) Sonnenaktivität mit jährlich gemittelten SWW verbunden waren, die zum Äquator (Südpol) hin verlagert waren (basierend auf einem „bottom-up“-Mechanismus).

Um den Einfluss der Stratosphäre und ihres Ozongehalts auf die Variabilität der SWW zu untersuchen, wurden zwei Simulationen (eine mit fester Ozonkonzentration und eine mit solarinduzierter stratosphärischer Ozonvariabilität) untersucht, die mit dem gekoppelten Atmosphäre-Ozean-Zirkulationsmodell EGMAM (ECHO-G with Middle Atmosphere Model) durchgeführt wurden und die Periode vom Späten Maunder-Minimum bis zum Beginn der industriellen Epoche umfassen (d.h. 1675-1790 n.Chr.). Die Ergebnisse dieser Analyse stehen in Einklang mit den Befunden, die aus den CCSM3-Simulationen gewonnen wurden. Demnach verlagern sich die Jahresmittel-SWW während Perioden geringerer Sonnenaktivität zum Äquator hin. Diese Verlagerung ist in der Simulation mit variierendem stratosphärischen Ozongehalt allerdings wesentlich signifikanter ausgeprägt als in der Simulation mit fester Ozonkonzentration. Hieraus kann ein wichtiger Beitrag der mittleren Atmosphäre über einen „top-down“-Mechanismus abgeleitet werden.

Um die Entwicklung der SWW unter orbitalem Antrieb zwischen dem mittleren Holozän (7 ka vor heute) und der vorindustriellen modernen Epoche (250 Jahre vor heute) zu untersuchen, wurden transiente Experimente mit CCSM3 durchgeführt. Zusätzlich wurde ein Zwischenmodellvergleich durchgeführt unter Verwendung orbital angetriebener transienter Holozän-Simulationen mit vier weiteren gekoppelten Klimamodellen. Analyse und Vergleich der Modellresultate deuten darauf hin, dass die jährlich und jahreszeitlich gemittelten SWW

einer Intensivierung und Verlagerung nach Süden im Verlauf des mittleren bis späten Holozän unterliegen. Eine Ausnahme stellt dabei der südhemisphärische Frühling dar, in dem die SWW einen entgegengesetzten Trend mit einer Verlagerung hin zum Äquator zeigen.

Table of Contents

Chapter 1

1. Introduction

1.1 Global atmospheric circulation

The general circulation of the atmosphere is referred to as the average movement of the world's wind. The unequal heating of the Earth's surface by solar radiation is its basic driving mechanism. Although, the energy received by the Earth as a whole is balanced by the energy radiated back into the space, there are certain locations with exceptions. The equatorial belt is one such location where it receives more heat than it radiates back to space and the polar region is another example where it loses more heat then it gains. The low-latitude regions between the tropics and the equator therefore, are constantly warm, whereas the polar regions are always colder. The mid-latitude region in between represents the zone of interpenetration between the warm tropical air and cold polar air. If there were no such exchange of warmth and cold, equatorial regions would become increasingly hotter and polar regions, increasingly colder. The atmosphere (as well as the ocean) provides the essential link between the equatorial and polar regions, by transporting heat from the warmer to the colder regions. The fundamental aspects of atmospheric (and oceanic) motions which help such exchange of heat thus constitute the general circulation of the atmosphere (as well as ocean).

The general circulation is one of the most dominant controlling factors in the distribution of world climatic zones. Much of the energy for the maintenance of global circulation comes from the tropical oceans, where evaporation transfers large amounts of latent heat to the atmosphere. The latitudinal difference in heating is expected to create a simple circulation of rising air in the warm equatorial region and cold polar region, the effects of Earth's rotation diverting the wind into gigantic whirling systems that are generally aligned in latitudinal belts.

In the 17th century, Halley (1686) pioneered the study of the trade winds with the then available data and speculated that the observed winds at the surface were associated with a direct thermally-driven circulation between a heat source and a heat sink, which reversed its direction between winter and summer seasons. An explanation for the formation of the trade winds along with their observed reversal of direction in the context of differential heating between the equator and the poles and with the rotation of the Earth was suggested by Hadley (1735). His argument was that a general equatorward drift of the trade winds at low levels

should be compensated by a poleward drift at high levels in order to prevent an accumulation of mass near the equator. In addition, a general westward drag by the trade winds near the Earth's surface at low latitudes, resulting from the rotation of the Earth, has to be balanced by an eastward drag by the westerlies in high latitudes so as to prevent a general slowing down of the Earth. Later, it was found that this general westward or eastward drift of the wind was required to conserve the Earth. The movement of the Earth is faster at the equator than at higher latitudes. This would force a parcel of air moving from high latitudes towards the equator, to acquire an increasingly eastward drift, in order to conserve the angular momentum of its native latitude.

However, Hadley's idealized single-cell concept had to undergo modifications demanded by later observations which proclaimed the presence of a high pressure belt over the subtropics and a low pressure belt further poleward near ~60° latitude. These pressure belts resulted in meridional pressure gradient associated with a poleward drift of air and also a compensating equatorward drift at some height, over the mid-latitudes. Later, it was found that the mid-latitude westerly winds were baroclinically unstable and were largely eddy-driven.

Introduction of the indirect cells that are characterized by a poleward flow near the surface and equatorward flow at higher levels, over the mid-latitudes, was first suggested by Ferrel (1859) and Thomson (1892) in a view to modify the idealized single-cell Hadley circulation model. The distinct role played by tropical circulation and the idea of a three-cell model of global atmospheric circulation was first put forward mainly by Rossby (1947). Rossby's three-cell meridional circulation model, in general, depicted a direct circulation cell over the tropics with rising air over the equatorial region and sinking air over the subtropical belt, an indirect circulation cell over the mid-latitudes and a direct circulation over the polar latitudes, along with a polar front located at a latitude of ~60° (Fig. 1).

Near the equator, where the average solar radiation is greatest, air is warmed at the surface and rises resulting in the formation of the band of low air pressure known as the Intertropical Convergence Zone (ITCZ), where the surface air is drawn from the subtropics. The subtropical air, on reaching the equator, rises into the tropopause due to convergence and convection and then begins flowing horizontally to the polar region (in both the hemispheres).

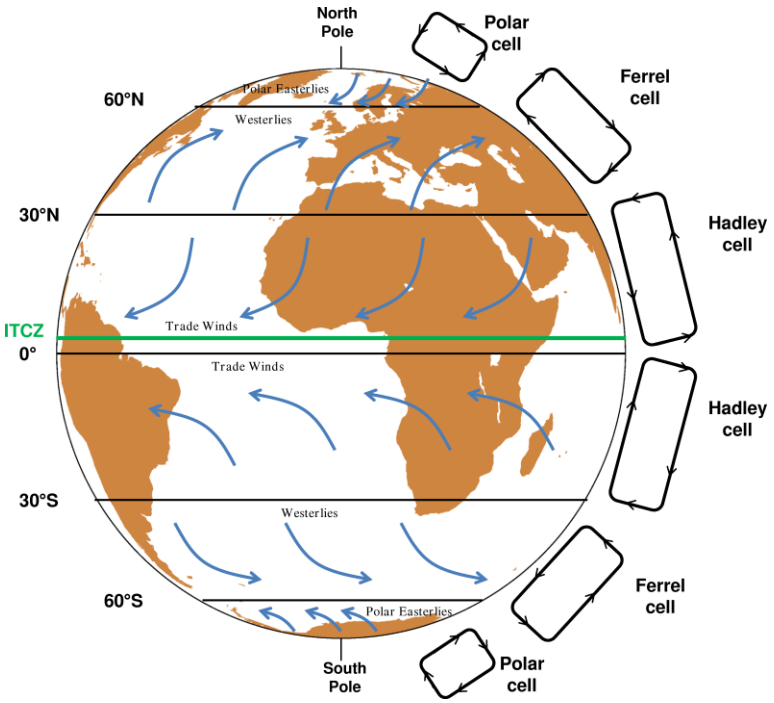

Fig. 1 Three-cell model for both the hemispheres representing the atmospheric general circulation.

This rising air comprises the circulation pattern called the ***Hadley Cell***, which is the major tropical circulation pattern (Fig. 1). The Hadley cell eventually returns air to the surface of the Earth near ~ 30° latitude. The descending portion of the Hadley Cell produces a band of high air pressure at these latitudes called the subtropical high, from where the surface air travels in two directions. Winds are generated between the subtropical high and the equatorial band of low pressure (i.e. ITCZ), as air moves from high surface pressure towards low surface pressure. These winds are deflected from east to west as they travel toward the equator by the Coriolis force, resulting in the trade winds or the tropical easterlies (Fig. 1). The other portion of the surface air moves towards the poles from the subtropical high zone. This air is also deflected by the Coriolis force, contributing towards the formation of the temperate (mid-latitude) westerlies (Fig. 1). ***The Ferrel cell*** has winds sinking at ~ 30° latitude which then starts travelling pole-ward as they reach the ground. This poleward branch diverges with the winds from the Hadley Cell (Fig. 1) providing the poleward component of the mid-latitude westerlies. These winds continue travelling poleward until they converge with winds in the ***Polar cell*** at ~ 60° latitude (Fig. 1). Finally, in the Polar cell, winds ascend at ~ 60° latitude and spread out poleward as they reach the upper troposphere. Here, the winds sink down at the poles and then diverge towards the equator until they reach ~ 60° latitude where they rise up again to complete the cell. They provide the equator-ward component of the polar easterlies.

Although climatologically this idealized model has certain utility, many aspects are missing which prevents it from describing the large scale circulation accurately mainly because of the facts that neither is the Earth made up of uniform material nor is the Sun always overhead at the equator. A large deviation of pressure pattern and the wind distribution over the globe in time and space occur due to the uneven land sea distribution on the Earth's surface, the physiography, the nature of the land surfaces, the apparent seasonal migration of the Sun from one solstice to the other etc. However, the three-cell model consisting of two direct Hadley-type cells, one over the tropics between the equator and about 30° latitudes and the second over the polar belt poleward of about 60° latitudes, and an indirect Thomson-Ferrel cell over the mid-latitudes is perhaps, the closest to what is observed in the real atmosphere over any part of the globe at any time of the year (e.g. Starr 1968).

As seen before, the dominant component of the large-scale atmospheric flow is the west-to-east circulation in the upper troposphere. However, this circulation alone is not sufficient to transport the heat and angular momentum poleward, which mainly requires a north-south flow. Though there exists a mean meridional circulation, dominated by the Hadley circulation of the tropical atmosphere which could transport heat and angular momentum poleward within the tropics, this circulation becomes much weaker on reaching the middle latitudes and cannot produce much transport there. Rather, in the extra-tropical atmosphere, the north-south flow is mainly driven by eddies (e.g. Oort 1971; Hartmann 1994).

A typical example for the eddy-driven flow in the atmospheric system is the mid-latitude jets of the Southern Hemisphere (SH) which are associated with the surface westerly winds. These surface westerlies which are controlled by large-scale eddy momentum fluxes are easily differentiable from the Hadley driven subtropical jet and are also present in all the seasons (Fig. 2). Also, the first EOF (Empirical Orthogonal Function) of zonal wind is almost independent of the season and represents meridional shifts of the eddy-driven jet (Hartmann and Lo, 1998). As seen in Fig. 2, the eddy meridional momentum flux is dominant in the southern mid-latitudes, extending throughout the troposphere, during both boreal winter as well as summer season. It is the balance between the convergence of this eddy meridional momentum flux and the surface drag which is mostly driving the mid-latitude Southern Hemisphere Westerly Winds (SWW).

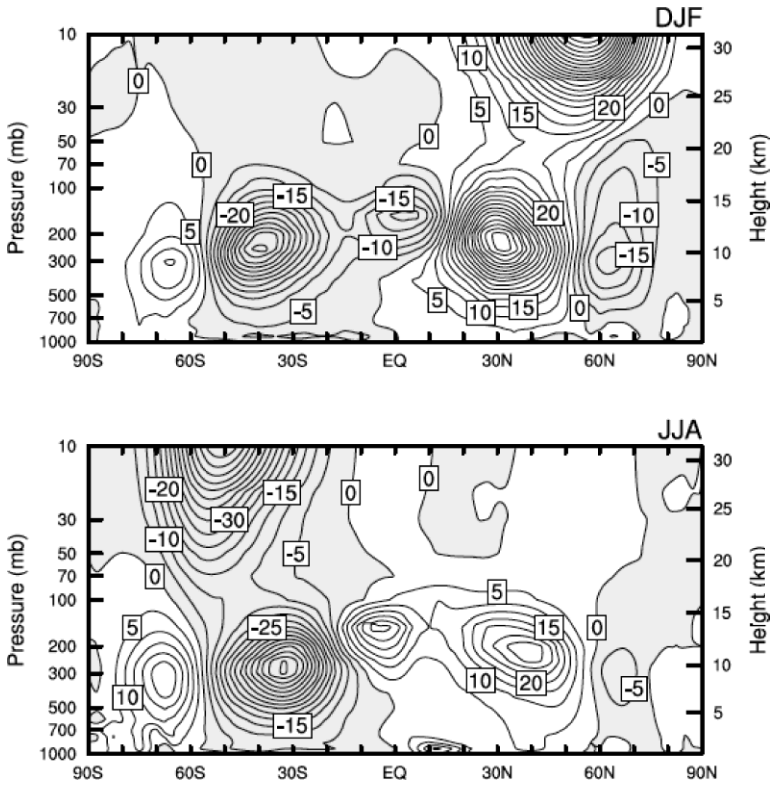

Fig. 2 Eddy meridional momentum flux (in m^2/s^2) climatology for the December/January/February and June/July/August seasons. Figure modified after Hartmann (2007).

The SWW, which are basically the prevailing winds in the mid-latitude belt of 30°S to 60°S, are the strongest time-averaged winds over the oceans in the world. Not only do they play a significant role in controlling the SH climate, but also are a crucial factor in affecting the global climate.

1.2 Southern Hemisphere Westerly Winds (SWW) in the climate system

The westerly winds are a major zonal circulation in both northern and southern hemispheres. They are especially well developed in the southern mid to high latitudes, due to the absence of vast land covered areas and also probably due to more pronounced temperature gradients caused by Antarctica (because of the fact that Antarctica is colder than the Arctic). These SWW have a substantial contribution that influences the ocean circulation through wind-driven upwelling of deep water in the Southern Ocean and thus on the global climate (Toggweiler and Samuels, 1995; Rahmstorf and England, 1997; Klinger et al., 2004, Kuhlbrodt et al., 2007; Sijp and England, 2009). In addition, the impact on the Indian-Atlantic Ocean water exchange by Agulhas leakage is another aspect through which the SWW affect the global ocean circulation (Sijp and England, 2009; Biastoch et al., 2009). By pushing the waters away from the Antarctic continent, the SWW raise a large amount of deep water to the ocean's surface south of the Antarctic Circumpolar Current (ACC). It has been

argued that the Ekman-driven upwelling and removal of deep water in the circumpolar belt may be quantitatively related to the formation of North Atlantic Deep Water (Toggweiler and Samuels, 1995) and may also affect atmospheric CO_2 contents (Toggweiler et al., 2006). The SWW are also suggested to have an impact on large-scale precipitation patterns as well as Antarctic temperatures (Shulmeister et al., 2004; Schneider et al., 2006). The changes in westerly intensity over time are suggested to enhance or diminish climatic controls like the El Niño-Southern Oscillation (e.g. Bertler et al., 2006; Toggweiler et al., 2006). Also, it is shown in a recent study that the positive phase of Southern Annular Mode (SAM), associated with poleward shifted westerlies, might account for an increased wildfire activity in Patagonia (Holz and Veblen, 2011). Accordingly, understanding the variability and the impact of various forcings on the SWW remains a significant area of investigation.

Although, the relative importance of SWW on influencing the climate variability is widely accepted, there are significant gaps in our understanding of how the strength and the latitudinal position of the westerlies have varied in the recent past. Most of the studies focussed on the time period of the Last Glacial Maximum (LGM) w.r.t the SWW variability. While some climate modelling studies suggested a poleward shift in storm tracks and SWW during the Last Glacial Maximum (Valdes, 2000; Wyroll et al., 2000; Kitoh et al., 2001; Shin et al., 2003; Rojas et al., 2009), other models simulated an equatorward (Kim et al., 2003) or no latitudinal displacement, but rather an intensification (Otto-Bliesner et al., 2006) of the mean westerlies. Likewise, proxy-based reconstructions of the glacial SWW provide contradictory views with claims of a poleward displacement (e.g. Markgraf, 1987; Markgraf et al., 1992) standing in contrast to the evidence of an equatorward shift (e.g. Heusser, 1989; Lamy et al., 1998, 1999; Shulmeister et al., 2004) compared to pre-industrial conditions. Holocene variability of SWW is also discussed in some modelling as well as proxy studies where also the disparities regarding the direction of the wind shifts persist (e.g. Heinz Veit, 1996; Lamy et al., 2001; Lamy et al., 2002; Gilli et al., 2005; Mayr et al., 2007; Lamy et al., 2010; Moreno et al., 2010, Waldmann et al., 2010; Varma et al., 2011). The paucity of multi-proxy paleoclimatic records in the SH is one of the main reasons for these controversial discussions about the past location of the SWW which also makes the validation of model results challenging.

1.3 Forcings on SWW

As described earlier, the climate system is always trying to minimize the energy gradients created by the unequal distribution of Sun's energy throughout the Earth's surface. The composition of the atmosphere (gases, aerosols, clouds etc) plays a significant role in driving the radiative processes, as these components are connected to chemical, thermal, and dynamical changes taking place in the atmosphere on vastly different time scales. Any change in these processes can force climate to change (Chapter 6 in Battarbee and Binney, 2008). The most important forcings on climate acting on decadal to millennial timescales are probably volcanic eruptions, changes in the concentration of greenhouse gases in the atmosphere, changes related to the output of energy from the Sun, changes in the seasonal insolation caused by the varying Earth orbital parameters etc. However, on a long-term (centennial to millennial timescales) perspective, the major natural forcings driving climate variability are considered to be the solar and the orbital forcings.

1.3.1 Solar forcing

On longer time scales there is an increasing evidence for solar forcing on climate change (e.g. van Geel et al., 1999; Renssen et al., 2000; Bond et al., 2001; Mauquoy et al., 2002; Hu et al., 2003; Versteegh 2005). The apparently large sensitivity of the climate system to comparatively small changes in solar activity is an indication for the amplification by feedback processes in the climate system. The sunspot record provides the longest historical record of solar activity representing the well known 11-year Schwabe cycle associated with a generally increasing trend from 1610 to the present. They also capture the distinct periods of low solar activity such as the Maunder Minimum (1645-1715 AD) and Dalton Minimum (1795-1820 AD). Proxy data derived from measurements of the cosmogenic radionuclides ^{10}Be and ^{14}C in natural archives such as ice cores and tree rings provide the extension of the solar activity record beyond the era of direct observations (e.g. Beer et al., 1990; Stuiver et al., 1991; Muscheler et al., 2004). The fluctuations in solar activity result in several cyclic features exhibiting periodicities around 11 years (Schwabe cycle), 87 years (Gleissberg cycle), 205 years (de Vries or Suess cycle), 2200 years (Halstatt cycle) etc., which have influence on climate (Stuiver and Braziunas, 1993; Chapter 6 in Batterbee and Binney, 2008).

Being a significant forcing on climate, solar activity could also be a potential driver for SWW variability. Van Geel et al. (2000) proposed solar activity as one of the possible factors for a shift in atmospheric circulation during the late Holocene around 2700 years BP. The abrupt

decrease in solar activity during this period might have acted as a trigger for the glacier advancement towards the equator due to an equatorward shift of climatic zones along with the SWW (Van Geel et al., 2000).

The influence of solar activity on climate is generally viewed in two ways: one through a 'bottom-up' mechanism and other through a 'top-down' mechanism. In the 'bottom-up' mechanism, total solar irradiance reaching the surface influences the climate mainly through the shortwave absorption by the surface (Meehl et al., 2009). In this concept, the stratospheric effect is not considered since there is less direct heating by solar radiation taking place at the higher levels of the atmosphere. The response of SWW under this mechanism is mostly dependent on the surface temperature gradients. In the 'top-down' mechanism, tropospheric climate is modulated mainly due to the stratospheric ozone responses to variations in the ultraviolet radiation (e.g. Haigh 1996). It has been suggested that during periods of enhanced solar activity, the summer stratosphere would get warmer due to the increase in solar ultraviolet (UV) radiation and ozone concentration which could be associated with the strengthening of the easterly winds there. Through thermal wind relations and dynamic coupling between the atmospheric layers, these easterly winds extending up to the tropical upper troposphere, could force the tropospheric westerly jets to move poleward (Haigh 1996; Haigh et al., 2005).

1.3.2 Orbital forcing

The total amount of radiation emitted by the Sun along with the relative position of Sun and Earth in space have a major influence on the seasonal and spatial distribution of the amount of solar radiation at the top of the atmosphere. While the processes taking place within the Sun determine the amount of radiation emitted, it is the variations caused to the Earth's orbit by the gravitational forces of the other planets which determine the relative positions of Sun and Earth (Laskar et al., 2004). The influence of orbital forcing is reflected mainly through three parameters namely the eccentricity (deviation of the orbit from a circle), the obliquity (tilt angle of the Earth's axis) and the precession of the equinoxes. The incoming solar radiation (insolation) at the top of the atmosphere is fully determined by these three parameters and this astronomical forcing is generally regarded as a dominant factor for glacial-interglacial climate changes (Milankovitch, 1941; Hays et al., 1976; Berger, 1978; Imbrie et al., 1992). Although the climate of the Holocene is generally being considered as relatively stable compared to the last glacial (e.g. Grootes and Stuiver, 1997), it has also been

suggested that there have been long-term trends in the spatial and temporal patterns of surface temperature during the Holocene (e.g. Battarbee and Binney, 2008). A considerable variation in the seasonal and latitudinal distribution of insolation, especially a decrease in austral winter-spring insolation accompanied by an increase in austral summer-fall insolation is observed between 7 kyr BP and present-day. These changes in seasonal insolation might have caused long-term variations in the structure, position and intensity of the SWW on multi-millennial timescales (e.g. Markgraf et al., 1992; Lamy et al., 2001; Jenny et al., 2003; Lamy et al., 2010).

1.4 Scientific questions addressed in this thesis

The Holocene – identified as the interglacial in the present ice age, is the geological epoch associated with most of the growth and development of the human species worldwide. Thus, in climate research the time period of Holocene deserves a special concern making the study of its variability, a necessity. The primary focus of this research is to understand the variability of SWW under the influence of two major natural forcings namely solar and orbital, during the period of Holocene. The Late Holocene response of the SWW to solar activity in the context of both 'bottom-up' and 'top-down' mechanisms described earlier is analysed in this study, through numerical modelling as well as comparison with proxy records.

The second natural forcing is the orbital forcing. The evolution of SWW under the influence of orbital forcing during the period from mid-Holocene to pre-industrial modern times (7 kyr BP to 250 yr BP) is studied implementing a multi-model inter-comparison approach, where the complexity of the model varies from high to intermediate.

Thus, through the application of numerical modelling and with the comparison of simulated results with the proxy records, this thesis intends to answer questions like:

i) Does the SWW show similar response patterns under both 'bottom-up' and 'top-down' mechanisms?

ii) Are these 'bottom-up' and 'top-down' processes mutually exclusive or do they complement each other towards a stronger total response in the SWW variability?

iii) How robust is the SWW response to orbital forcing in various models used in this study?

iv) Are the model results identifiable with the results from reconstructed data in depicting the latitudinal shifts observed during the Holocene?

The various models used in this study along with their experimental set-ups are described in the following section.

1.5 Models and Experimental set-up

1.5.1 Models

To study the response of SWW under solar and orbital forcings during the Holocene, an approach of numerical modelling is applied where several models are used whose degree of complexity varies from high to intermediate. Most of the results discussed in this study are from the General Circulation Models (GCMs) which represent the climate scenarios in a more detailed frame with a higher degree of complexity. In addition, results from the Earth System Models of Intermediate Complexity (EMICs) which describe the dynamics of the atmosphere and/or ocean with simplified physics, are also analysed. Although the GCMs can include almost all the important aspects of climate system such as atmospheric and oceanic circulations, sea-ice dynamics, land vegetation etc, a major limitation in their application is the high computational cost involved, at times hindering the long-term as well as large member ensemble simulations that are often required for paleoclimate studies. EMIC's are simple enough to allow long-term climate simulations over several thousands of years or even glacial cycles describing most of the processes implicit in comprehensive models, albeit in a more reduced or a more parameterized form (Claussen et al., 2002). Thus, the EMICs bridge the gap between the comprehensive GCMs and simplified conceptual models (where the limitations are not the computational costs involved but the lack of many important processes and feedbacks operating in the real world). On the other hand, the utilization of EMICs in studies that require high spatial resolution is not plausible which could be performed only with GCMs. However, EMICs are an aid in the assessment of uncertainties which sometimes the GCMs could do only to a lesser extent (Claussen et al., 2002). Accordingly, this spectrum of models complements each other in the attempt of representing the Earth system, as close to reality as possible, with minimum flaws. A brief description of the various models used in this study is given in the following sections.

1.5.1.1 CCSM3

The main model used in this study for carrying out climate simulations is the CCSM3 (Community Climate System Model version 3). NCAR's (National Centre for Atmospheric Research) CCSM3 is a state-of-the-art fully coupled GCM, composed of four separate components representing atmosphere, ocean, land and sea-ice connected by a flux coupler. The component models are CAM3 (Community Atmosphere Model version 3; Collins et al., 2004, 2006a, b), POP (Parallel Ocean Program version 1.4.3; Smith and Gent, 2002), CLM3 (Community Land surface Model version 3; Oleson et al., 2004; Dickinson et al., 2006) and CSIM5 (Community Sea Ice Model version 5; Briegleb et al., 2004). A low-resolution version is employed in all CCSM3 simulations where the resolution of the atmospheric component is given by T31 (3.75° transform grid), with 26 layers in the vertical. The ocean has a nominal resolution of 3° (like the sea-ice component) with a vertical resolution of 25 levels. Since this study focuses on the behaviour of the zonal wind system in the SH, results from the atmospheric component of CCSM3 (i.e. CAM3) are of main interest and hence analysed. The basic dynamics and physics used in CAM3 are described below.

1.5.1.1.1 CAM3 dynamics and physics

The CAM3 can be used both in stand-alone as well as coupled modes. The coupled mode (as used in this study) of the CAM3 is suitable for studying the interactions of the atmosphere, ocean, sea-ice and land surface on seasonal to millennial time scales, where it is integrated together with the CLM, CSIM5 and the POP. The CAM3 simulations presented here are based on the Eulerian dynamical core.

In CAM3, the physical parameterisations are separated from the dynamical core which makes it easier to replace or modify in isolation. Williamson (2002) describes coupling of the parameterisation suite with the dynamical core using time-split as well as process-split methods which are also applied in CAM3 (Collins et al., 2006a). In the process-split coupling, all the calculations involving the dynamical and physical tendencies for prognostic variables are based upon the same past state and these tendencies are added to produce the updated state. In the time-split coupling, the tendencies are computed sequentially, each based upon the state produced by the other (Williamson (2002)).

The CAM3 is designed to produce simulations with reasonable reliability for several dynamical cores and horizontal resolutions under different configurations. In order to run

CAM3 in a stable coupled environment, the energy balance in each configuration is established by adjusting the parameters governing the cloud condensate, cloud amount, precipitation processes, and biharmonic diffusion (Collins et al., 2004). CAM3 also employs its horizontal diffusion operator to satisfy the Courant–Friedrichs–Levy (CFL) condition for the upper layers (Collins et al., 2004).

The basic laws which govern the behaviour of the atmosphere (e.g. Chapter 5 in McGuffie and Sellers, 1997) take the form of fundamental equations representing:

a) Conservation of momentum

$$\frac{\mathrm{D}\mathbf{v}}{\mathrm{D}t} = -2\boldsymbol{\Omega}\times\mathbf{v} - \rho^{-1}\nabla p + \mathbf{g} + \mathbf{F} \tag{1.1}$$

b) Conservation of mass

$$\frac{\mathrm{D}\rho}{\mathrm{D}t} = -\rho\nabla\cdot\mathbf{v} + C - E \tag{1.2}$$

c) Conservation of energy

$$\frac{\mathrm{D}I}{\mathrm{D}t} = -p\frac{\mathrm{d}\rho^{-1}}{\mathrm{d}t} + Q \tag{1.3}$$

and

d) Ideal gas law

$$p = \rho RT \tag{1.4}$$

where $\mathbf{v}$ = velocity relative to the rotating Earth, t = time, $\frac{\mathrm{D}}{\mathrm{D}t} = \left[\frac{\partial}{\partial t} + \mathbf{v}\cdot\nabla\right]$ which is the total time derivative, $\boldsymbol{\Omega}$ = angular velocity vector of the Earth, ρ = atmospheric density, $\mathbf{g}$ = acceleration due to gravity, p = atmospheric pressure, $\mathbf{F}$ = force per unit mass, C = rate of creation of atmospheric constituents, E = rate of destruction of atmospheric constituents, $I = c_v T$ which is the internal energy per unit mass (c_v is specific heat of air at constant volume and T is the temperature), Q = heating rate per unit mass and R = universal gas constant.

Although there are several other aspects of the atmospheric flow that are to be considered, the equations (1.1) to (1.4), collectively known as the primitive equations, are the fundamental equations to formulate any Atmospheric GCM (AGCM) (e.g. Chapter 5 in McGuffie and Sellers, 1997). These equations can be represented in pressure coordinates as scalar equations such as:

$$\left(\frac{du}{dt}\right)_p - \left(f + u\frac{\tan\phi}{a}\right)v = -\frac{1}{a\cos\phi}\frac{\partial \boldsymbol{\Phi}}{\partial\lambda} + D_\lambda \tag{1.5}$$

$$\left(\frac{dv}{dt}\right)_p + \left(f + u\frac{\tan\phi}{a}\right)u = -\frac{1}{a}\frac{\partial \boldsymbol{\Phi}}{\partial\phi} + D_\phi \tag{1.6}$$

$$\frac{\partial \boldsymbol{\Phi}}{\partial p} = \frac{RT}{p} \tag{1.7}$$

$$\frac{1}{a\cos\phi}\frac{\partial u}{\partial\lambda} + \frac{1}{a\cos\phi}\frac{\partial}{\partial\phi}(v\cos\phi) + \frac{\partial\omega}{\partial p} = 0 \tag{1.8}$$

$$c_p\left(\frac{dT}{dt}\right)_p - \frac{RT}{p}\omega = Q \tag{1.9}$$

$$\left(\frac{d}{dt}\right)_p = \frac{\partial}{\partial t} + \frac{u}{a\cos\phi}\left(\frac{\partial}{\partial\lambda}\right)_p + \frac{v}{a}\left(\frac{\partial}{\partial\phi}\right)_p + \omega\frac{\partial}{\partial p} \tag{1.10}$$

$$\omega = \frac{dp}{dt} \tag{1.11}$$

where λ = longitude, ϕ = latitude, a = radius of Earth, f = Coriolis parameter, ω = vertical velocity, $\boldsymbol{\Phi}$ = geopotential height, u and v = zonal and meridional velocities.

Applying the two-dimensional curl and divergence to the horizontal velocity, $\mathbf{V}_h = (u, v)$ in equations (1.5) and (1.6) will result in the vorticity and divergence equations as follows:

$$\frac{\partial\zeta}{\partial t} + \mathbf{V}_h\cdot\nabla_p(\zeta + f) + \omega\frac{\partial\zeta}{\partial p} = -(\zeta + f)\nabla_p\cdot\mathbf{V}_h + \mathbf{k}\cdot\left(\frac{\partial\mathbf{V}_h}{\partial p}\times\nabla_p\omega\right) + \mathbf{k}\cdot\nabla_p\times\mathbf{D} \tag{1.12}$$

$$\frac{\partial \delta}{\partial t} + \nabla_p \cdot \left(\mathbf{V}_h \cdot \nabla_p \mathbf{V}_h \right) + \nabla_p \omega \cdot \frac{\partial \mathbf{V}_h}{\partial p} + \omega \frac{\partial \delta}{\partial p} = -\nabla_p^2 \mathbf{\Phi} - \nabla_p \cdot \left(f\mathbf{k} \times \mathbf{V}_h \right) + \nabla_p \cdot \mathbf{D} \qquad (1.13)$$

where ζ = vorticity, δ = divergence, **k** = unit vector in the z coordinate, **D** = drag (frictional shear stress).

This is the most fundamental form of the equations governing the horizontal motion and they still have to be further modified in order to convert them to the final form that can be solved by CAM3, the details of which are given in Collins et al. (2004).

The governing equations are solved using the spectral method in the horizontal and only the vertical and time differences are treated using the finite difference method. The model makes use of the spectral transform method described in Machenhauer (1979) for all nonlinear terms. The vorticity, divergence, thermodynamic equations and surface pressure tendency are transformed to spectral space by performing Fourier operations on each in such a way that the Fourier transform is performed first and then the differentiation is carried out in the spectral space.

A brief overview of the CAM3 physics model mentioning the major schemes and methods applied is described in the following paragraphs of this section. Collins et al. (2004) describes the physics in greater detail.

The total parameterization package in CAM3 is consisted of a sequence of components which are moist precipitation processes, clouds and radiation, surface model, and turbulent mixing. The parameterization scheme developed by Zhang and McFarlane (1995) is used to treat the deep convection processes, also dealing with upward and downward ensembles, the constituent transport via convection etc under certain numerical approximations. The evaporation of the convective precipitation, as it makes its way to the surface, is treated according to Sundqvist (1988). For the parameterization of non-convective cloud processes in CAM3, the method employed follows that of Rasch and Kristjánsson (1998) and Zhang et al. (2003) which consists of two components namely a macro-scale component describing the exchange of water substance between the condensate and the vapour phase and the associated temperature change arising from that phase change and a bulk microphysical component that controls the conversion from condensate to precipitate. CAM3 also employs the inclusion of a dry adiabatic adjustment if a layer is unstable with respect to the dry adiabatic lapse rate. Cloud amount and the associated optical properties, are evaluated based on the scheme

introduced by Slingo (1987), with variations according to Hack et al., (1993), Kiehl et al., (1998) and Rasch and Kristjánsson (1998).

The longwave and shortwave heating rates are computed only for every model hour. In CAM3, insolation is computed using the method of Berger (1978). CAM3 has the provision to determine the insolation for any time within 10^6 years of 1950 AD facilitating the use of CAM3 for paleoclimate simulations in particular.

For the formulation of shortwave solution, the δ - Eddington approximation of Joseph et al. (1976) and Coakley et al. (1983) is adopted. The δ - Eddington approximation is an extension of the Eddington approximation where the equations of radiative transfer were dealt only in terms of just two functions of optical depth, for which a pair of ordinary differential equations were required. However, the Eddington approximation was incapable of coping with the highly asymmetric phase functions which are typical of particulate scattering (Joseph et al., 1976). In the δ - Eddington scheme, the forward peak of the phase function is approximated using a Dirac delta function thus providing a more accurate and analytically simple parameterization of radiation, the details of which are given in (Joseph et al., 1976). The solar spectrum is represented in 19 discrete spectral and pseudo-spectral intervals (7 for O_3, 1 for the visible, 7 for H_2O, 3 for CO_2, and 1 for the near-infrared following Collins (1998)). The surface albedo is specified in two wavebands (0.2-0.7 μm, and 0.7-5.0 μm) which distinguish albedos for direct and diffuse incident radiation. The ocean surfaces, geographically varying land surfaces, and sea ice surfaces are distinguished using different albedos. For the parameterization of longwave radiation, the method by Ramanathan and Downey (1986) is employed.

1.5.1.2 ECHO-G

The second GCM is the coupled climate model ECHO-G (The Hamburg Atmosphere-Ocean coupled Circulation Model; Legutke and Voss, 1999) whose Holocene transient simulations carried out by Lorenz and Lohmann, (2004) and Wagner et al. (2007) are analysed to monitor the role of orbital forcing on SWW variability. ECHO-G consists of two-component models, an atmosphere general circulation model (AGCM) and an ocean-sea ice general circulation model (OGCM). While ECHAM4 (Roeckner et al., 1996) represents the atmospheric component of the model, HOPE (Hamburg Ocean Primitive Equation model; Wolff et al., 1997) represents that of the ocean component. In ECHAM4, the three-dimensional transport of water vapour, cloud water, trace constituents etc. is calculated according to the semi-

Lagrangian scheme described by Williamson and Rasch (1994). The dataset for annual mean land surface parameters are compiled according to Claussen et al. (1994). The ECHAM4-model is also based on primitive equations as described for CAM3. The prognostic variables include vorticity, divergence, logarithm of surface pressure, temperature, specific humidity and mixing ratio of total cloud water. The vertical extension reaches up to a pressure level of 10 hPa, which corresponds to a height of approximately 30 km. The ocean model HOPE is also based on primitive equations with the representation of thermodynamic processes. It is a non-eddy resolving circulation model. The coupling software OASIS (Terray et al., 1998) controls the interpolation as well as the coupling between the atmosphere and ocean components. Further aspects of the exchange processes are flux corrections due to the interactive coupling between ocean and atmosphere in order to prevent climate drift. This flux adjustment is constant in time and its global average vanishes.

1.5.1.3 COSMOS

The third GCM is the COSMOS (Community Earth System Models), whose orbitally forced Holocene transient simulation by Pfeiffer and Lohmann (2011) is analysed to study the SWW variability. Similar to the earlier mentioned GCMs, COSMOS is also composed of an AGCM called ECHAM5 (Roeckner et al., 2003) and an OGCM named MPI-OM (Max Planck Institute Ocean Model; Marsland et al., 2003). ECHAM5 differs from its predecessor ECHAM4 in terms of numerics as well as physics which are described in detail in Roeckner et al. (2003). As an overview, the major changes include the introduction of a semi-Lagrangian transport scheme for positive definite variables like water components and chemical tracers according to Lin and Rood (1996). While ECHAM4 applied an emissivity method, the modified ECHAM5 makes use of a new longwave radiation code developed by Mlawer et al. (1997) which has a higher spectral resolution and is computationally more efficient. The number of spectral bands was increased from 2 to 4 in the new version. Further changes are the inclusion of separate prognostic equations for cloud liquid water and cloud ice along with a new cloud microphysical scheme and a prognostic-statistical cloud cover parameterization. The representation of land surface processes is also modified including an implicit coupling between the surface and the atmosphere, and the representation of orographic drag forces. In addition, a new dataset of land surface parameters based on Hagemann (2002) has also been compiled for the new model ECHAM5 (Roeckner et al., 2003). The prognostic variables of ECHAM5 are vorticity, divergence, logarithm of surface pressure, temperature, mass mixing ratios of water vapour, cloud liquid water, cloud ice etc.

COSMOS differs from ECHO-G in terms of its OGCM as well. While ECHO-G used the HOPE OGCM, COSMOS uses the MPI-OM. The major modification made to MPI-OM, compared to its predecessor HOPE, is the implementation of an orthogonal curvilinear C-grid for the horizontal discretization treatment along with improvements in subgridscale mixing, isopycnal diffusion scheme, eddy-induced mixing parameterization etc. (Marsland et al., 2003). The ocean model also includes a dynamic-thermodynamic sea-ice model with viscous-plastic rheology. A dynamic vegetation module is coupled to the land surface model JSBACH allowing an interactive adaptation of the terrestrial biosphere to varying climate conditions (Brovkin et al., 2009).

1.5.1.4 EGMAM

The coupled Atmosphere-Ocean GCM (AOGCM), EGMAM (Huebner et al., 2007) is based on the AOGCM ECHO-G (Legutke and Voss 1999) which is described earlier. The atmospheric component is ECHAM4 which is the same as explained for ECHO-G (Roeckner et al., 1996) with T30/L19 spatial resolution (~ 3.75° and 19 levels in vertical), but extended for the middle atmosphere (Manzini and Mcfarlane, 1998), with additional 20 levels in vertical i.e. spatial resolution corresponding to T30/L39. The oceanic component is HOPE-G (Hamburg Ocean Primitive Equation Global Model) as for ECHO-G.

1.5.1.5 ECBilt-CLIO-VECODE

This model belongs to the category of EMICs. The atmospheric component is ECBilt as described in Opsteegh et al. (1998). The model is realistic in the sense that it contains the minimum amount of physics that is necessary to simulate the mid-latitude planetary and synoptic-scale circulations in the atmosphere as well as its variability on various time-scales. It is a coupled atmosphere/ocean/sea-ice/land surface model containing simplified parameterisations of the sub-grid scale physical processes. CLIO is the oceanic component and consists of a free-surface, primitive-equation ocean general circulation model coupled to a dynamic-thermodynamic sea-ice model (Goosse and Fichefet, 1999). A three-layer sea-ice model, which takes into account sensible and latent heat storage in the snow-ice system, simulates the changes of snow and ice thickness in response to surface and bottom heat fluxes. VECODE is a dynamic global vegetation model (DGVM) which interactively simulates the dynamics of trees and grasses (Brovkin et al., 2002). Being an EMIC, ECBilt is computationally more efficient than comprehensive GCMs.

1.5.1.6 CLIMBER2-LPJ

CLIMBER2-LPJ also belongs to the category of EMIC, consisting of CLIMBER2 (Petoukhov et al., 2000), coupled to the DGVM LPJ (Sitch et al., 2003). CLIMBER2 also contains oceanic biogeochemistry, a model for marine biota, and a sediment model (Archer, 1996; Brovkin et al., 2002, 2007). To this EMIC, the DGVM LPJ is coupled in order to investigate land surface processes at a significantly higher resolution of 0.5°x0.5°. DGVMs include process-oriented formulations of biogeochemical fluxes as well as vegetation dynamics. Basic units of the LPJ model are "Plant Functional Types" which are designed to capture the major types of plants in the biosphere.

1.5.2 Experimental set-up

To study the influence of solar activity on SWW, two sets of idealized solar forcing experiments are carried out using the comprehensive GCM, CCSM3. In the first set, two simulations are performed varying the total solar irradiance (TSI) values by 2 W/m^2. While the control simulation has a TSI of 1365 W/m^2 (Merkel et al., 2010), the sensitivity experiments have a reduced TSI of 1363 W/m^2. All the simulations maintained the preindustrial boundary conditions. This genre of idealized experiments provides a platform to isolate and study the influence of a particular forcing on climate simulations, which in this framework, is the solar forcing. That the sensitivity of the model is sufficient enough to detect recurring solar-forced SWW shifts and if the response is dependent on the Holocene background climate, is tested through an additional set of three experiments with idealized solar forcing where the TSI varied sinusoidally with an amplitude of 1 W/m^2 and a period of 200 years. The 200-year period is chosen to mimic one of the most prominent solar cycles during the Holocene, which is the de Vries solar cycle (e.g. Knudsen et al., 2009). The TSI reduction between the solar maximum and minimum in the model experiments is consistent with recent observation as well as physics-based estimates (e.g. Steinhilber et al., 2009).

The model results are also validated using proxy data through the comparison of a high resolution iron record from the Chilean continental slope (which is interpreted to reflect changes in the position of SWW; Lamy et al., 2001) with reconstructed solar activity based on ^{10}Be (Vonmoos et al., 2006) and ^{14}C (Solanki et al., 2004), for the period of late Holocene.

The details of these solar forcing experiments are given in Chapter 2.

Since a low resolution version of CCSM3 is employed, influence of solar activity through the stratosphere and its ozone content cannot be verified. To this point, an AOGCM called EGMAM with extended middle atmosphere is used. Spangehl et al. (2010) performed transient simulations covering the period from Maunder Minimum to present-day (1630-2000 AD) to study the influence of stratospheric ozone on climate with fixed as well as solar induced varying stratospheric ozone along with greenhouse gas (GHG) concentrations, focussing mainly on the NH. Those simulations are analysed in this study to examine the behaviour of SWW. Even though the simulations are carried out with GHG forcing as well, the analyses are done so as to isolate the solar forcing alone, by focussing on the time period from Late Maunder Minimum to Pre-Industrial (1675-1790 AD), where the contribution from natural forcing is dominant.

A detailed description of the EGMAM results is given in Chapter 4.

In order to study the influence of orbital forcing on the evolution of SWW during the Holocene, a multi-model inter-comparison approach is adopted. Orbitally forced transient simulations are carried out using CCSM3 under pre-industrial boundary conditions and these simulation results are compared with a range of climate models belonging to the category of GCMs as well as EMICs. Here, the sole forcing acting on the Holocene transient simulations is that of orbital forcing.

The details of the CCSM3 results along with the model inter-comparison results are shown in Chapter 3.

1.6 Outline of chapters

Chapter 2: Solar-forced shifts of the Southern Hemisphere Westerlies during the Holocene

V. Varma, M. Prange, F. Lamy, U. Merkel and M. Schulz

(Published in *Climate of the Past*, doi:10.5194/cp-7-339-2011)

This chapter focuses on the solar influence on SWW during the period of Late Holocene. It is shown that a high-resolution iron record from the Chilean continental slope (41°S), which is interpreted to reflect changes in the position of the SWW, is significantly correlated with reconstructed solar activity during the past 3000 years. In addition, CCSM3 simulations are also presented to support the evidence for a potential solar forcing on SWW through 'bottom-up' mechanism.

Chapter 3: Holocene Evolution of the Southern Hemisphere Westerly Winds in Transient Simulations with Global Climate Models

V. Varma, M. Prange, U. Merkel, T. Kleinen, G. Lohmann, M. Pfeiffer, H. Renssen, A. Wagner, S. Wagner, and M. Schulz

(Under review for publication in *Climate of the Past*; doi:10.5194/cpd-7-1797-2011)

In this study, the evolution of the SWW under orbital forcing from the mid-Holocene (7 kyr BP) to pre-industrial modern times (250 yr BP) is examined with transient experiments using the comprehensive coupled global climate model CCSM3. In addition, a model inter-comparison is carried out using orbitally forced Holocene transient simulations from four other coupled global climate models namely ECHO-G, COSMOS, ECBilt-CLIO-VECODE and CLIMBER2-LPJ.

Chapter 4: Impact of solar-induced stratospheric ozone decline on Southern Hemisphere Westerlies during the Late Maunder Minimum

V. Varma, M. Prange, T. Spangehl, F. Lamy, U. Cubasch and M. Schulz

(Submitted to *Geophysical Research Letters*)

This chapter focuses on the solar influence on SWW through 'top-down' mechanism. In this study, the response of the SWW to the changes in solar activity in the middle atmosphere, during the period from Late Maunder Minimum (1675-1715 AD) to Pre-industrial (1716-1790 AD) is presented through the analyses of the AOGCM EGMAM transient simulations using both fixed as well as solar-induced varying stratospheric ozone. Comparison between a high-resolution iron record from the Chilean continental slope (41°S), which is interpreted to reflect changes in the position of the SWW, and reconstructed solar activity for the past 500 years before present shows a significant correlation supporting the model evidence for an influence of solar activity on SWW variability.

Chapter 5 provides the summary and conclusions of this study with an outlook for future work.

1.7 References

Archer, D.: A data-driven model of the global calcite lysocline, Global Biogeochem. Cycles, 10, 511-526, **1996.**

Battarbee, R.W., and Binney, H.A.: Natural Climate Variability and Global Warming: A Holocene Perspective, Wiley-Blackwell, ISBN: 978-1-4051-5905-0, **2008.**

Beer, J., Blinov, A., Bonani, G., Finkel, R. C., Hofmann, H. J., Lehmann, B., Oesschger, H., Sigg, A., Schwander, J., Staffelbach, T., Stauffer, B., Suter, M., and Wötfli, W.: Use of ^{10}Be in polar ice to trace the 11-year cycle of solar activity, Nature, 347, 164-166, **1990.**

Berger, A.L.: Long-term variations of daily insolation and Quaternary climatic changes, J. Atmos. Sci., 35, 2362-2367, **1978.**

Bertler, N.A.N., Naish, T.R., Oerter, H., Kipfstuhl, S., Barrett, P.J., Mayewski, P.A., and Kreutz, K.: The effects of joint ENSO-Antarctic Oscillation forcing on the McMurdo Dry Valleys, Antarctica, Antarctic Science, 18, 507–514, doi: 10.1017/S0954102006000551, **2006.**

Biastoch, A., Böning, C.W., Schwarzkopf, F.U., and Lutjeharms, J.R.E.: Increase in Agulhas leakage due to poleward shift of Southern Hemisphere westerlies, Nature, 462, 495-498, **2009.**

Bond, G., Kromer, B., Beer, J., Muscheler, R., Evans, M. N., Showers, W., Hoffmann, S., Lotti-Bond, R., Hajdas, I., and Bonani, G.: Persistent solar influence on North Atlantic climate during the Holocene, Science, 294, 2130-2136, **2001.**

Briegleb, B. P.: Delta-Eddington approximation for solar radiation in the NCAR Community Climate Model, J. Geophys. Res., 97, 7603-7612, **1992.**

Briegleb, B. P., Bitz, C. M., Hunke, E. C., Lipscomb, W. H., Holland, M. M., Schramm, J. L., and Moritz, R. E.: Scientific description of the sea ice component in the Community Climate System Model, Version Three, Tech. Rep. NCAR/TN-463+STR, NCAR, Boulder, CO, **2004.**

Brovkin, V., J. Bendtsen, M. Claussen, A. Ganopolski, C. Kubatzki, V. Petoukhov, and A. Andreev.: Carbon cycle, vegetation, and climate dynamics in the Holocene: Experiments with the CLIMBER-2 model, Global Biogeochem. Cycles, 16, 1139, doi:10.1029/ 2001GB001662, **2002.**

Brovkin, V., A. Ganopolski, D. Archer, and S. Rahmstorf.: Lowering of glacial atmospheric CO_2 in response to changes in oceanic circulation and marine biogeochemistry, Paleoceanography, 22, PA4202, doi:10.1029/2006PA001380, **2007.**

Brovkin, V., Raddatz, T., Christian H. Reick, C.H., Claussen, M., Gayler, V.: Global biogeophysical interactions between forest and climate, Geophys. Res. Lett., 36, doi:10.1029/2009GL037543, **2009.**

Claussen, M., Lohmann, U., Roeckner, E., and Schulzweida, U.: A global dataset of land-surface parameters, Report 135, MPI Hamburg, **1994.**

Claussen, M., Mysak, L. A., Weaver, A. J., Crucifix, M., Fichefet, T., Loutre, M. –F., Weber, S. L., Alcamo, J., Alexeev, V. A., Berger, A., Calov, R., Ganopolski, A., Goosse, H., Lohman, G., Lunkeit, F., Mokhov, I.I., Petoukhov, V., Stone, P., Wang, Zh.: Earth System Models of Intermediate Complexity: Closing the Gap in the Spectrum of Climate System Models, Clim. Dyn., 18, 579-586, **2002.**

Coakley, J. A., Cess, R. D., and Yurevich, F. B.: The effect of tropospheric aerosols on the Earth's radiation budget: A parameterization for climate models, J. Atmos. Sci., 40, 116-138, **1983.**

Collins, W. D.: A global signature of enhanced shortwave absorption by clouds, J. Geophys. Res., 103, 31669-31679, **1998.**

Collins, W. D., Rasch, P. J., Boville, B. A., Hack, J. J., McCaa, J. R., Williamson, D. L., Kiehl, J. T., Briegleb, B., Bitz, C., Jiann Lin, S., Zhang, M., and Dai, Y.: Description of the NCAR Community Atmosphere Model (CAM 3.0), Technical Report NCAR/TN-464+STR, NCAR, Boulder, CO, **2004.**

Collins, W. D., Bitz, C. M., Blackmon, M. L., Bonan, G. B., Bretherton, C. S., Carton, J. A., Chang, P., Doney, S. C., Hack, J. J., Henderson, T. B., Kiehl, J. T., Large, W. G., McKenna, D. S., Santer, B. D., and Smith, R. D.:: The Community Climate System Model version 3 (CCSM3), J. Clim., 19, 2122–2143, **2006a.**

Collins, W. D., Rasch, P. J., Boville, B. A., Hack, J. J., McCaa, J. R., Williamson, D. L., Briegleb, B., Bitz, C., Jiann Lin, S., and Zhang, M.: The formulation and atmospheric simulation of the Community Atmosphere Model version 3 (CAM3), J. Clim., 19, 2144–2161, **2006b.**

Ferrel, W.: The motions of fluids and solids relative to the Earth's surface, Math Monthly 1, 140, 210, 300, 366, 397, **1859.**

Gilli, A., Ariztegui, D., Anselmetti, F. S., Bradbury, J. P., McKenzie, J. A., Markgraf, V., Hajdas, I., and McCulloch, R. D.: Mid-Holocene strengthening of the Southern Westerlies in South America: sedimentological evidences from Lago Cardiel, Argentina (49° S), Global and Planetary Change, 49, 75–93, **2005.**

Grootes, P. M., and Stuiver, M.: Oxygen 18/16 variability in Greenland snow and ice with 10^{-3}- to 10^{5}-year time resolution, J. Geophys. Res., 102, 455-470, **1997.**

Goosse, H., and Fichefet, T.: Importance of ice-ocean interactions for the global ocean circulation: a model study, J. Geophys. Res., 104, 23337-23355, **1999.**

Hack, J. J., Boville, B. A., Briegleb, B. P., Kiehl, J. T., Rasch, P. J., and Williamson, D. L.: Description of the NCAR Community Climate Model (CCM2), Tech. Rep. NCAR/TN-382+STR, NCAR, Boulder, CO, 120 pp, **1993.**

Hadley, G.: Concerning the cause of the general trade winds, Phil. Trans. Roy. Soc. London, 39, 58-62, **1735.**

Hagemann, S.: An improved land surface parameter dataset for global and regional climate models, Report 336, MPI Hamburg, **2002.**

Haigh, J. D.: The impact of solar variability on climate, Science, 272, 981-984, doi:10.1126/science.272.5264.981, **1996.**

Haigh, J. D., Blackburn, M., and Day, R.: The response of tropospheric circulation to perturbations in lower-stratospheric temperature, J. Clim., 18, 3672-3685, doi: 10.1175/JCLI3472.1, **2005.**

Halley, E.: An historical account of the Trade Winds, and Monsoons, Observable in the seas between and near the Tropicks, with an attempt to assign the Physical cause of the said Winds, Philos. Trans. R. Soc. London, 16, 153-168, **1686.**

Hartmann, D. L.: Global physical climatology, Academic Press ISBN 0-12-328530-5, **1994.**

Hartmann, D. L., and Lo, F.: Wave-Driven Zonal Flow Vacillation in the Southern Hemisphere, J. Atmos. Sci., 55, 1303-1315, **1998.**

Hartmann, D. L.: The Atmospheric General Circulation and its variability, J. Meteor. Soc. Japan., 85B, 123-143, **2007.**

Hays, J.D., Imbrie, J., and Shackleton, N.J.: Variations in the Earth's orbit: Pacemaker of the ice ages, Science, 194, 1121-1132, **1976.**

Heinz Veit.: Southern Westerlies during the Holocene deduced from geomorphological and pedological studies in the Norte Chico, Northern Chile (27-33°S), Palaeogeogr. Palaeoclimatol. Palaeoecol., 123, 107-119, **1996.**

Heusser, C. J.: Polar perspective of Late Quaternary climates in the Southern Hemisphere, Quat. Res., 32, 60–71, **1989.**

Holz, A., and Veblen, T. T.: Variability in the Southern Annular Mode determines wildfire activity in Patagonia, Geophys. Res. Lett., 38, doi:10.1029/2011GL047674, **2011.**

Hu, F. S., Kaufman, D., Yoneji, S., Nelson, D., Shemesh, A., Huang, Y., Tian, J., Bond, G., Clegg, B., and Brown, T.: Cyclic variation and solar forcing of Holocene climate in the Alaskan subarctic, Science, 301, 1890-1893, **2003.**

Huebener, H., Cubasch, U., Langematz, U., Spangehl, T., Niehörster, F., Fast, I., and Kunze, M.: Ensemble climate simulations using a fully coupled ocean-troposphere-stratosphere general circulation model, Philos. Trans. R. Soc. Ser. A., 365, 2089-2101, **2007.**

Imbrie, J., Boyle, E. A., Clemens, S. C., Duffy, A., Howard, W. R., Kukla, G., kutzbach, J., Martinson, D. G., McIntyre, A., Mix, A. C., Molfino, B., Morley, J. J., Peterson, L. C., Pisias, N. G., Prell, W. L., Raymo, M. E., Shackleton, N. J., and Toggweiler, J. R.: On the Structure and Origin of Major Glaciation Cycles 1. Linear Responses to Milankovitch Forcing, Paleoceanography, 7, 701–738, doi:10.1029/92PA02253, **1992.**

Jenny, B., Wilhelm, D., and Valero-Garcés, B.L.: The Southern Westerlies in Central Chile: Holocene precipitation estimates based on a water balance model for Laguna Aculeo (33°50'S), Clim. Dyn., 20, 269-280, **2003.**

Joseph, J. H., Wiscombe, W. J., and Weinman, J. A.: The delta-Eddington approximation for radiative flux transfer, J. Atmos. Sci., 33, 2452-2459, **1976.**

Kasahara, A.: Various vertical coordinate systems used for numerical weather prediction, Mon. Wea. Rev., 102, 509-522, **1974.**

Kiehl, J. T., Hack, J. J, Bonan, G. B., Boville, A. B., Williamson, D. L., and Rasch, P. J.: The NCAR Community Climate Model: CCM3, J. Clim., 11, 1131-1149, **1998.**

Kim, S.J., Flato, G.M., and Boer, G.J.: A coupled climate simulation of the last glacial maximum, Part 2: approach to equilibrium, Clim. Dyn., 20, 635-661, **2003.**

Kitoh, A., Murakami, S., and Kiode, H.: A simulation of the last glacial maximum with a coupled atmosphere-ocean GCM, Geophys. Res. Lett., 28, 2221-2224, **2001.**

Klinger, B. A., Drijfhout, S., Marotzke, J., Scott, J. R.: Remote Wind-Driven Overturning in the Absence of the Drake Passage Effect, J. Phys. Oceanogr., 34, 1036-1049, **2004.**

Knudsen, M.F., Riisager, P., Jacobsen, B.H., Muscheler, R., Snowball, I., and Seidenkrantz, M. S.: Taking the pulse of the Sun during the Holocene by joint analysis of ^{14}C and ^{10}Be, Geophys. Res. Lett., 36, doi:10.1029/2009GL039439, **2009.**

Kuhlbrodt, T., Griesel, A., Montoya, M., Levermann, A., Hofmann, M., and Rahmstorf, F.: On the driving processes of the Atlantic meridional overturning circulation, Rev. Geophys., 45, RG2001, doi:10.1029/2004RG000166, **2007.**

Lamy, F., Hebbeln, D., and Wefer, G.: Late quaternary precessional cycles of terrigenous sediment input off the Norte Chico, Chile (27.5°S) and palaeoclimatic implications. Palaeogeogr. Palaeoclimatol. Palaeoecol., 140, 233–244, **1998.**

Lamy, F., Hebbeln, D., and Wefer, G.: High-resolution marine record of climatic change in mid-latitude Chile during the last 28,000 years based on terrigenous sediment parameters, Quat. Res., 51, 83-93, **1999.**

Lamy, F., Hebbeln, D., Rohl, U., and Wefer, G.: Holocene rainfall variability in southern Chile: a marine record of latitudinal shifts of the Southern Westerlies, Earth Planet. Sc. Lett., 185, 369-382, **2001.**

Lamy, F., Ruhlemann, C., Hebbeln, D., and Wefer, G.: High- and low latitude climate control on the position of the southern Peru–Chile current during the Holocene, Paleoceanography, 17, 16.11-16.10, **2002.**

Lamy, F., Kilian, R., Arz, H.W., Francois, J.P., Kaiser, J., Prange, M., and Steinke, T.: Holocene changes in the position and intensity of the southern westerly wind belt, Nat. Geo., 3, 695-699, **2010.**

Laskar, J., Robutel, P., Joutel, F., Gastineau, M., Correia, A. C. M and Levrad, B.: A long-term numerical solution for the insolation quantities of the Earth, Astronom. & Astrophys., 428, 261-285, **2004.**

Legutke, S., and Voss, R.: The Hamburg atmosphere-ocean coupled circulation model ECHO-G, Technical Report 18, Deutsches Klimarechenzentrum, Hamburg, **1999.**

Lin, S. –J., and Rood, R. B.: Multidimensional flux from form semi-lagrangian transport schemes, Mon. Wea. Rev., 124, 2046-2070, **1996.**

Lin, S. –J.: A vertically Lagrangian finite-volume dynamical core for globe models, Mon. Wea. Rev., 132, 2293-2307, **2004.**

Lorenz, S.J, and Lohmann, G.: Acceleration technique for Milankovitch type forcing in a coupled atmosphere-ocean circulation model: method and application for the Holocene, Clim. Dyn., 23, 727-743, doi: 10.1007/s00382-004-0469-y, **2004.**

Machenhauer, B.: The spectral method, in Numerical Methods used in Atmospheric Models, World Meteorological Organization, Geneva, Switzerland, **1979.**

Manzini, E., and McFarlane, N. A.: The effect of varying the source spectrum of a gravity wave parameterization in a middle atmosphere general circulation model, J. Geophys. Res., 103, 31523-31539, **1998.**

Markgraf, V.: Paleoenvironmental changes at the northern limit of the subantarctic Nothofagus forest, Lat 37°S. Quat. Res., 28, 119–129, **1987.**

Markgraf, V., Dodson, J.R., Kershaw, P.A., McGlone, M.S., and Nicholls, N.: Evolution of late Pleistocene and Holocene climates in the circum-South Pacific land areas, Clim. Dyn., 6, 193-211, **1992.**

Marsland, S. J., Haak, H., Jungclaus, J. H., Latif, M., and Roske, F.: The Max-Planck Institute global ocean/sea ice model with orthogonal curvilinear coordinates, Ocean model., 5, 91-127, **2003.**

Mauquoy, D., van Geel, B., Blaauw, M., and van der Pflicht, J.: Evidence from northwest European bogs shows "Little Ice Age" climatic changes driven by variations in solar activity, The Holocene, 12, 1-6, **2002.**

Mayr, C., Wille, M., Haberzettl, T., Fey, M., Janssen, S., Lucke, A., Ohlendorf, C., Oliva, G., Schabitz, F., Schleser, G.H., Zolitschka, B.: Holocene variability of the Southern Hemisphere westerlies in Argentinean Patagonia (52°S), Quat. Sci. Rev., 26, 579–584, **2007.**

McGuffie, K., and Henderson-Sellers, A.: A Climate Modelling Primer, Second Edition. John Wiley & Sons, New York, ISBN 0-471-95558-2, **1997.**

Meehl, G.A., Arblaster, J.M., Matthes, K., Sassi, F., and van Loon, H.: Amplifying the Pacific Climate System Response to a Small 11-Year Solar Cycle Forcing, Science, 325, 1114–1118, **2009.**

Merkel U., Prange M., and Schulz M.: ENSO variability and teleconnections during glacial climates, Quat. Sci. Rev., 29, 86-100, **2010.**

Milankovitch, M.: Kanon der Erdbestrahlungen und seine Anwendung auf das Eiszeitenproblem, Spec Publ, 132, 633, R. Serb. Acad., Belgrade, **1941.**

Mlawer, E. J., Taubman, S. J., Brown, P. D., Iacono, M. J., and Clough, S. A.: Radiative transfer for inhomogeneous atmospheres: RRTM a validated correlated-k model for the longwave, J. Geophys. Res., 102, 16663-16682, **1997.**

Moreno, P. I., Francois, J. P., Moy, C. M., and Villa-Martinez, R.: Covariability of the Southern Westerlies and atmospheric CO_2 during the Holocene, Geology, 38, 727-730, doi:10.1130/G30962.1, **2010.**

Muscheler, R., Beer, J., Wagner, G., et al.: Changes in the carbon cycle during the last deglaciation as indicated by the comparison of ^{10}Be and ^{14}C records, Earth Planet Sci. Lett., 219, 325-340, **2004.**

Oleson, K. W., and Co-authors: Technical description of the Community Land Model (CLM), Tech. Rep. NCAR/TN-461+STR, NCAR, Boulder, CO, **2004.**

Oort, A. H.: The observed annual cycle in the meridional transport of atmospheric energy, J. Atmos. Sci., 28, 325-339, **1971.**

Opsteegh, J. D., Haarsma, R. J., Selten, F. M., and Kattenberg, A.: ECBILT: a dynamic alternative to mixed boundary conditions in ocean models, Tellus A, 50 (3), 348-367, **1998.**

Otto-Bliesner, B., Brady, E., Clauzet, G., Thomas, R., Levis, S., and Kothavala, Z.: Last glacial maximum and Holocene climate in CCSM3, J. Clim., 19, 2526-2544, **2006.**

Petoukhov, V., A. Ganopolski, V. Brovkin, M. Claussen, A. Eliseev, C. Kubatzki, and S. Rahmstorf.: CLIMBER-2: A climate system model of intermediate complexity. Part I: Model description and performance for present climate, Clim. Dyn., 16, 1– 17, **2000.**

Pfeiffer, M., and Lohmann, G.: Interglacial climate evolution: a comparison between the Marine Isotope Stages 1 and 5, Clim. Dyn., in preparation, **2011.**

Rahmstorf, S., and England, M. H.: The influence of southern hemisphere winds on North Atlantic deep water flow, J. Phys. Oceanogr., 27, 2040-2054, **1997.**

Ramanathan, V., and Downey, P.: A nonisothermal emissivity and absorptivity formulation for water vapour, J. Geophys. Res., 91, 8649-8666, **1986.**

Rasch, P. J., and Kristjánsson, J. E.: A comparison of the CCM3 model climate using diagnosed and predicted condensate parameterizations, J. Clim., 11, 1587-1614, **1998.**

Renssen, H., van Geel, B., van der Plicht, J., and Magny, M.: Reduced solar activity as a trigger for the start of the Younger Dryas?, Quatern. Internat., 68-71, 373-383, **2000.**

Roeckner, E., Arpe, K., Bengtsson, L., Christoph, M., Claussen, M., Dümenil, L., Esch, M., Giorgetta, M., Schlese, U., and Schulzweida, U.: The atmospheric general circulation model ECHAM-4: model description and simulation of the present day climate, Report 218. Max-Planck-Institut fur Meteorologie, **1996.**

Roeckner, E., Bäuml, G., Bonaventura, L., Brokopf, R., Esch, M., Giorgetta, M., Hagemann, S., Kirchner, I., Kornblueh, L., Manzini, E., Rhodin, A., Schlese, U., Schulzweida, U., and Tompkins, A.: The atmospheric general circulation model ECHAM5. Part I: Model description. Max Planck Institute for Meteorology Rep. 349, 127 pp. [available from MPI for Meteorology, Bundesstr. 53, 20146 Hamburg, Germany], **2003.**

Rossby, C. G.: On the distributions of angular velocity in gaseous envelopes under influence of large-scale horizontal mixing processes, Bull. Amer. Meteor. Soc., 28, 53-68, **1947.**

Schneider, D. P., Steig, E. J., Van Ommen, T. D., Dixon, D. A., Mayewski, P. A., Jones, J. M., and Bitz, C. M.: Antarctic temperatures over the past two centuries from ice cores, Geophys. Res. Lett., 33, doi:10.1029/2006GL027057, **2009.**

Shin, S.I., Lui, Z., Otto-Bliesner, B., Brady, E.C., Kutzback, J.E., and Harrison, S.P.: A simulation of the last glacial maximum climate using NCAR CCSM, Clim. Dyn., 20, 127-151, doi:10.1007/s00382-002-0260-x, **2003.**

Shulmeister, J., Goodwin, I., Renwick, J., Harle, K., Armand, L., McGlone, M.S., Cook, E., Dodson, J., Hesse, P.P., Mayewski, P., and Curran, M.: The Southern Hemisphere westerlies in the Australasian sector over the last glacial cycle: a synthesis, Quatern. Int., 118-119, 23-53, **2004.**

Sijp, W.P., and England, M.H.: Southern Hemisphere Westerly Wind Control over the Ocean's Thermohaline Circulation, J. Clim., 22, 1277-1286, **2009.**

Sitch, S., Smith, B., Prentice, I. C., Arneth, A., Bondeau, A., Cramer, W., Kaplan, J. O., Levis, S., Lucht, W., Sykes, M. T., Thonicke, K., and Venevsky, S.: Evaluation of ecosystem dynamics, plant geography and terrestrial carbon cycling in the LPJ dynamic global vegetation model, Global Change Biol., 9, 161-185, **2003.**

Slingo, J. M.: The development and verification of a cloud prediction scheme for the ECMWF model, Q. J. R. Meteorol. Soc., 113, 899-927, **1987.**

Smith, R. D., and Gent, P. R.: Reference manual for the Parallel Ocean Program (POP), ocean component of the Community Climate System Model (CCSM2.0 and 3.0), Technical Report. LA-UR-02-2484, Los Alamos National Laboratory, **2002.**

Solanki, S.K., Usoskin, I.G., Kromer, B., Schüssler, M., and Beer, J.: Unusual activity of the Sun during recent decades compared to the previous 11,000 years, Nature, 431, 1084 – 1087, **2004.**

Spangehl, T., Cubasch, U., Raible, C. C., Schimanke, S., Körper, J., and Hofer, D.: Transient climate simulations from the Maunder Minimum to present day: Role of the Stratosphere, J. Geophys. Res-Atmos., 115, D00I10, doi:10.1029/2009JD012358, **2010.**

Starr, V. P.: Physics of negative viscosity phenomena, New York, McGraw-Hill, **1958.**

Steinhilber, F., Beer, J., and Fröhlich, C.: Total solar irradiance during the Holocene, Geophys. Res. Lett., 36, doi:10.1029/2009GL040142, **2009.**

Stuiver, M., Braziunas, T. F., Becker, B., and Kromer, B.: Climatic, solar, oceanic and geomagnetic influences on Late-Glacial and Holocene atmospheric $^{14}C/^{12}C$ change, Quat. Res., 35, 1-24, **1991.**

Stuiver, M., and Braziunas, T. F.: Sun, ocean, climate and atmospheric $^{14}CO_2$, an evaluation of causal and spectral relationships, The Holocene, 3, 289-305, **1993.**

Sundqvist, H.: Parameterization of condensation and associated clouds in models for weather prediction and general circulation simulation, in Physically-based Modeling and

Simulation of Climate and Climate Change, 1, edited by M. E. Schlesinger, 433-461, Kluwer Academic, **1988.**

Terray, L., Valcke, S., and Piacentini, A.: The oasis coupler user guide. Version 2.2, Tech. Rep. TR/CMGC/98-05, CERFAS, **1998.**

Thomson, J.: On the grand currents of atmospheric circulation, British Association Meeting, Dublin, Phil. Trans. Roy. Soc. London (A), 183, 653-684, **1892.**

Toggweiler, J.R., and Samuels, B.: Effect of Drake Passage on the global thermohaline circulation, Deep-Sea Res. Pt 1., 42, 477-500, **1995.**

Toggweiler, J.R., Russel, J. L., and Carson, S.R.: Midlatitude westerlies, atmospheric CO_2 and climate change during the ice ages, Paleoceanography, 21, PA2005, doi:10.1029/2005PA001154, **2006.**

Valdes, P.J.: South American palaeoclimate model simulations: how reliable are the models?, J. Quaternary Sci., 15, 357-368, **2000.**

van Geel, B., Heusser, C.J., Renssen, H., and Schuurmans, J.E.: Climatic change in Chile at around 2700 BP and global evidence for solar forcing: a hypothesis, Holocene, 10, 659-664, **2000.**

Varma, V., Prange, M., Lamy, F., Merkel, U., and Schulz, M.: Solar-forced shifts of the Southern Hemisphere Westerlies during the Holocene, Clim. Past, 7, 339-347, doi:10.5194/cp-7-339-2011, **2011.**

Versteegh, G.J.M.: Solar forcing of climate. 2: Evidence from the Past, Space Sci. Rev., 120, 243–286, **2005.**

Vonmoos, M., Beer, J., and Muscheler, R.: Large variations in Holocene solar activity: Constraints from ^{10}Be in the Greenland Ice Core Project ice core, J. Geophys. Res-Space, 111, A10105, doi:10.1029/2005JA011500, **2006.**

Wagner, S., Widmann, M., Jones, J., Haberzettl, T., Lücke, A., Mayr, C., Ohlendorf, C., Schäbitz, F., and Zolitschka, B.: Transient simulations, empirical constructions and forcing mechanisms for the Mid-holocene hydrological climate in southern Patagonia, Clim. Dyn., doi 10.1007/s00382-007-0229-x, **2007.**

Waldmann, N., Ariztegui, D., Anselmetti, F. S., Austin, Jr J. A., Moy, C. M., Stern, C., Recasens, C., Dunbar, R. B.: Holocene climatic fluctuations and positioning of the Southern Hemisphere westerlies in Tierra del Fuego (548 S), Patagonia. J. Quaternary Sci., Vol. 25 pp. 1063–1075. ISSN 0267-8179, **2010.**

Williamson, D. L., and Olson, J. G.: Climate simulations with a semi-Lagrangian version of the NCAR Community Climate Model, Mon. Wea. Rev., 122, 1594-1610, **1994.**

Williamson, D. L., and Rasch, P. J.: Water transport in the NCAR CCM2, Tellus 46 A, 34-51, **1994.**

Williamson, D. L.: Time-spit versus process-split coupling of parameterizations and dynamical core, Mon. Wea. Rev., 130, 2024-2041, **2002.**

Wolff, J., Maier-Reimer, E., and Legutke, S.: The Hamburg Primitive Equation Model HOPE, Tech. Rep. 18, German Climate Center (DKRZ), **1997.**

Wyroll, K-H., Dong, B., and Valdes, P.J.: On the position of southern westerlies at the last glacial maximum: an outline of AGCM simulation results and evaluation of their implications, Quat. Sci. Rev., 19, 881-898, **2000.**

Zhang, G. J., and McFarlane, N. A.: Sensitivity of climate simulations to the parameterization of cumulus convection in the Canadian Climate Centre general circulation model, Atmosphere-Ocean, 33, 407-446, **1995.**

Zhang, M., Lin, W., Bretherton, C. S., Hack, J. J., and Rasch, P. J.: A modified formulation of fractional stratiform condensation rate in the NCAR community atmospheric model CAM2, J. Geophys. Res., 108(D1), **2003.**

Chapter 2

2. Solar-forced shifts of the Southern Hemisphere Westerlies during the Holocene

V. Varma, M. Prange, F. Lamy, U. Merkel and M. Schulz

(Published in *Climate of the Past*, doi:10.5194/cp-7-339-2011)

2.1 Abstract

The Southern Hemisphere Westerly Winds (SWW) constitute an important zonal circulation that influences large-scale precipitation patterns and ocean circulation. Variations in their intensity and latitudinal position have been suggested to exert a strong influence on the CO_2 budget in the Southern Ocean, thus making them a potential factor affecting the global climate. In the present study, the possible influence of solar forcing on SWW variability during the Holocene is addressed. It is shown that a high-resolution iron record from the Chilean continental slope (41°S), which is interpreted to reflect changes in the position of the SWW, is significantly correlated with reconstructed solar activity during the past 3000 years. In addition, solar sensitivity experiments with a comprehensive global climate model (CCSM3) were carried out to study the response of SWW to solar variability. Taken together, the proxy and model results suggest that centennial-scale periods of lower (higher) solar activity caused equatorward (southward) shifts of the annual mean SWW.

2.2 Introduction

The Southern Hemisphere Westerly Winds (SWW) constitute an important zonal circulation system that dominates the dynamics of Southern Hemisphere mid-latitude climate (e.g. Thresher, 2002; Shulmeister et al., 2004). Furthermore, they may influence the global ocean circulation through wind driven upwelling of deep water in the Southern Ocean (Toggweiler and Samuels, 1995; Kuhlbrodt et al., 2007; Sijp and England, 2009) and through the impact on the Indian-Atlantic Ocean water exchange by Agulhas leakage (Sijp and England, 2009;

Biastoch et al., 2009). The significance of the SWW in the global climate system through their influence on the CO_2 budget in the Southern Ocean has been discussed controversially (Toggweiler et al., 2006; Menviel et al., 2008; Tschumi et al., 2008; Anderson et al., 2009). Accordingly, understanding the variability and the impact of various forcings on the SWW remains a significant area of investigation. Earlier studies have provided evidence for an equatorward displacement of the northern SWW margin during glacial periods (Lamy et al., 2004; Kaiser et al., 2005). Toggweiler et al. (2006) postulated feedback mechanisms involving the Southern Ocean CO_2 air-sea gas exchanges, global temperature and position of SWW, whereby cooler climates would correspond to a more equatorward location of the SWW. Driving mechanisms and dynamics behind the variability in SWW are still unclear. During the Holocene, changes in seasonal insolation might have caused long-term variations in the structure, position and intensity of the SWW (Markgraf et al., 1992; Lamy et al., 2001; Jenny et al., 2003; Lamy et al., 2010).

Another significant forcing that influences climate on decadal to millennial time-scales is solar activity (e.g. Haigh, 1996; Cubasch et al., 1997; Bond et al., 2001; Versteegh, 2005; Spangehl et al., 2010), which could also be a potential driver for SWW variability. Van Geel et al. (2000) proposed solar activity as one of the possible factors for a shift in atmospheric circulation during the late Holocene around 2700 yr BP. The abrupt decrease in solar activity during this period might have acted as a trigger for the glacier advancement towards the equator due to an equatorward shift of climatic zones along with the SWW (Van Geel et al., 2000). Solar-induced changes in stratospheric ozone through enhanced variability in the ultraviolet part of the solar spectrum were a postulated factor for shifting the SWW by influencing the tropospheric subtropical westerly jet through dynamical coupling between the atmospheric layers (Haigh, 1996). The potential role of solar forcing in Southern Hemisphere mid-latitude climate variability on the quasi-decadal timescale has been investigated by Thresher (2002), using observational data from the instrumental period. For longer timescales, the study of proxy data from natural archives is necessary. Here, we investigate the influence of centennial scale total solar irradiance (TSI) variations on the SWW using proxy data from the late Holocene in combination with sensitivity experiments, employing a state-of-the-art comprehensive global climate model. The results will lead us to the

suggestion that equatorward (southward) shifts of the annual mean SWW occurred during centennial-scale periods of lower (higher) solar activity.

2.3 Hints of solar-forced SWW shifts in a marine sediment core

The mid-latitudes of Chile exhibit an extreme north-south precipitation gradient controlled by the latitudinal position of the SWW. Furthermore, local correlation analyses have shown that, in central and southern Chile, rainfall on the western side of the Andes is almost entirely determined by the westerlies (Garreaud, 2007). Therefore, any paleoclimate proxy that is primarily controlled by precipitation changes is a potential recorder of past changes of the SWW in this region. High-accumulation rate marine sediment core GeoB3313-1 from the Chilean continental slope (41°S, 74.45°W) provides a mid-to-late Holocene record of rainfall variability through its iron content (Lamy et al., 2001). Figure 1 shows the core location and illustrates the pattern of seasonal precipitation and zonal surface wind.

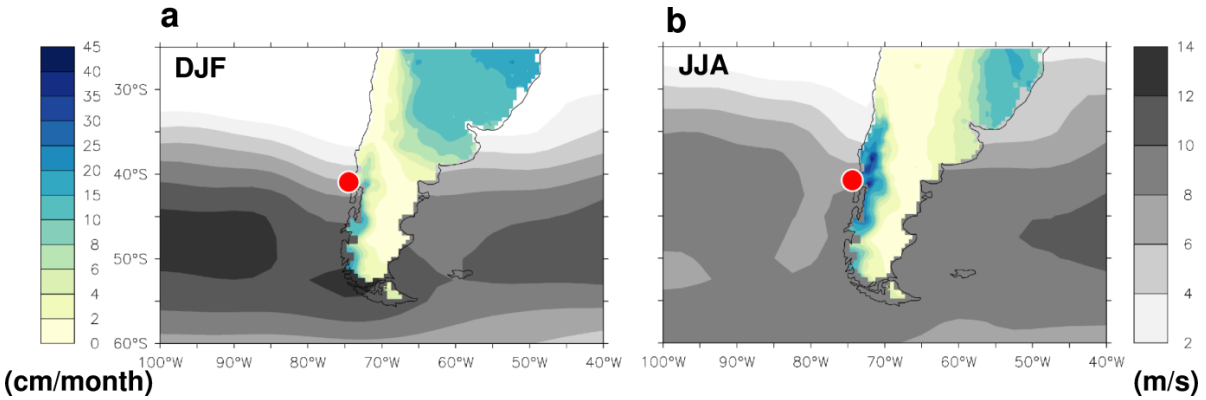

Fig. 1 Long-term climatological distribution of precipitation over land and 1000 hPa zonal wind over oceans in the region of marine sediment core GeoB3313-1 located at 41°S, 74.45°W (red dot) for (a) austral summer (December/January/February) and (b) austral winter (June/July/August). During summer, the winds are more confined towards the south, resulting in decreased precipitation over the catchment represented by the core. During winter, surface winds (shown in grey shades) move towards the north, resulting in enhanced precipitation (shown in bluish shades) over the catchment represented by the core. Data: University of Delaware precipitation (http://climate.geog.udel.edu/~climate/), NCEP-NCAR reanalysis winds (Kalnay et al., 1996).

During the austral summer, the northern margin of the SWW moves southwards and the core of the westerlies at around 50°S intensifies. The latitudinal movement of the wind belt's

northern margin results in decreased precipitation over the catchment represented by the sediment core (Fig. 1a). Conversely, during the austral winter, the northern margin of the westerly wind belt is shifted towards the equator resulting in enhanced precipitation over the catchment represented by the sediment core (Fig. 1b). Given the strong influence of the SWW on the precipitation pattern, the iron data from core GeoB3313-1, which primarily reflect changes in paleoprecipitation, are likely to provide information on the SWW position. A higher content of iron in the sediment core region indicates drier conditions, probably due to southward shifted SWW, whereas a lower iron concentration might be indicative of wetter conditions suggesting northward shifted SWW (Lamy et al., 2001).

In order to find a possible correlation of the iron record with Holocene solar forcing, we use reconstructions of solar activity based on ^{14}C (Solanki et al., 2004) and ^{10}Be (Vonmoos et al., 2006). Comparison of the records suggests a possible link between the Sun's radiative output and the SWW, indicating an equatorward (southward) shift of the annual mean SWW during periods of lower (higher) solar activity during the last 3000 years (Fig. 2).

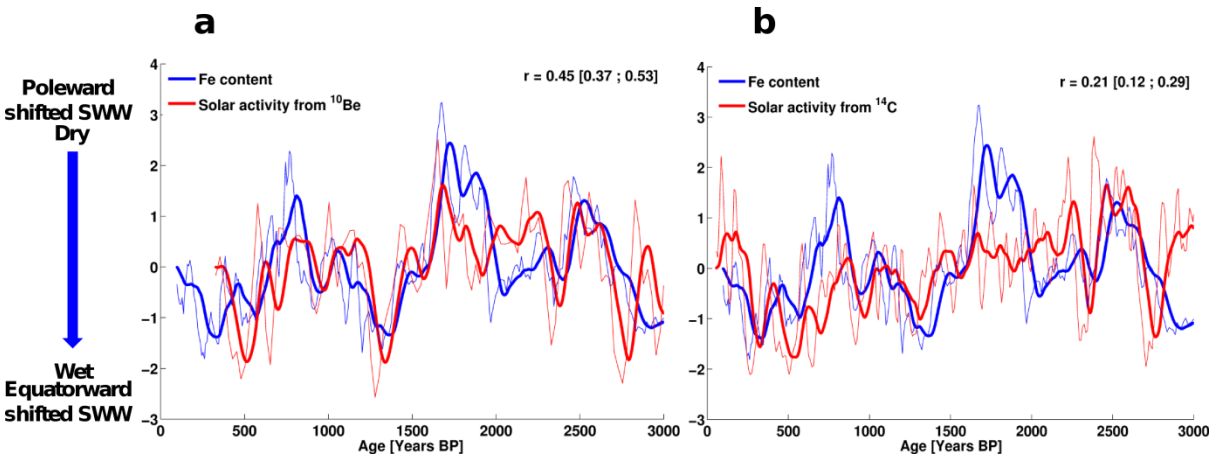

Fig. 2 Reconstructions of precipitation and hence, the position of the SWW (based on the GeoB3313-1 iron record) versus solar activity for the late Holocene. (a) Solar activity based on ^{10}Be (Vonmoos et al., 2006), (b) solar activity based on ^{14}C (Solanki et al., 2004). The time series have been linearly detrended and standardized. The bold curves show 100-year running means and the thin curves show the unsmoothed data. A lower content of iron stands for wetter conditions, suggesting northward shifted SWW (Lamy et al., 2001). Conversely, a higher content of iron reflects drier conditions essentially due to southward shifted SWW. Pearson correlation coefficients (r) were calculated from the unsmoothed data. 95% confidence intervals (in brackets) were calculated using a bootstrap method, where autocorrelation has been taken into account (Mudelsee, 2003).

Linear correlations over this time interval, calculated using the Pearson coefficient are significant for both solar reconstructions. While the correlation coefficient (r) for ^{14}C is relatively small (but statistically significant), the large correlation coefficient for ^{10}Be would suggest that ca. 20% (i.e., r2) of late Holocene rainfall and hence SWW variability could be attributable to solar forcing.

2.4 Model evidence for solar-forced SWW shifts

To investigate the effect of TSI on the SWW, we carried out two sets of idealized experiments with constant and sinusoidal solar forcings using the comprehensive global climate model CCSM3 (Community Climate System Model version 3). NCAR's (National Center for Atmospheric Research) CCSM3 is a state-of-the-art fully-coupled model, composed of four separate components representing atmosphere, ocean, land and sea-ice (Collins et al., 2006). Here, we employed the low-resolution version described in detail by Yeager et al. (2006). In this version, the resolution of the atmospheric component is given by T31 (3.75° transform grid), with 26 layers in the vertical, while the ocean has a nominal resolution of 3° (like the sea-ice component) with a vertical resolution of 25 levels.

2.4.1 Ensemble experiments with constant solar forcing

Model runs were carried out with constant solar forcing, with the control run having a solar constant of 1365 Wm^{-2} and the solar sensitivity experiments with a lower solar irradiance value of 1363 Wm^{-2} (i.e. reduction by 0.15%). Preindustrial boundary conditions were applied in all simulations following the protocol established by the Paleoclimate Modelling Intercomparison Project, Phase II (Braconnot et al., 2007). This forcing represents the average conditions of the late Holocene before the significant impact of humans, rather than a specific date, and it accounts for concentrations of greenhouse gases (e.g. CO_2 concentration of 280 ppmv), ozone, sulphate and carbonaceous aerosols (Otto-Bliesner et al., 2006). After a 600-year spin-up, the control simulation (Merkel et al., 2010) was run for another 150 years while three sensitivity runs with a reduced solar constant were branched off at model years 600, 640 and 680, respectively. Each sensitivity run was integrated for 70 years, which is a typical timescale for the duration of solar "Grand minima" like the Wolf (1280–1350 AD), Spörer (1450–1550 AD) or Maunder (1645–1715AD) Minimum. Our choice of TSI reduction

of 2 Wm^{-2} between solar maximum and solar minimum in the model experiments is consistent with recent observation and physics-based estimates (Steinhilber et al., 2009).

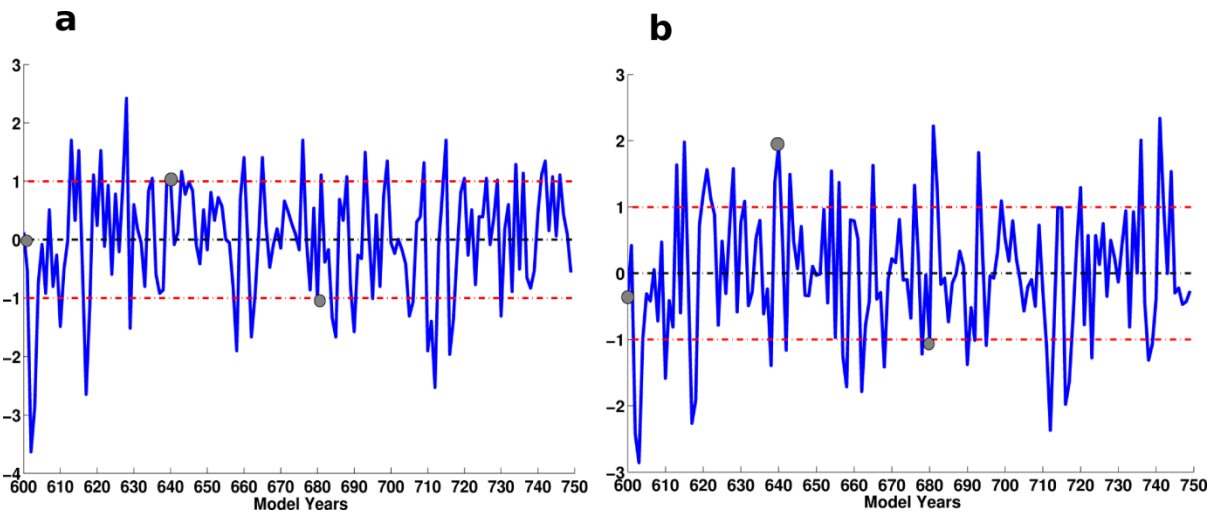

Fig. 3 Indices for annual-mean SWW intensity and position, respectively, in the model control run. (a) Zonally averaged zonal wind velocity at 1000 hPa averaged between 55°S and 35°S. (b) Difference in zonally averaged 1000 hPa zonal winds between 55°S and 35°S. Both indices have been standardized and ±1σ denote one standard deviation (red dashed horizontal lines) while zero denotes the mean (black dashed horizontal lines). The years from which the three constant TSI sensitivity runs were branched off are marked as grey solid circles.

The three TSI sensitivity runs were branched off from very different SWW states (Fig. 3) and it could be noted from the time series of both intensity and position that the initial conditions for the different sensitivity runs were clearly different from each other and spanned the full range of ±1σ. Indices of both the intensity and position of the annual mean SWW have been defined in terms of the average and difference between the latitudes 55°S (southern part of SWW belt) and 35°S (northern part of SWW belt) respectively. Spectral analyses performed for both SWW indices from the control run showed no decadal or multi-decadal cycles at the 95% significance level (not shown), thus ruling out a possible influence of low-frequency variability on the SWW response to reduced solar activity. Similar results hold for seasonal analyses (not shown). Moreover, we note that the three different TSI sensitivity experiments showed similar responses to reduced solar activity despite their different initial states. Taken together, we are therefore confident that the results from our three 70-year sensitivity

experiments are robust with respect to the response of the SWW to TSI reduction. The difference between sensitivity and control run (i.e. low minus high TSI simulation for a specific 70-year interval) was calculated for each ensemble member and, subsequently, the ensemble mean was taken and subjected to statistical analyses using a Student's t-test. Figure 4a shows the 70- year-averaged annual mean zonal wind anomaly at 1000 hPa in response to lower solar activity, for the ensemble mean. The model results suggest a shift of surface wind fields towards the equator in response to TSI reduction, consistent with the interpretation of the marine iron record discussed above. Figure 4b depicts the zonally averaged annual mean zonal wind anomaly as a function of latitude and height, showing that the equatorward SWW shift takes place at all levels in the troposphere. The wind anomaly patterns exhibit opposite signs for the different seasons, i.e. for lower solar activity, the SWW experience an equatorward shift during austral summer and a poleward shift during austral winter (Fig. 5).

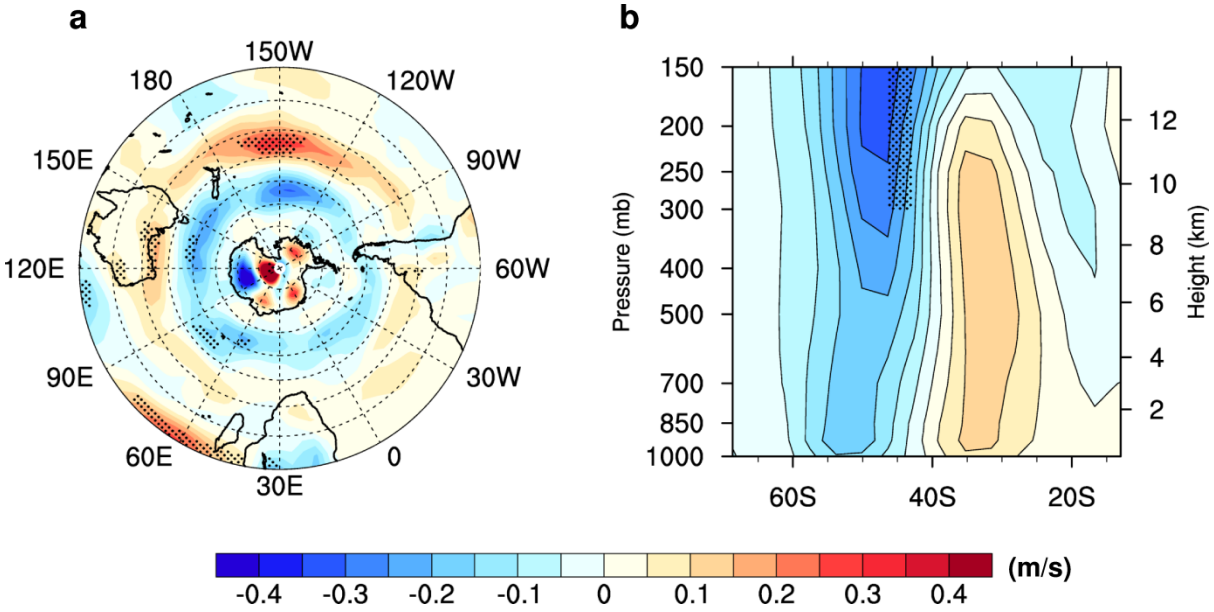

Fig. 4 Annual mean zonal wind anomaly (low minus high total solar irradiance) in the model ensemble mean, averaged over the entire 70- year interval of the constant solar forcing experiment. (a) Zonal wind anomaly in the Southern Hemisphere at 1000 hPa, showing the clear equatorward shift of SWW. Latitudes marked start from 10°S and are placed at a 10° interval. (b) Zonally averaged zonal wind anomaly for the Southern Hemisphere showing that the equatorward shift of SWW is pronounced even at upper levels of the troposphere. Stippling indicates significance of the anomaly at the 0.05 level (applying a Student's t-test).

However, it is the austral summer pattern (December/January/February) which dominates the annual mean distribution, as can be seen by comparing Figs. 4 and 5. An equatorward shift of the SWW should result in increased precipitation over central Chile. Since a low resolution version of CCSM3 has been used here, local features and in particular, orographic rainfall at the Andes cannot be fully captured. The model still simulates positive precipitation anomalies over the Chilean regions of enhanced westerlies, albeit with a very small magnitude and statistically not significant at the 0.05 significance level according to a t-test (not shown). We further note that a direct geographical comparison between model output and proxy data from a specific location could be affected by the fact that the summer SWW in CCSM3 are biased towards north (see http://www.ccsm.ucar.edu/experiments/ccsm3.0/atm/b30.031-obs_801-820/set4/set4_DJF_U_NCEP_obsc.png for the present-day control run). The position of the maximum wind speed is simulated further equatorward, which is a common shortcoming in most coarse-resolution climate models (Rojas et al., 2009). This implies that the response of the SWW is likely simulated somewhat too far north.

2.4.2 Experiments with sinusoidal solar forcing

In order to test if the sensitivity of the model is sufficient to detect recurring solar-forced SWW shifts and if the response is dependent on the Holocene background climate, we carried out an additional set of experiments with idealized solar forcing. Each of these idealized experiments was initialized from an orbitally forced transient Holocene run (9 kyr BP to the present day) by taking the model years having orbital forcing corresponding to 8.5 kyr BP, 5.5 kyr BP and 2.5 kyr BP, respectively (all other boundary conditions were set to the pre-industrial levels described above; an in depth analysis of the Holocene transient experiment will be the subject of a forthcoming study*). From these initial conditions, the model was integrated for another 500 years to reach quasi-equilibrium for each of the three time slices. Subsequently, a sinusoidally varying solar irradiance forcing with a period of 200 years and an amplitude of 1 Wm^{-2} was applied to the model for each time slice. The 200-year period was chosen to mimic the de Vries solar cycle, which is one of the most prominent solar cycles during the Holocene (e.g. Knudsen et al., 2009).

*See Chapter 3 for details.

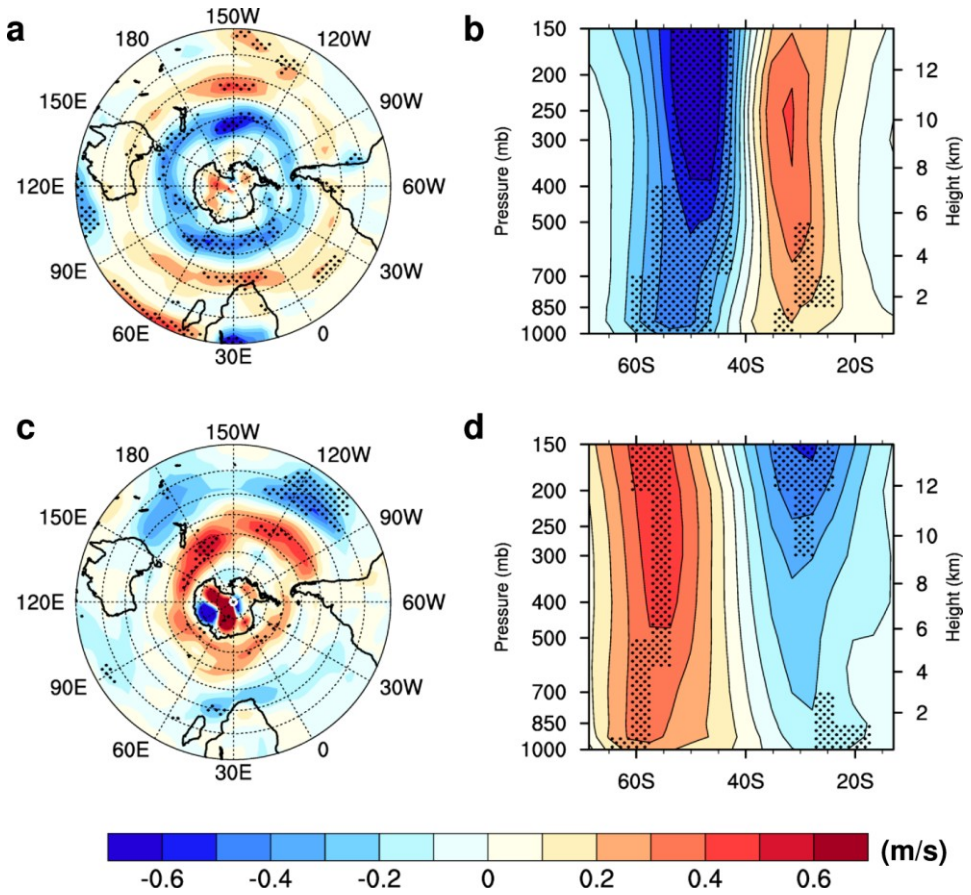

Fig. 5 Seasonal mean zonal wind anomaly (low minus high total solar irradiance) in the model ensemble mean, averaged over the entire 70-year interval of the constant solar forcing experiment. (a) and (c) Zonal wind anomaly in the Southern Hemisphere at 1000 hPa for austral summer (December/January/February) and austral winter (June/July/August), respectively. The wind anomaly patterns exhibit opposite signs for the different seasons, i.e. for lower solar activity, the SWW experience an equatorward shift during austral summer and a poleward shift during austral winter. Latitudes marked start from 10°S and are placed at 10° interval. (b) and (d) Zonally averaged zonal wind anomaly for the Southern Hemisphere for austral summer (December/January/February) and austral winter (June/July/August), respectively. Stippling indicates significance of the anomaly at the 0.05 level (applying a Student's t-test).

With 700 years of model integration having sinusoidally varying solar irradiance, it was possible to include 3.5 de Vries solar cycles in each of the three experiments. Figure 6 shows the TSI forcing along with the position of the SWW (defined in terms of the difference between the latitudes 55°S and 35°S which represent the southern and northern parts of the SWW belt, respectively) for the early, mid and late Holocene experiments. In each experiment, forcing and response exhibit a strikingly similar temporal pattern, i.e. higher

(lower) solar activity resulted in a poleward (equatorward) shift of the SWW. The three time series of the SWW position showed a statistical correlation with TSI significant at the 95% confidence level for centennial-scale variations. In addition, cross-spectral coherency was significant (95% level) at the period of 200 years using unsmoothed time series (not shown).

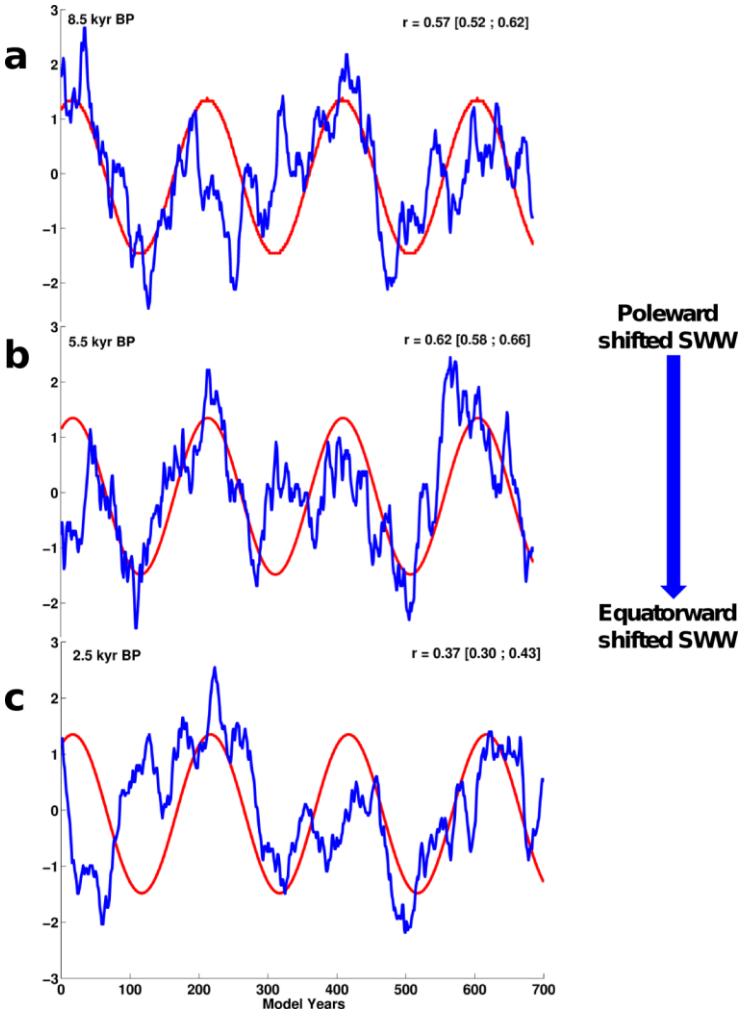

Fig. 6 Total solar irradiance (red curves) along with the position of annual mean SWW at 1000 hPa (blue curves; defined in terms of the difference between the latitudes 55°S and 35°S which represent the southern and northern parts of the SWW belt) in the idealized sinusoidal solar-forcing experiments for early (a), mid (b) and late (c) Holocene. All time series have been standardized. The Pearson correlation coefficients (r) were calculated after low-pass filtering using 70-year smoothing on zonal wind. 95% bias corrected bootstrap confidence intervals (in brackets) were calculated using 10000 sub-samplings.

2.5 Discussion

Even though the influence and importance of the SWW on a global scale has been identified in previous studies, little is known about its variability and forcings. Correlation analysis between the GeoB3313-1 iron record and solar activity reconstructions suggests a significant influence of the Sun's radiative output on the position of the SWW for the last 3000 years on a (multi-)centennial timescale. Though, for the early and mid-Holocene (i.e. prior to 3000 yr

BP), the correlation based on proxy records is close to zero (not shown), the model results from the sinusoidal solar forcing experiments do not suggest a weakening of the solar influence on the SWW in the early and mid-Holocene (Fig. 6). It is possible that this incongruity is due to dating uncertainties in the deeper section of core GeoB3313-1. We emphasize that all the proxy records used in this study are given on their own age scale, which may have adverse or positive effects on the correlation. The climate model used in this study has a poorly resolved stratosphere and does not include feedbacks associated with the effect of enhanced variability in the ultraviolet part of the solar spectrum on photochemical dissociation rates and the subsequent impact on stratospheric ozone (Haigh, 1999; Rind et al., 2008). Instead, applied changes in TSI mostly affect the climate system through shortwave absorption by the surface, whereas less direct heating by solar radiation takes place at higher levels of the atmosphere. Note that almost 70% of shortwave radiation that enters the atmosphere and is not reflected back to space, is absorbed at the surface (Kiehl and Trenberth, 1997, and also in our model simulations). Therefore, the climate response in our experiment is mainly through "bottom-up mechanisms" (Meehl et al., 2009). By contrast, a "top-down" mechanism, which influences the troposphere via stratospheric ozone responses to variations in ultraviolet radiation, has been proposed by Haigh (1996). In her model, increase in ultraviolet radiation and resulting rise in ozone concentration, induced heating in the lower stratosphere during the Southern Hemisphere summer. As a consequence, strengthened stratosphere easterly winds caused the tropospheric subtropical westerly jets to move poleward, the tropical Hadley cell to broaden, and the SWW to move southward. "Bottom-up" and "top-down" mechanisms are not mutually exclusive. The model by Haigh (1996) used fixed sea surface temperatures and, hence, is unable to simulate "bottom-up" mechanisms that are important in our coupled climate model. We therefore suggest that the processes linking solar variability to the SWW in the two different models may complement each other, thus leading to a stronger total response than given by each individual process alone. In order to get some insight into the "bottom-up" processes involved in our low-TSI experiment, simulated surface temperature anomalies are analyzed from the ensemble experiments with constant (70-year long) solar forcing (Fig. 7). As expected, a general surface cooling is induced by the TSI reduction (Fig. 7a). In addition to this general cooling, a more pronounced reduction in surface temperature is observed in the mid latitudes of, e.g., the central South Pacific sector (Fig. 7a, c, and d). By means of general atmospheric

circulation modelling and scaling arguments, it has recently been shown that a reduction of the mean global surface temperature decreases the width of the Hadley cell (Frierson et al., 2007) and shifts the eddy-driven surface westerlies that result from the balance between vertically integrated eddy momentum convergence and surface drag towards the equator (Lu et al., 2010).

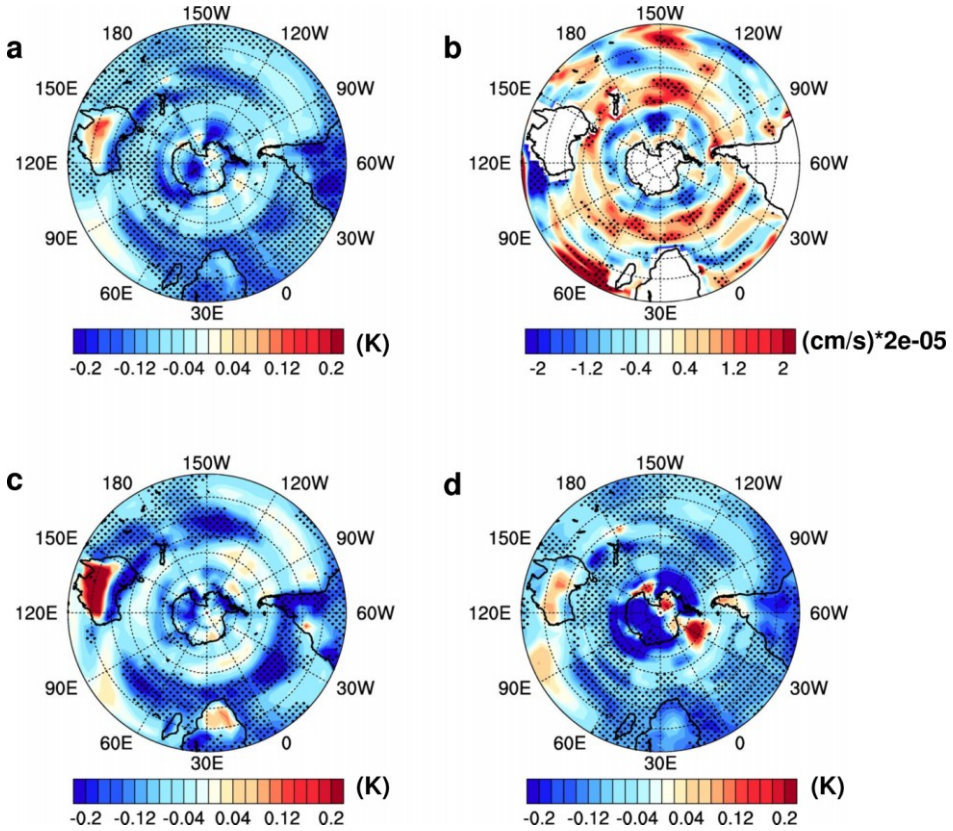

Fig. 7 Surface temperature anomalies (low minus high total solar irradiance) and the austral summer upwelling anomaly in the model ensemble mean, averaged over the entire 70-year interval of the constant solar forcing experiment. (a), (c) and (d) Surface temperature anomaly in the Southern Hemisphere for annual mean, austral summer (December/January/February) and austral winter (June/July/August), respectively. (b) Austral summer (December/January/February) upwelling (vertical velocity) anomaly at 30m depth in the Southern Hemisphere. Stippling indicates significance of the anomaly at the 0.05 level (applying a Student's t-test). Latitudes marked start from 10°S and are placed at 10° interval.

Since the reduction in TSI is only 0.15%, the global cooling effect is small and additional feedbacks are required to induce a significant change in the westerlies. One important feedback is associated with enhanced Ekman divergence and resulting upwelling (vertical velocity) around ~40°S in austral summer (Fig. 7b). The upwelled cold water is transported northward in the Ekman surface layer, leading to enhanced SST cooling just north of ~40°S (Fig. 7c). This cooling results in a meridional SST gradient anomaly that lies very close to (or just equatorward of) the subtropical jet. It has been shown that such an anomalous subtropical surface temperature gradient causes a strengthening of the jet along with an equatorward shift of the eddy-driven surface westerlies (Brayshaw et al., 2008; Lu et al., 2010), thus providing a positive feedback on the initial SWW shift in our simulations. In austral winter, the coldest surface temperature anomalies are found around Antarctica (Fig. 7d), mainly due to increased sea-ice concentrations (up to 7%) reducing ocean atmosphere heat fluxes and increasing the surface albedo. The resulting stronger meridional surface temperature gradient at high latitudes, however, is accompanied by a poleward shift of the surface westerlies (Chen et al., 2010; Lu et al., 2010), due to enhanced high-latitude baroclinic wave generation. This results in a winter SWW shift that is opposite to the other seasons.

2.6 Conclusions

Evidence for a significant solar influence on climate is rapidly growing based on natural archives from the Northern Hemisphere. Proxy data from the Southern Hemisphere, however, are notoriously sparse (Versteegh, 2005). Here, we presented proxy and model evidence that centennial scale variability in the position of the annual mean SWW has been influenced by fluctuations in solar activity at least during the past 3000 years. Periods of lower solar activity were associated with annual-mean equatorward shifts of the SWW, whereas periods of higher solar activity were linked to annual-mean poleward displacements of the SWW. Our idealized experiments with sinusoidal solar forcing show that the model response to solar forcing on the centennial time scale is a robust feature, independent of the Holocene background climate state. Based on our model evidence, as well as the proxy indication, we propose that the role of the Sun in modifying Southern Hemisphere tropospheric circulation patterns has probably been underestimated in model simulations of past climate change. The potential role of solar forcing, along with feedbacks involving ocean and sea-ice dynamics, may further complicate the prediction of future SWW shifts.

2.7 Acknowledgements

This work was funded through the DFG (Deutsche Forschungsgemeinschaft, German Research Foundation) Priority Programme "INTERDYNAMIK" and through the DFG Research Center/Cluster of Excellence "The Ocean in the Earth System". We are indebted to Jürg Beer and Sami Solanki for providing the solar activity reconstructions as well as to Bruce Briegleb and Bette Otto-Bliesner for providing CCSM3 pre-industrial boundary conditions. We thank Axel Timmermann for stimulating discussions. We are also thankful to the two anonymous reviewers for their valuable comments and suggestions for improving the paper. We also thank PAGES for sponsoring the publication of this article. CCSM3 simulations were performed on the IBM supercomputer of the Norddeutscher Verbund für Hoch und Höchstleistungsrechnen (HLRN). We also acknowledge the use of the NCAR Command Language (NCL) and NOAA/PMEL's Ferret in our data analysis and visualization herein. SimStat (Statistical Analysis and Simulation Software) was used to calculate the bootstrap confidence intervals.

2.8 References

Anderson, R.F., Ali, S., Bradtmiller, L.I., Nielsen, S.H.H., Fleisher, M.Q., Anderson, B.E., and Burckle, L.H.: Wind-Driven Upwelling in the Southern Ocean and the Deglacial Rise in Atmospheric CO_2, Science, 323, 1443 – 1448, **2009.**

Biastoch, A., Böning, C.W., Schwarzkopf, F.U., and Lutjeharms, J.R.E.: Increase in Agulhas leakage due to poleward shift of Southern Hemisphere westerlies, Nature, 462, 495-498, **2009.**

Bond, G., Kromer, B., Beer, J., Muscheler, R., Evans, M.N., Showers, W., Hoffmann, S., Lotti-Bond, R., Hajdas, I., and Bonani, G.: Persistent Solar Influence on North Atlantic Climate During the Holocene, Science, 294, 2130 – 2136, **2001.**

Braconnot, P., Otto-Bliesner, B., Harrison, S., Joussaume, S., Peterchmitt, J.-Y., Abe-Ouchi, A., Crucifix, M., Driesschaert, E., Fichefet, Th., Hewitt, C.D., Kageyama, M., Kitoh, A., Laîné, A., Loutre, M.-F., Marti, O., Merkel, U., Ramstein, G., Valdes, P., Weber, S.L., Yu, Y., and Zhao, Y.: Results of PMIP2 coupled simulations of the Mid-Holocene and Last Glacial Maximum Part 1: experiments and large-scale features, Clim. Past., 3, 261–277, **2007.**

Brayshaw, D.J., Hoskins, B., Blackburn, M.: The Storm-Track Response to Idealized SST Perturbations in an Aquaplanet GCM, J. Atmos. Sci., 65, 2842-2860, doi:10.1175/2008JAS2657.1, **2008.**

Chen, G., Plumb, R.A., and Lu, J.: Sensitivities of zonal mean atmospheric circulation to SST warming in an aqua-planet model, Geophys. Res. Lett., 37, L12701, doi:10.1029/2010GL043473, **2010.**

Collins, W.D., Bitz, C.M., Blackmon, M.L., Bonan, G.B., Bretherton, C.S., Carton, J.A., Chang, P., Doney, S.C., Hack, J.J., Henderson, T.B., Kiehl, J.T., Large, W.G., McKenna, D.S., Santer, B.D., and Smith, R.D.: The Community Climate System Model Version 3 (CCSM3), J. Clim., 19, 2122-2143, **2006.**

Cubasch, U., Voss, R., Hegerl, G.C., Waszkewitz, J., and Crowley, T.J.: Simulation of the influence of solar radiation variations on the global climate with an ocean-atmosphere general circulation model, Clim. Dyn., 13, 757-767, **1997.**

Frierson, D.M.W., Lu, J., and Chen, G.: Width of the Hadley cell in simple and comprehensive general circulation models, Geophys. Res. Lett., 34, L18804, doi:10.1029/2007GL031115, **2007.**

Garreaud, R.D.: Precipitation and Circulation Covariability in the Extratropics, J. Clim., 20, 4789–4797, **2007.**

Haigh, J.D.: The impact of solar variability on Climate, Science, 272, 981 – 984, **1996.**

Haigh, J.D.: Modelling the impact of solar variability on climate, J. Atmos. Sol-Terr. Phy., 61, 63-72, **1999.**

Jenny, B., Wilhelm, D., and Valero-Garcés, B.L.: The Southern Westerlies in Central Chile: Holocene precipitation estimates based on a water balance model for Laguna Aculeo (33°50'S), Clim. Dyn., 20, 269-280, **2003.**

Kaiser, J., Lamy, F., and Hebbeln, D.: A 70-kyr sea surface temperature record off southern Chile (Ocean Drilling Program Site 1233), Paleoceanography, 20, PA4009, doi:10.1029/2005PA001146, **2005.**

Kalnay, E., Kanamitsu, M., Kistler, R., Collins, W., Deaven, D., Gandin, L., Iredell, M., Saha, S., White, G., Woollen, J., Zhu, Y., Leetmaa, A., Reynolds, R., Chelliah, M., Ebisuzaki, W., Higgins, W., Janowiak, J., Mo, K.C., Ropelewski, C., Wang, J., Jenne, R., and Joseph, D.: The NCEP/NCAR 40-Year Reanalysis Project, B. Am. Meteorol. Soc., 77, 437-471, **1996.**

Kiehl, J., and Trenberth, K.: Earth's annual global mean energy budget, B. Am. Meteorol. Soc., 78, 197-206, **1997.**

Knudsen, M.F., Riisager, P., Jacobsen, B.H., Muscheler, R., Snowball, I., and Seidenkrantz, M. S.: Taking the pulse of the Sun during the Holocene by joint analysis of ^{14}C and ^{10}Be, Geophys. Res. Lett., 36, doi:10.1029/2009GL039439, **2009.**

Kuhlbrodt, T., Griesel, A., Montoya, M., Levermann, A., Hofmann, M., and Rahmstorf, F.: On the driving processes of the Atlantic meridional overturning circulation, Rev. Geophys., 45, RG2001, doi:10.1029/2004RG000166, **2007.**

Lamy, F., Hebbeln, D., Rohl, U., and Wefer, G.: Holocene rainfall variability in southern Chile: a marine record of latitudinal shifts of the Southern Westerlies, Earth Planetary Sci. Lett., 185, 369-382, **2001.**

Lamy, F., Kaiser, J., Ninnemann, U., Hebbeln, D., Arz, H.W., and Stoner, J.: Antarctic Timing of Surface Water Changes off Chile and Patagonian Ice Sheet Response, Science, 304, 1959 – 1962, **2004.**

Lamy, F., Kilian, R., Arz, H.W., Francois, J.P., Kaiser, J., Prange, M., and Steinke, T.: Holocene changes in the position and intensity of the southern westerly wind belt, Nat. Geo., 3, 695-699, **2010.**

Lu, J., Chen, G., and Frierson, D.M.W. : The position of the midlatitude storm track and eddy-driven westerlies in aquaplanet AGCMs, J. Atmos. Sci., 67, 3984-4000, **2010.**

Markgraf, V., Dodson, J.R., Kershaw, P.A., McGlone, M.S., and Nicholls, N.: Evolution of late Pleistocene and Holocene climates in the circum-South Pacific land areas, Clim. Dyn., 6, 193-211, **1992.**

Meehl, G.A., Arblaster, J.M., Matthes, K., Sassi, F., and van Loon, H.: Amplifying the Pacific Climate System Response to a Small 11-Year Solar Cycle Forcing, Science, 325, 1114–1118, **2009.**

Menviel, L., Timmermann, A., Mouchet, A., and Timm, O.: Meridional reorganizations of marine and terrestrial productivity during Heinrich events, Paleoceanography, 23, PA1203, doi:10.1029/2007PA001445, **2008.**

Merkel U., Prange M., and Schulz M.: ENSO variability and teleconnections during glacial climates, Quat. Sci. Rev., 29, 86-100, **2010.**

Mudelsee, M.: Estimating Pearson's correlation coefficient with bootstrap confidence interval from serially dependent time series, Math. Geol., 35, 651-665, **2003.**

Otto-Bliesner, B.L., Tomas, R., Brady, E.C., Ammann, C., Kothavala, Z., and Clauzet, G.: Climate sensitivity of moderate- and low-resolution versions of CCSM3 to preindustrial forcing, J. Clim., 19, 2567-2583, **2006.**

Rind, D., Lean, J., Lerner, J., Lonergan, P., and Leboissitie, A.: Exploring the stratospheric/tropospheric response to solar forcing, J. Geophys. Res-Atmos., 113, D24103, doi:10.1029/2008JD010114, **2008.**

Rojas, M., Moreno, P., Kageyama, M., Crucifix, M., Hewitt, C., Abe-Ouchi, A., Ohgaito, R., Brady, E. C., and Hope, P.: The Southern Westerlies during the last glacial maximum in PMIP2 simulations, Clim. Dyn., 32, 525-548, DOI:10.1007/s00382-008-0421-7, **2009.**

Shulmeister, J., Goodwin, I., Renwick, J., Harle, K., Armand, L., McGlone, M.S., Cook, E., Dodson, J., Hesse, P.P., Mayewski, P., and Curran, M.: The Southern Hemisphere westerlies

in the Australasian sector over the last glacial cycle: a synthesis, Quatern. Int., 118-119, 23-53, **2004.**

Sijp, W.P., and England, M.H.: Southern Hemisphere Westerly Wind Control over the Ocean's Thermohaline Circulation, J. Clim., 22, 1277-1286, **2009.**

Solanki, S.K., Usoskin, I.G., Kromer, B., Schüssler, M., and Beer, J.: Unusual activity of the Sun during recent decades compared to the previous 11,000 years, Nature, 431, 1084 – 1087, **2004.**

Spangehl, T., Cubasch, U., Raible, C.C., Schimanke, S., Körper, J., and Hofer, D.: Transient climate simulations from the Maunder Minimum to present day: Role of the Stratosphere, J. Geophys. Res-Atmos., 115, doi:10.1029/2009JD012358, **2010.**

Steinhilber, F., Beer, J., and Fröhlich, C.: Total solar irradiance during the Holocene, Geophys. Res. Lett., 36, L19704, doi:10.1029/2009GL040142, **2009.**

Thresher, R.E.: Solar correlates of Southern Hemisphere mid-latitude climate variability, Int. J. Climatol., 22, 901-915, **2002.**

Toggweiler, J.R., and Samuels, B.: Effect of Drake Passage on the global thermohaline circulation, Deep-Sea Res. Pt 1., 42, 477-500, **1995.**

Toggweiler, J.R., Russel, J. L., and Carson, S.R.: Midlatitude westerlies, atmospheric CO_2 and climate change during the ice ages, Paleoceanography, 21, PA2005, doi:10.1029/2005PA001154, **2006.**

Tschumi, T., Joos, F., and Parekh, P.: How important are Southern Hemisphere wind changes for low glacial carbon dioxide? A model study, Paleoceanography, 23, PA4208, doi:10.1029/2008PA001592, **2008.**

van Geel, B., Heusser, C.J., Renssen, H., and Schuurmans, J.E.: Climatic change in Chile at around 2700 BP and global evidence for solar forcing: a hypothesis, Holocene, 10, 659-664, **2000.**

Versteegh, G.J.M.: Solar forcing of climate. 2: Evidence from the Past, Space Sci. Rev., 120, 243–286, **2005.**

Vonmoos, M., Beer, J., and Muscheler, R.: Large variations in Holocene solar activity: Constraints from ^{10}Be in the Greenland Ice Core Project ice core, J. Geophys. Res-Space, 111, A10105, doi:10.1029/2005JA011500, **2006.**

Yeager, S.G., Shields, C.A., Larger, W.G., and Hack, J.J.: The low-resolution CCSM3, J. Clim., 19, 2545-2566, **2006.**

Chapter 3

3. Holocene Evolution of the Southern Hemisphere Westerly Winds in Transient Simulations with Global Climate Models

V. Varma, M. Prange, U. Merkel, T. Kleinen, G. Lohmann, M. Pfeiffer, H. Renssen, A. Wagner, S. Wagner, M. Schulz

(Under review for publication in *Climate of the Past*; doi:10.5194/cpd-7-1797-2011)

3.1 Abstract

The Southern Hemisphere Westerly Winds (SWW) have been suggested to exert a critical influence on global climate through wind-driven upwelling of deep water in the Southern Ocean and the potentially resulting atmospheric CO_2 variations. The investigation of the temporal and spatial evolution of the SWW along with forcings and feedbacks remains a significant challenge in climate research. In this study, the evolution of the SWW under orbital forcing from the mid-Holocene (7 kyr BP) to pre-industrial modern times (250 yr BP) is examined with transient experiments using the comprehensive coupled global climate model CCSM3. In addition, a model inter-comparison is carried out using orbitally forced Holocene transient simulations from four other coupled global climate models. Analyses and comparison of the model results suggest that the annual and seasonal mean SWW were subject to an overall strengthening and poleward shifting trend during the course of the mid-to-late Holocene under the influence of orbital forcing, except for the austral spring season, where the SWW exhibited an opposite trend of shifting towards the equator.

3.2 Introduction

Mid-latitude westerly winds belong to the prominent features of the global tropospheric circulation. The present day positions of the Southern Hemisphere Westerly Winds (SWW) during austral summer (December-January-February) and winter (June-July-August) are illustrated in Fig. 1. The SWW dominate climate dynamics and influence the precipitation patterns between ~30°S and 70°S (e.g. Thresher, 2002; Shulmeister et al., 2004). Changes in

strength and position of the SWW may affect the large-scale Atlantic hydrography and circulation through the impact on the Indian-Atlantic Ocean water exchange by Agulhas leakage (Sijp and England, 2009; Biastoch et al., 2009). Furthermore, it has been suggested that the SWW exert a crucial influence on the global ocean circulation through wind-driven upwelling of deep water in the Southern Ocean (Toggweiler and Samuels, 1995; Kuhlbrodt et al., 2007; Sijp and England, 2009). The potentially resulting influence on atmospheric CO_2 variations on orbital timescales has been controversially discussed (Toggweiler et al., 2006; Menviel et al., 2008; Tschumi et al., 2008; Anderson et al., 2009; Moreno et al., 2010; d'Orgeville et al., 2010). Therefore, understanding the variability and the impact of various forcings on the SWW remains a significant area of investigation.

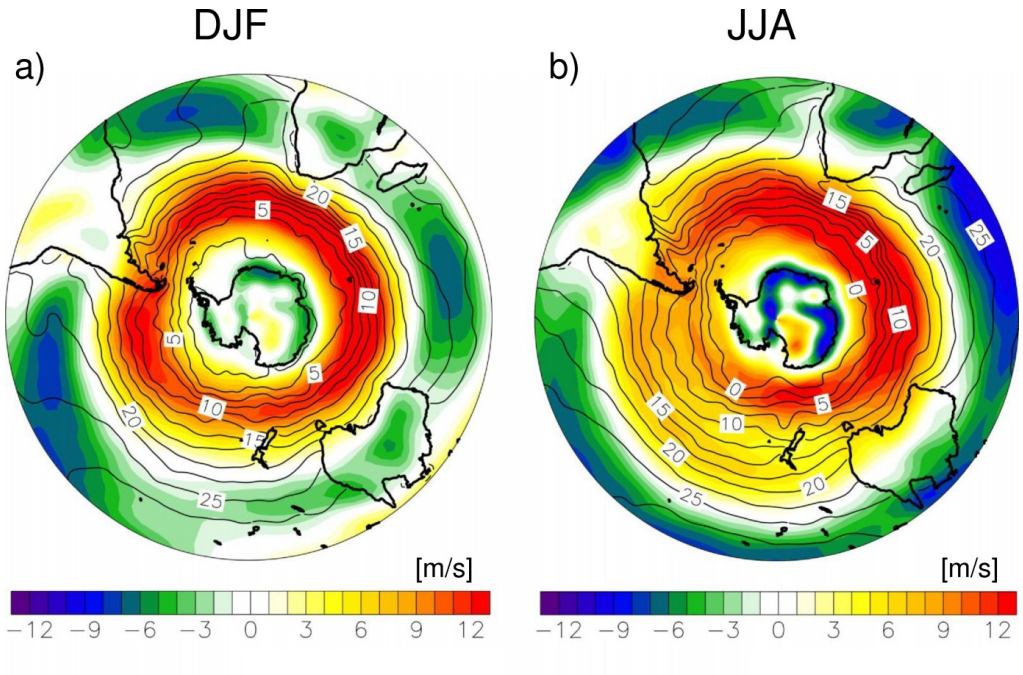

Fig. 1 Present-day Southern Hemisphere zonal wind climatology at 850 hPa for (a) austral summer (DJF) and (b) austral winter (JJA), based on NCEP/NCAR reanalysis data (1968–1996; Kalnay et al., 1996). Overlaid isotherms (contours) represent the climatological sea surface temperatures (°C) for the corresponding seasons based on the NODC World Ocean Atlas (Levitus et al., 1998). During DJF, the northern margin of the zonal wind shows a more southward confined pattern, while during JJA, it extends further to the north. In general, the surface westerly winds cover the region between ~30°S and 70°S, with the present-day strongest wind centred at around ~50°S.

The variability of the SWW on glacial-interglacial timescales has been discussed in some earlier works, in which contradicting results regarding the direction of meridional shift of the mean wind were presented. While some climate modelling studies suggested a poleward shift

in storm tracks and SWW during the Last Glacial Maximum (Valdes, 2000; Wyroll et al., 2000; Kitoh et al., 2001; Shin et al., 2003), other models simulated an equatorward (Kim et al., 2003) or no latitudinal displacement, but rather an intensification (Otto-Bliesner et al., 2006) of the mean westerlies. Likewise, proxy based reconstructions of the glacial SWW provided contradictory views with claims of a poleward displacement (e.g. Markgraf, 1987; Markgraf et al., 1992) standing in contrast to evidence of an equatorward shift (e.g. Heusser, 1989; Lamy et al., 1998, 1999; Shulmeister et al., 2004) compared to the pre-industrial conditions. Lamy et al. (2010) suggested that past variations in the SWW were not only characterized by latitudinal shifts but also by expansions and contractions of the wind belt. During the deglacial peak warmth in Antarctica (~12–9 kyr ago), they provided evidence for a minimal latitudinal extent of the belt, analogous to its present-day summer configuration.

An important forcing of global climate on longer time scales is accomplished by changes in the seasonal insolation caused by the varying Earth orbital parameters. This astronomical forcing is generally regarded as a dominant factor for glacial interglacial climate changes (Milankovitch, 1941; Hays et al., 1976; Berger, 1978; Imbrie et al., 1992). Although the climate of the Holocene is generally being considered as relatively stable compared to the last glacial (e.g. Grootes and Stuiver, 1997), it has also been suggested that there have been long-term trends in the spatial and temporal patterns of surface temperature during the Holocene (e.g. Battarbee and Binney, 2008). A considerable variation in the seasonal and latitudinal distribution of insolation, especially a decrease in austral winter-spring insolation accompanied by an increase in austral summer-fall insolation, can be observed between 7 kyr BP and present-day (Fig. 2). These changes in seasonal insolation might have caused long-term variations in the structure, position and intensity of the SWW on multi-millennial timescales (e.g. Markgraf et al., 1992; Lamy et al., 2001; Jenny et al., 2003; Lamy et al., 2010). The aim of this study is to analyze the response of the SWW to the changes in insolation during the mid-to-late Holocene using transient experiments with the comprehensive global climate model CCSM3. In addition, we compare this simulated Holocene evolution of the SWW under orbital forcing with transient experiments from a range of other global climate models. The analyses will lead us to the suggestion that the annual and seasonal mean SWW experienced a poleward shifting trend in general – except for the austral spring season – during the course of the Holocene under orbital forcing, consistently in all climate models used for this inter-comparison.

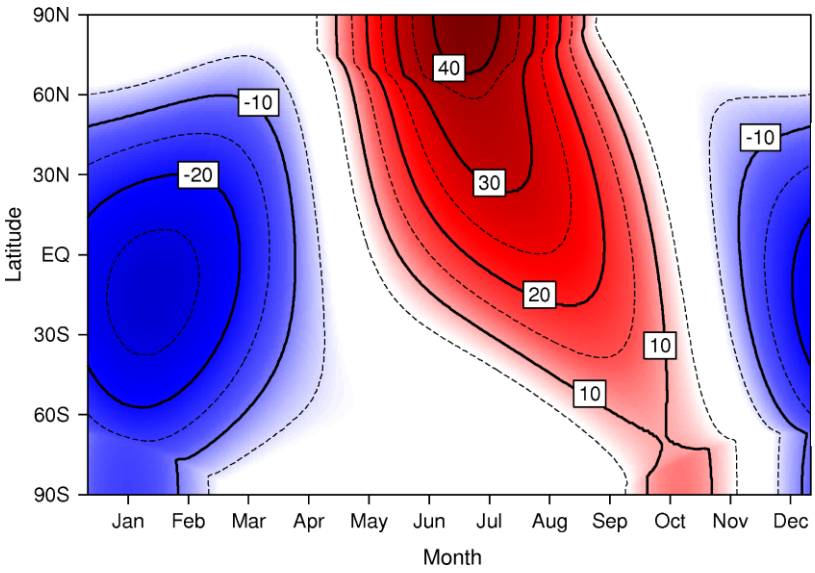

Fig. 2 Latitudinal distribution of insolation in Wm^{-2} at the top-of-the-atmosphere for 7 kyr BP minus present-day, calculated after Berger (1978), through the year.

3.3 Methods

To study the Holocene evolution of SWW under the influence of orbital forcing, transient experiments have been carried out using the comprehensive global climate model CCSM3 (Community Climate System Model version 3). NCAR's (National Center for Atmospheric Research) CCSM3 is a state-of-the-art fully coupled model, composed of four separate components representing atmosphere, ocean, land and sea-ice (Collins et al., 2006). Here, we employ the low-resolution version described in detail by Yeager et al. (2006). In this version the resolution of the atmospheric component is given by T31 (3.75° transform grid), with 26 layers in the vertical, while the ocean has a nominal resolution of 3° (like the sea-ice component) with refined meridional resolution (0.9°) around the equator and a vertical resolution of 25 levels.

3.3.1 Experimental setup for CCSM3

From a pre-industrial equilibrium simulation (Merkel et al., 2010), the model was integrated for 400 yr with conditions representing 9 kyr BP orbital forcing to reach a new quasi-equilibrium. After this spin-up, transient experiments were carried out by applying an acceleration (by a factor of 10) to the orbital forcing year until present day. The underlying assumptions for the application of this acceleration technique are that orbital forcing operates on much longer timescales (> millennia) than those inherent in the atmosphere and surface mixed layer of the ocean (months to years), and that climate changes related to long-term

variability of the thermohaline circulation during the time period considered are negligible in comparison with orbitally-driven surface temperature variations (Lorenz and Lohmann, 2004; Lorenz et al., 2006). Climate trends of the last 9000 yr, imposed by the external orbitally driven insolation changes, are represented in the experiments with only 900 simulation years with the application of acceleration by a factor 10. Thus, it was possible to conduct three Holocene transient experiments with different initial conditions within the available computer resources. While the first transient run was initialized with the quasi-equilibrated 9 kyr BP state, the second and third transient runs used the 8.9 and 8.8 kyr BP climates from the first transient run as initial conditions at 9 kyr BP. Throughout the Holocene experiments, greenhouse gas concentrations as well as aerosol and ozone distributions were kept at pre-industrial values as prescribed by the protocol of the Paleoclimate Modelling Intercomparison Project (PMIP), Phase II (Braconnot et al., 2007). Besides, variations in the Sun's output of energy and changes in continental ice-sheets were ignored such that variations in the orbital parameters were the sole external forcing in the model simulations.

3.3.2 Model inter-comparison

In addition to our CCSM3 experiments, results from five other Holocene transient climate model simulations are analyzed here in order to study the evolution of the SWW under insolation changes. These models are ECHO-G (Lorenz and Lohmann, 2004; Wagner et al., 2007), COSMOS (Pfeiffer and Lohmann, 2011), ECBilt-CLIO-VECODE (Renssen et al., 2009) and CLIMBER2-LPJ (Kleinen et al., 2010). As in the CCSM3 transient runs, all these models have been forced by orbital variations only, keeping greenhouse gas concentrations constant at their pre-industrial levels. A short and very general overview of these simulations is given below and detailed descriptions are available from the given references.

3.3.2.1 ECHO-G (I)

Holocene climate has been simulated using the coupled atmosphere-ocean general circulation model ECHO–G (Legutke and Voss, 1999). The atmospheric part of this model is the fourth generation of the European Centre atmospheric model of Hamburg (ECHAM4, Roeckner et al., 1996). The prognostic variables are calculated in the spectral domain with a triangular truncation at wave number 30 (T30), which corresponds to a Gaussian longitude–latitude grid of approximately 3.8°. The vertical domain is represented by 19 levels. The ocean model

includes a dynamic-thermodynamic sea-ice model and is defined on a grid with approximately 2.8° resolution (increased meridional resolution of 0.5° in the tropics to allow a more realistic representation of the ENSO phenomenon) and 20 irregularly spaced levels in the vertical. Acceleration by a factor 10 has been applied to the orbital forcing in these experiments to produce a two-member ensemble of transient Holocene runs covering the last 7000 yr (Lorenz and Lohmann, 2004).

3.3.2.2 ECHO-G (II)

Model and forcing are identical to ECHO-G (I), except for the fact that there is no acceleration applied on the orbital forcing for the Holocene transient run. Comparing the results of the non-accelerated ECHO-G (II) experiment with those from the accelerated ECHO-G (I) allows an assessment of the effect of orbital acceleration on the Holocene simulation of the SWW.

3.3.2.3 COSMOS

The core of COSMOS consists of the atmosphere model ECHAM5 (Roeckner et al., 2003) and the ocean model MPI-OM (Marsland et al., 2003). For long-term integrations, a low-resolution version of this model is applied with spectral T31 (3.75° transform grid) resolution in the atmosphere and approximately 3°5 horizontal resolution in the ocean. In the vertical, atmosphere and ocean model grids are defined on 19 and 40 levels, respectively. The ocean model includes a dynamic-thermodynamic sea-ice model with viscous-plastic rheology. A dynamic vegetation module is coupled to the land surface model JSBACH allowing an interactive adaptation of the terrestrial biosphere to varying climate conditions (Brovkin et al., 2009). Orbital acceleration with a factor 10 has been applied to simulate the past 8000 yr. Besides the simulations with coupled general circulation models described above, two Holocene runs with Earth system Models of Intermediate Complexity (EMICs) are also included in this study, they being, ECBilt-CLIO-VECODE and CLIMBER2-LPJ.

3.3.2.4 ECBilt-CLIO-VECODE

The first EMIC transient run was carried out with version 3 of ECBilt-CLIO-VECODE. The atmospheric component is ECBilt, a quasi-geostrophic model with 3 layers in the vertical and T21 (~5.6°) horizontal resolution (Opsteegh et al., 1998). CLIO is the oceanic component and

consists of a free-surface, primitive-equation ocean general circulation model coupled to a dynamic-thermodynamic sea-ice model (Goosse and Fichefet, 1999). CLIO is defined on 20 levels in the vertical and has a 3° horizontal resolution. VECODE interactively simulates the dynamics of trees and grasses (Brovkin et al., 2002). Orbital forcing without acceleration was applied to simulate the past 9000 yr.

3.3.2.5 CLIMBER2-LPJ

The second EMIC used in this inter-comparison is CLIMBER2-LPJ (Petoukhov et al., 2000). The model consists of a 2.5-dimensional statistical-dynamical atmosphere with a resolution of approximately 51° (longitude) by 10° (latitude), a zonally averaged ocean resolving three basins with a latitudinal resolution of 2.5°, and a sea-ice model. CLIMBER2-LPJ also contains dynamic vegetation, oceanic biogeochemistry, a model for marine biota, and a sediment model (Archer, 1996; Brovkin et al., 2002, 2007). The transient simulations were carried out with non-accelerated orbital forcing for the past 8000 yr, keeping greenhouse gas forcing fixed as in the other model experiments to pre-industrial levels.

The model descriptions are summarized in Table 1. The spatial distribution of the annual mean SWW for the period 7 kyr BP to 250 yr BP represented in various models is given in Fig. 1 of the Supplement*.

3.4 Results

In this section, we present the simulated insolation-forced SWW Holocene trends for all climate models used for the inter-comparison. As the strength and position of the SWW are strongly related to meridional surface temperature gradients (Brayshaw et al., 2008; Lu et al., 2010; Chen et al., 2010) we will also analyse the modelled trends in surface temperature. In order to have a time period of comparison which is common for all model simulations, all analyses are done for the period 7 kyr BP to 250 yr BP. For CCSM3 and ECHO-G (I) we have used the three-member and two-member ensemble means, respectively.

*See Appendix 1

Model Name	Orbital Acceleration	Resolution
CCSM3	by a factor of 10 ; 3 member ensemble	T31 - Atmosphere & Land : 3.75° ; 26 layers Ocean & Ice : 3.6°x1.6°; 25 layers
ECHO-G (I)	by a factor of 10 ; 2 member ensemble	T30 - Atmosphere & Land : 3.8° ; 19 layers Ocean & Ice : 2.8° ; 20 layers
ECHO-G (II)	non-accelerated ; 1 simulation	T30 - Atmosphere & Land : 3.8° ; 19 layers Ocean & Ice : 2.8° ; 20 layers
COSMOS	by a factor of 10 ; 1 simulation	T31 - Atmosphere & Land : 3.75° ; 19 layers Ocean & Ice : 3° ; 40 layers
ECBilt-CLIO-VECODE	non-accelerated ; 1 simulation	T21 - Atmosphere : 5.6° ; 3 layers Ocean : 3° ; 20 layers
CLIMBER2-LPJ	non-accelerated ; 1 simulation	Atmosphere : 51°x10° Ocean : Zonally averaged, with 2.5° latitudinal resolution ; 11 layers

Table 1 Brief summary of the climate models used for inter-comparison.

3.4.1 Annual and seasonal mean trends in SWW

The spatial distribution of Holocene trends in the annual-mean low-level zonal wind in the Southern Hemisphere for the period 7 kyr BP to 250 yr BP for all models is represented in Fig. 3. The zonal wind trends are plotted at 850 hPa for CCSM3, ECHO-G (I and II) and COSMOS, and at the lowermost model level for ECBilt-CLIO-VECODE (800 hPa) and CLIMBER2-LPJ. All models exhibit a general trend of strengthening in the southern and central SWW region and a weakening trend in the northern part of the SWW belt, which can be interpreted as a poleward displacement of the annual mean westerly circulation during the course of the mid-to-late Holocene (Fig. 3). This spatio-temporal wind pattern resembles a long-term trend of the Southern Annular Mode (or Antarctic Oscillation) towards its positive phase (e.g. Sen Gupta and England, 2006). Strengthening of the SWW in the latitudinal belt between about 40°S and 60°S (i.e. the SWW core region) is most intense and continuous in ECHO-G (I and II), followed by CCSM3.

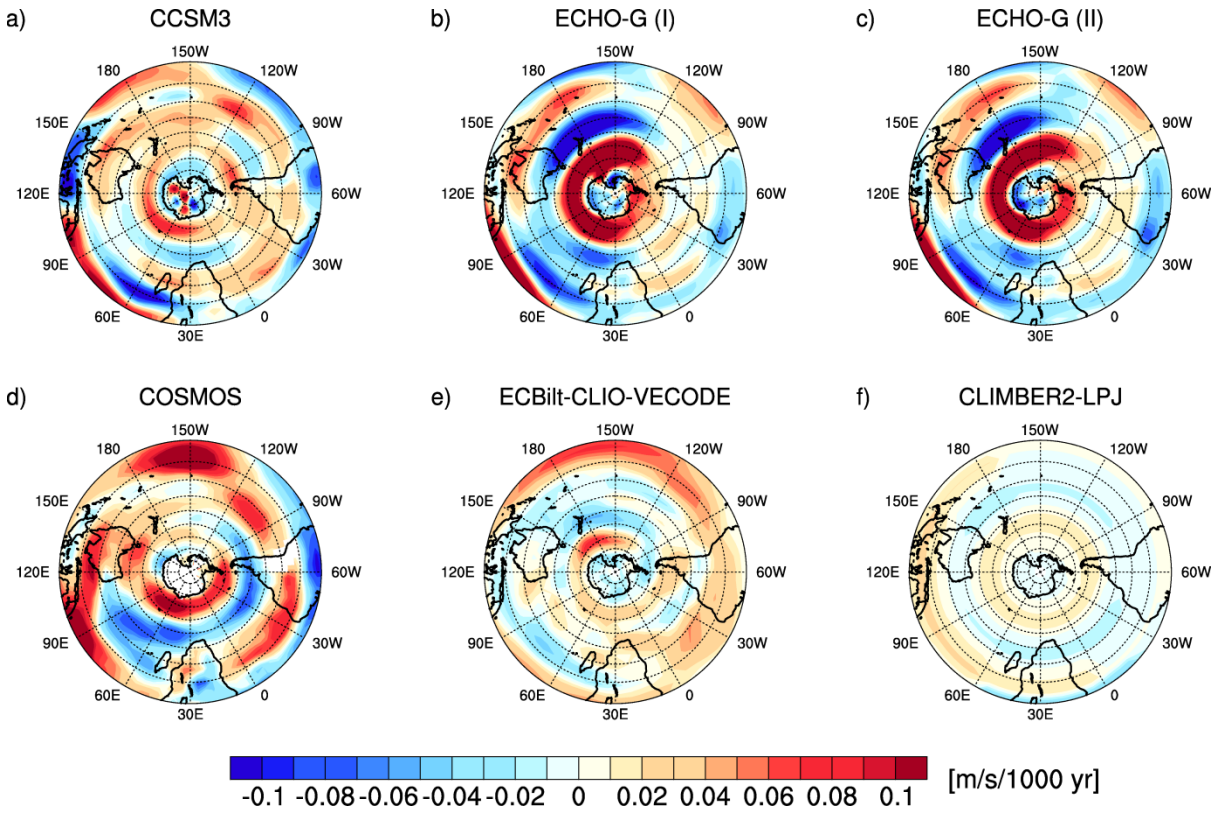

Fig. 3 Trend in the annual mean low-level zonal wind in (a) CCSM3, (b) ECHO-G (I), (c) ECHO-G (II), (d) COSMOS, (e) ECBilt-CLIO-VECODE, and (f) CLIMBER2-LPJ for the period 7 kyr BP to 250 yr BP. All polar stereographic plots represent the Southern Hemisphere, with latitudes placed at 10° interval, starting from equator to 90° S.

While COSMOS shows a pronounced strengthening of the SWW in the region between ~50°S and 70°S, ECBilt-CLIO-VECODE simulates a less annular pattern, but, with respect to the zonal mean, a strengthening in the core SWW latitude belt is seen. CLIMBER2-LPJ produces the weakest trends, probably due to its simplified dynamics that does not explicitly simulate eddy momentum transports.

The simulated timeseries of the annual-mean SWW temporal evolution in all models used for inter-comparison are represented by an index and is displayed in Fig. 4. The index is defined as the difference of the zonally averaged zonal low-level winds between the latitudes 55°S and 35°S and is a measure for latitudinal displacements of the SWW belt (Varma et al., 2011). An evident trend observed in all the models is the strengthening of the low-level winds towards 55°S during the course of Holocene (Fig. 4). The strongest changes occur during the mid-Holocene (4000 to 6000 yr BP) in almost all the models. Again, ECHO-G (I) and

ECHO-G (II) are very similar, CLIMBER2-LPJ follows the deterministic insolation, CCSM3 and COSMOS show pronounced internal variability for the last 3000 yr.

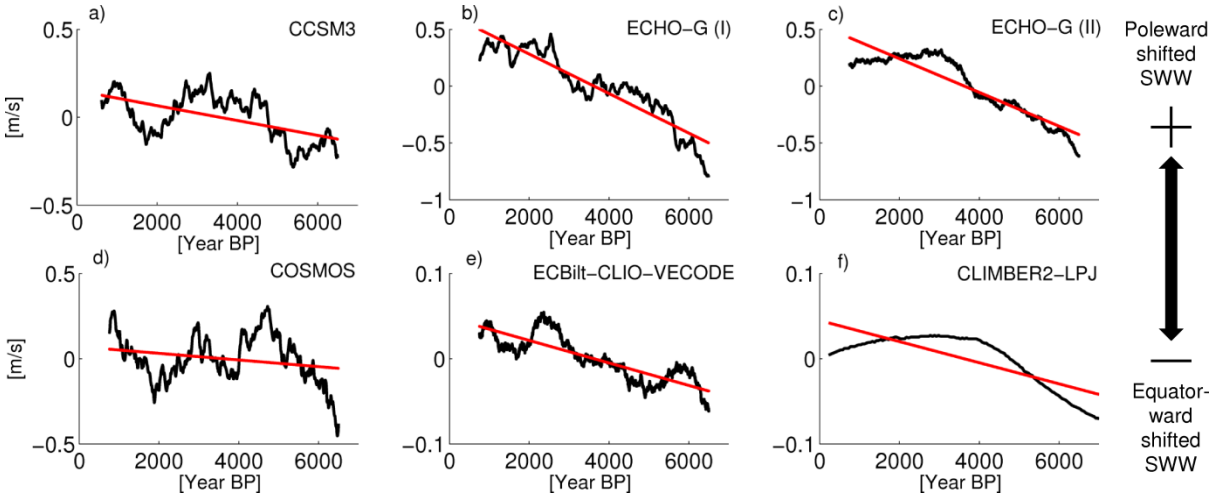

Fig. 4 Temporal evolution of annual mean SWW position during the period 7 kyr BP to 250 yr BP in (a) CCSM3, (b) ECHO-G (I), (c) ECHO-G (II), (d) COSMOS, (e) ECBilt-CLIOVECODE, and (f) CLIMBER2-LPJ, defined in terms of the difference between the latitudes 55°S and 35°S (southern and northern parts of the SWW belt respectively) of the zonally averaged low-level zonal winds (black curves). Time axis is plotted against the anomaly of the mean wind position. A 1000 yr boxcar smoothing with respect to orbital year has been applied to all the time series except for CLIMBER2-LPJ. Linear regression lines for the time series are shown in red. Note the different ordinate scales.

The zonally averaged simulated Holocene trends in low-level zonal winds separately for each season are represented in Fig. 5 (see Supplement for the maps of seasonal trends in Southern Hemisphere zonal winds*). For the March-April-May (MAM) season, all models show the most pronounced southward shift and strengthening of SWW in the latitudinal belt between about 40°S and 60°S. During the June-July-August (JJA) season, CCSM3, ECHO-G (I and II) and CLIMBER2-LPJ sustain the pattern of SWW strengthening in that latitudinal belt, whereas ECBilt-CLIO-VECODE exhibits a weakening in this region. The most striking feature in Figure 5 is the SWW behaviour during the September-October-November (SON) season. This season shows the trend of a SWW weakening (between the latitudes ~40°S and 60°S) and northward shift in all the models, i.e. opposite to the annual-mean trend.

*See Appendix 1

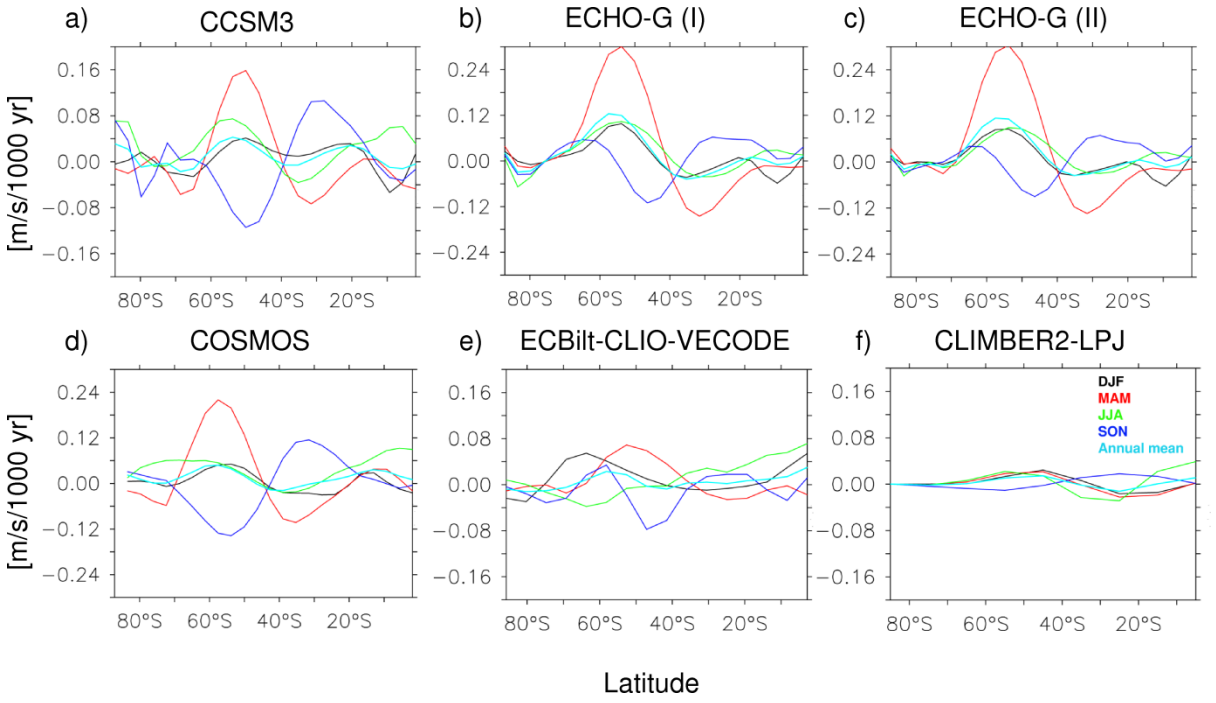

Fig. 5 Zonally averaged seasonal and annual mean trends in the low-level zonal wind in (a) CCSM3, (b) ECHO-G (I), (c) ECHO-G (II), (d) COSMOS, (e) ECBilt-CLIO-VECODE, and (f) CLIMBER2-LPJ for the Southern Hemisphere. Note the different ordinate scales.

3.4.2 Annual and seasonal mean trends in surface temperature

The spatial distributions of Holocene trends in Southern Hemisphere annual-mean surface temperature for the period 7 kyr BP to 250 yr BP is shown in Fig. 6. The most noticeable trend pattern in all models relates to an intense cooling in the southern high latitudes especially around Antarctica. In low latitudes, the temperature trend patterns are more heterogeneous among the different models. For instance, CCSM3 exhibits a large-scale (albeit weak) tropical warming trend, while ECHO-G (II) shows more of a tropical cooling (Fig. 6c). The seasonal response pattern of Holocene surface temperature trends in the Southern Hemisphere caused by variations in orbital forcing is more entangled. The zonally averaged trends in the surface temperature on a seasonal basis as simulated by the different models is displayed in Fig. 7 (see Supplement for the Southern Hemisphere maps of seasonal trends in surface temperature*). Austral summers (DJF) experience a lower-than-present insolation during the early Holocene (Fig. 2) resulting in a general warming trend in the Southern Hemisphere during the course of the Holocene, which is most pronounced over the continents (Fig. 8 of Supplement*).

*See Appendix 1

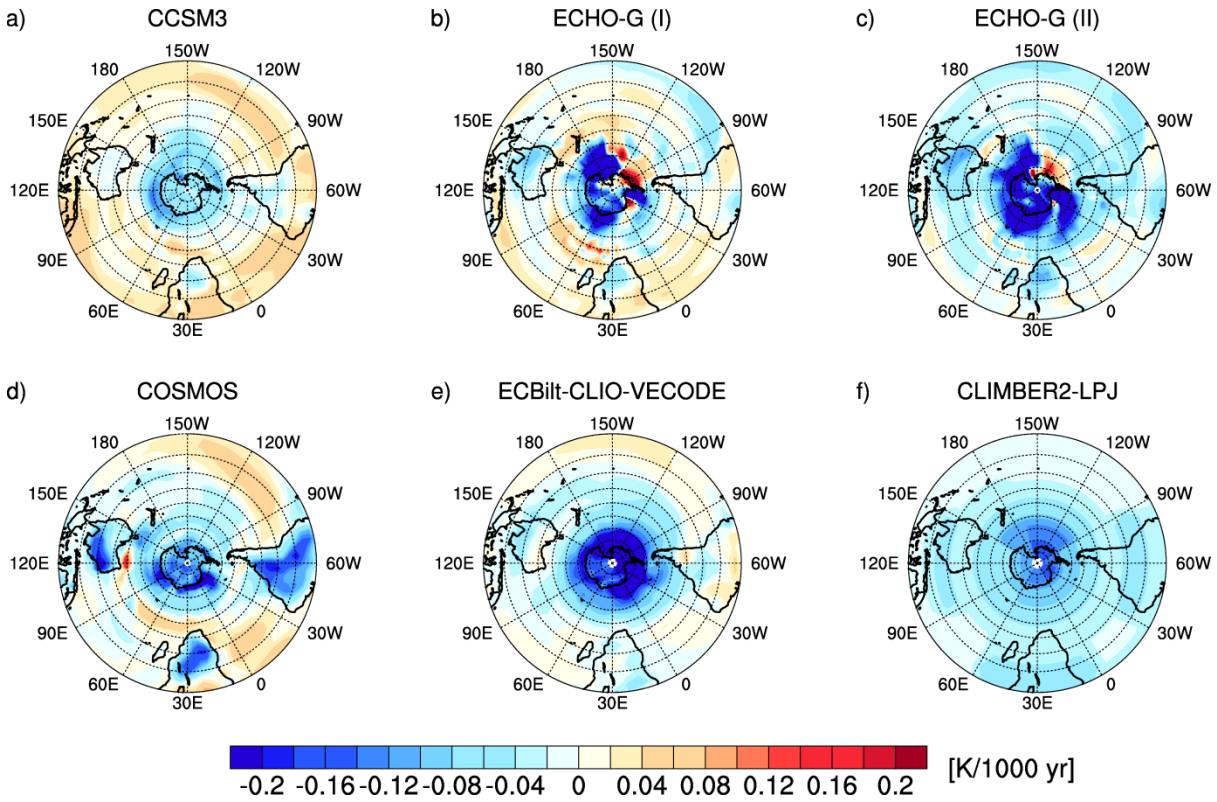

Fig. 6 Trend in the annual mean surface temperature in (a) CCSM3, (b) ECHO-G (I), (c) ECHO-G (II), (d) COSMOS, (e) ECBilt-CLIO-VECODE, and (f) CLIMBER2-LPJ for the period 7 kyr BP to 250 yr BP.

By contrast, the austral winter season (JJA) shows strong cooling trends over the Southern Hemisphere continents as a direct response to decreasing insolation (Fig. 6 of Supplement). The MAM and SON seasons exhibit the most uniform trends on a hemispherical scale over both Southern Hemisphere land and ocean in all the models (Figs. 5 and 7 of Supplement). Among all the seasons, the austral spring (SON) shows the strongest seasonal cooling trend, whereas the austral fall (MAM) exhibits the strongest seasonal warming trend (Fig. 7) as a result of insolation changes in combination with a delayed response of the climate system by 1–3 months owing to the thermal inertia of the surface ocean (cf. Renssen et al., 2005). However, even during the MAM season, the Southern Ocean regions around Antarctica show a cooling trend, opposite to what would be expected from the local insolation trend (Fig. 2). This regional cooling trend has been attributed to a long memory of the Southern Ocean through the storage of late winter-spring surface temperature anomalies in the deep upper-ocean winter layer in combination with sea ice-albedo and ice-insulation feedbacks (Renssen

et al., 2005). While the study of Renssen et al. (2005) is based on a single coupled model, our multi-model inter-comparison supports their results and reveals that this is a robust feature captured by all models. As a result, all models show a year-round Holocene cooling trend in the Southern Ocean (Figs. 6, 7).

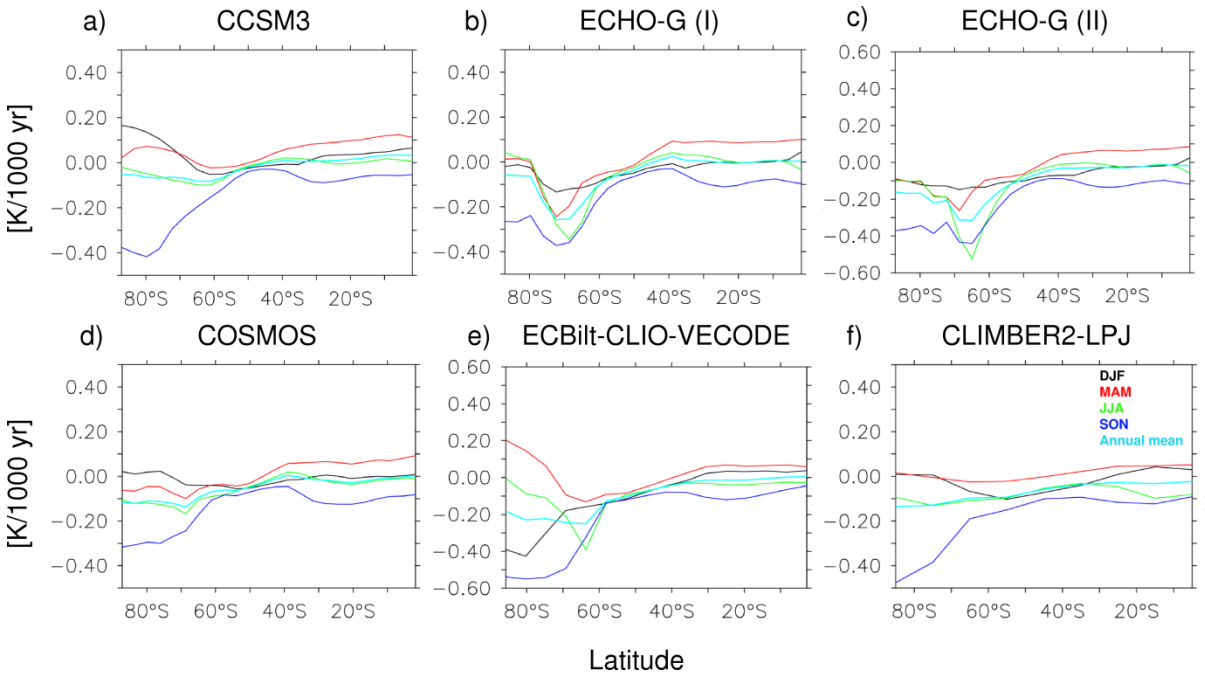

Fig. 7 Zonally averaged seasonal and annual mean trends in the surface temperature in (a) CCSM3, (b) ECHO-G (I), (c) ECHO-G (II), (d) COSMOS, (e) ECBilt-CLIO-VECODE, and (f) CLIMBER2-LPJ for the Southern Hemisphere. Note the different ordinate scales.

3.5 Discussion

Surface westerlies result from the westerly momentum flux convergence by transient eddies acting against losses by surface friction. The eddies, in turn, are driven by the potential energy available in the meridional temperature gradient (e.g. Vallis, 2006). Consequently, strength and position of the SWW depends to a large extent on surface temperature patterns (Brayshaw et al., 2008; Lu et al., 2010; Chen et al., 2010). The most significant pattern that could be noted in both annual and seasonal means is the strong cooling trend in the southern high latitudes, especially around Antarctica (Figs. 6, 7). Ice cores indeed provide evidence for a widespread Antarctic Holocene cooling trend (Masson et al., 2000) underpinned by

palaeoclimate reconstructions from the Ross Sea (Steig et al., 1998) and the Palmer Deep (Domack et al., 2001).

The southern high-latitude cooling trend results in a steepening of the pole-to-equator surface temperature gradient. Recent theoretical and modelling studies have shown that an enhanced meridional temperature gradient does not only lead to an overall strengthening of the SWW, but that the surface temperature pattern also influences the position of the wind belt (Brayshaw et al., 2008; Lu et al., 2010; Chen et al., 2010). Accordingly, a stronger meridional surface temperature gradient at high latitudes is accompanied by a poleward shift of the surface westerlies due to enhanced high-latitude baroclinic wave generation. This may explain the overall poleward shifting trend of the SWW that prevails in the annual mean in all the models. During the MAM season, when this trend is strongest, two additional effects contribute to the southward movement of the westerlies: increasing insolation during the austral late summer with highest values in low latitudes (i.e. increasing meridional insolation gradient; Fig. 2) in combination with the 1–3 months time lag, owing to the thermal inertia of the surface climate system (Renssen et al., 2005), leads to a further increase in the meridional temperature gradient as well as to a hemispheric-scale warming trend during the austral fall (Fig. 7). By means of general atmospheric circulation modelling and scaling arguments, it has recently been shown that an increase in the global (or hemispheric-scale) surface temperature increases the latitudinal extent of the Hadley cell (Frierson et al., 2007) and shifts the eddy-driven surface westerlies towards the pole (Lu et al., 2010), thus contributing to the maximum insolation-response of the SWW during the MAM season (Fig. 5). During the SON season, the trend in insolation-forcing is of opposite sign (Fig. 2), leading to a hemispheric-scale cooling trend and hence an equatorward movement of the SWW (Fig. 5). The model results consistently suggest that the annual and seasonal mean SWW exhibit an overall strengthening and poleward shifting trend during the course of the mid-to-late Holocene under the influence of orbital forcing, except for the austral spring season, where the SWW exhibit an opposite trend of shifting towards the equator. Our findings for Holocene SWW shifts are largely consistent with a recent study by Rojas and Moreno (2010) who analyzed a multi-model-mean of PMIP2 simulations for 6 kyr BP. They found an enhanced annual-mean westerly flow between ~35°S and 45°S and a weakening south of ~45°S for the mid-Holocene time slice relative to the present.

Validating the model results with reconstructions of the paleo-SWW proves still to be elusive, as there is a substantial incongruity between different proxy records. For the SWW core region around 51°–53°S, for instance, terrestrial ecosystem proxy records from western Patagonia (Moreno et al., 2010) suggest a trend of increasing SWW strength during the past 7000 yr that is not supported by sedimentological and pollen based reconstructions of South Patagonian precipitation by Lamy et al. (2010). As a cautionary note, we emphasize again that the model simulations suggest opposite Holocene trends in SWW variations for different seasons (Fig. 5) which may affect the proxy records and their interpretation.

3.6 Conclusions

The investigation of the temporal and spatial evolution of the SWW along with forcings and feedbacks remains a significant challenge in climate research. In this study, we examined the Holocene evolution of SWW under the influence of orbital forcing with transient experiments using the state-of-the-art comprehensive coupled global climate model CCSM3. In addition, a model inter-comparison has been conducted using Holocene transient simulations from four other coupled global climate models, namely, ECHO-G, COSMOS, ECBilt-CLIO-VECODE and CLIMBER2-LPJ. Analyses and comparison of the model results suggest that the annual and seasonal mean SWW were subject to an overall strengthening and poleward shifting trend during the course of the mid-to-late Holocene under the influence of orbital forcing, except for the austral spring season, where the SWW exhibited an opposite trend of shifting towards the equator. The comparison between an accelerated and a non-accelerated ECHO-G experiment revealed that the simulation of these trends is unaffected by the orbital acceleration technique employed in some of the transient runs. In view of a substantial incongruity between different SWW simulations for the Last Glacial Maximum (Rojas et al., 2009), the agreement among the different models with respect to Holocene SWW trends is encouraging. However, the magnitude of SWW shift is much smaller in EMICs compared to the comprehensive general circulation models. Therefore, the potential feedbacks in their climate/carbon cycle simulations may be underestimated.

Whether the simulated shifts in the SWW had the potential to affect atmospheric CO_2 concentrations through degassing of the deep ocean via changes in wind-driven upwelling in the Southern Ocean (Moreno et al., 2010) remains elusive at the time being. Moreover, the

effect of increasing greenhouse gases from the mid to the late Holocene (e.g. Raynaud et al., 2000) is not included in the orbital-forced model simulations presented here, although there is strong evidence for a CO_2-induced strengthening and poleward shift of the SWW over the past four decades (e.g. Arblaster and Meehl, 2006; Toggweiler and Russell, 2008). In future studies, the combined effects of orbital and greenhouse gas forcing should be explored using comprehensive climate models in order to put the Southern Hemisphere circulation changes of the last decades into a long-term context.

3.7 Acknowledgements

This work was funded through the DFG (Deutsche Forschungsgemeinschaft) Priority Programme "INTERDYNAMIK" and through the DFG Research Center/Excellence Cluster "The Ocean in the Earth System". CCSM3 simulations were performed on the SGI Altix supercomputer of the Norddeutscher Verbund für Hoch und Höchstleistungsrechnen (HLRN). We also acknowledge the use of the NCAR Command Language (NCL) and NOAA/PMEL's Ferret in our data analysis and visualization herein.

3.8 References

Anderson, R.F., Ali, S., Bradtmiller, L.I., Nielsen, S.H.H., Fleisher, M.Q., Anderson, B.E., and Burckle, L.H.: Wind-Driven Upwelling in the Southern Ocean and the Deglacial Rise in Atmospheric CO_2, Science, 323, 1443 – 1448, **2009.**

Arblaster, J, M., and Meehl, G. A.: Contributions of External Forcings to Southern Annular Mode Trends, J. Clim., 19, 2896–2905, doi: 10.1175/JCLI3774.1, **2006.**

Archer, D.: A data-driven model of the global calcite lysocline, Global Biogeochem. Cycles, 10, 511 – 526, **1996.**

Battarbee, R.W., and Binney, H.A.: Natural Climate Variability and Global Warming: A Holocene Perspective, Wiley-Blackwell, ISBN: 978-1-4051-5905-0, **2008.**

Berger, A.L.: Long-term variations of daily insolation and Quaternary climatic changes, J. Atmos. Sci., 35, 2362-2367, **1978.**

Biastoch, A., Böning, C. W., Schwarzkopf, F. U., and Lutjeharms, J. R. E.: Increase in Agulhas leakage due to poleward shift of Southern Hemisphere westerlies, Nature, 462, 495–498, **2009.**

Braconnot, P., Otto-Bliesner, B., Harrison, S., Joussaume, S., Peterchmitt, J.-Y., Abe-Ouchi, A., Crucifix, M., Driesschaert, E., Fichefet, Th., Hewitt, C.D., Kageyama, M., Kitoh, A., Laîné, A., Loutre, M.-F., Marti, O., Merkel, U., Ramstein, G., Valdes, P., Weber, S.L., Yu, Y., and Zhao, Y.: Results of PMIP2 coupled simulations of the Mid-Holocene and Last Glacial Maximum Part 1: experiments and large-scale features, Clim. Past., 3, 261–277, **2007.**

Brayshaw, D.J., Hoskins, B., Blackburn, M.: The Storm-Track Response to Idealized SST Perturbations in an Aquaplanet GCM, J. Atmos. Sci., 65, 2842-2860, doi:10.1175/2008JAS2657.1, **2008.**

Brovkin, V., Bendtsen, J., Claussen, M., Ganopolski, A., Kubatzki, C., Petoukhov, V., and Andreev, A.: Carbon cycle, vegetation, and climate dynamics in the Holocene: Experiments with the CLIMBER-2 model, Global Biogeochem. Cycles, 16, 1139, doi:10.1029/2001GB001662, **2002.**

Brovkin, V., Ganopolski, A., Archer, D., and Rahmstorf, S.: Lowering of glacial atmospheric CO_2 in response to changes in oceanic circulation and marine biogeochemistry, Paleoceanography, 22, PA4202, doi:10.1029/2006PA001380, **2007.**

Brovkin, V., Raddatz, T., Christian H. Reick, C.H., Claussen, M., Gayler, V.: Global biogeophysical interactions between forest and climate, Geophys. Res. Lett., 36, doi:10.1029/2009GL037543, **2009.**

Chen, G., Plumb, R.A., and Lu, J.: Sensitivities of zonal mean atmospheric circulation to SST warming in an aqua-planet model, Geophys. Res. Lett., 37, L12701, doi:10.1029/2010GL043473, **2010.**

Collins, W.D., Bitz, C.M., Blackmon, M.L., Bonan, G.B., Bretherton, C.S., Carton, J.A., Chang, P., Doney, S.C., Hack, J.J., Henderson, T.B., Kiehl, J.T., Large, W.G., McKenna, D.S., Santer, B.D., and Smith, R.D.: The Community Climate System Model Version 3 (CCSM3), J. Clim., 19, 2122-2143, **2006.**

Domack, E. W., Leventer, A., Dunbar, R., Taylor,F., Brachfeld, S., Sjunneskog, C., and ODP Leg 178 Scientific Party.: Chronology of the Palmer Deep site, Antarctic Peninsula: a Holocene palaeoenvironmental reference for the circum-Antarctic, The Holocene, 11, 1-9, **2001.**

Frierson, D.M.W., Lu, J., and Chen, G.: Width of the Hadley cell in simple and comprehensive general circulation models, Geophys. Res. Lett., 34, doi:10.1029/2007GL031115, **2007.**

Goosse, H., and Fichefet, T.: Importance of ice-ocean interactions for the global ocean circulation: a model study, J. Geophys. Res., 104, 23337-23355, **1999.**

Grootes, P. M., and Stuiver, M.: Oxygen 18/16 variability in Greenland snow and ice with 10^{-3}- to 10^{5}-year time resolution, J. Geophys. Res., 102, 455-470, **1997.**

Hays, J.D., Imbrie, J., and Shackleton, N.J.: Variations in the Earth's orbit: Pacemaker of the ice ages, Science, 194, 1121-1132, **1976.**

Heusser, C. J.: Polar perspective of Late Quaternary climates in the Southern Hemisphere, Quat., Res., 32, 60–71, **1989.**

Imbrie, J., Boyle, E. A., Clemens, S. C., Duffy, A., Howard, W. R., Kukla, G., kutzbach, J., Martinson, D. G., McIntyre, A., Mix, A. C., Molfino, B., Morley, J. J., Peterson, L. C., Pisias, N. G., Prell, W. L., Raymo, M. E., Shackleton, N. J., and Toggweiler, J. R.: On the Structure and Origin of Major Glaciation Cycles 1. Linear Responses to Milankovitch Forcing, Paleoceanography, 7, 701–738, doi:10.1029/92PA02253, **1992.**

Jenny, B., Wilhelm, D., and Valero-Garcés, B.L.: The Southern Westerlies in Central Chile: Holocene precipitation estimates based on a water balance model for Laguna Aculeo (33°50'S), Clim. Dyn., 20, 269-280, **2003.**

Kalnay, E., Kanamitsu, M., Kistler, R., Collins, W., Deaven, D., Gandin, L., Iredell, M., Saha, S., White, G., Woollen, J., Zhu, Y., Leetmaa, A., Reynolds, R., Chelliah, M., Ebisuzaki, W., Higgins, W., Janowiak, J., Mo, K.C., Ropelewski, C., Wang, J., Jenne, R., and Joseph, D.: The NCEP/NCAR 40-Year Reanalysis Project, B. Am. Meteorol. Soc., 77, 437-471, **1996.**

Kim, S.J., Flato, G.M., and Boer, G.J.: A coupled climate simulation of the last glacial maximum, Part 2: approach to equilibrium, Clim. Dyn., 20, 635-661, **2003.**

Kitoh, A., Murakami, S., and Kiode, H.: A simulation of the last glacial maximum with a coupled atmosphere-ocean GCM, Geophys. Res. Lett., 28, 2221-2224, **2001.**

Kleinen, T., Brovkin, V., von Bloh, W., Archer, D., and Munhoven, G.: Holocene carbon cycle dynamics, Geophys. Res. Lett., 37, doi:10.1029/2009GL041391, **2010.**

Kuhlbrodt, T., Griesel, A., Montoya, M., Levermann, A., Hofmann, M., and Rahmstorf, F.: On the driving processes of the Atlantic meridional overturning circulation, Rev. Geophys., 45, RG2001, doi:10.1029/2004RG000166, **2007.**

Lamy, F., Hebbeln, D., and Wefer, G.: Late quaternary precessional cycles of terrigenous sediment input off the Norte Chico, Chile (27.5°S) and palaeoclimatic implications. Palaeogeogr. Palaeoclimatol. Palaeoecol., 140, 233–244, **1998.**

Lamy, F., Hebbeln, D., and Wefer, G.: High-resolution marine record of climatic change in mid-latitude Chile during the last 28,000 years based on terrigenous sediment parameters, Quat. Res., 51, 83-93, **1999.**

Lamy, F., Hebbeln, D., Rohl, U., and Wefer, G.: Holocene rainfall variability in southern Chile: a marine record of latitudinal shifts of the Southern Westerlies, Earth Planetary Sci. Lett., 185, 369-382, **2001.**

Lamy, F., Kilian, R., Arz, H.W., Francois, J.P., Kaiser, J., Prange, M., and Steinke, T.: Holocene changes in the position and intensity of the southern westerly wind belt, Nat. Geosci., 3, 695-699, **2010.**

Legutke, S., and Voss, R.: The Hamburg atmosphere-ocean coupled circulation model ECHO-G, Technical Report 18, Deutsches Klimarechenzentrum, Hamburg, **1999.**

Levitus, S., Boyer, T., Conkright, M., Johnson, D., O'Brien, T., Antonov, J., Stephens, C., and Gelfeld, R.: Introduction. Vol. 1, World Ocean Database 1998, NOAA Atlas NESDIS 18, 346, **1998.**

Lorenz, S.J, and Lohmann, G.: Acceleration technique for Milankovitch type forcing in a coupled atmosphere-ocean circulation model: method and application for the Holocene, Clim. Dyn., 23, 727-743, doi: 10.1007/s00382-004-0469-y, **2004.**

Lorenz, S.J., Kim, J-H., Rimbu, N., Schneider, R.R., and Lohmann, G.: Orbitally driven insolation forcing on Holocene climate trends: Evidence from alkenone data and climate modeling, Paleoceanography, 21, doi:10.1029/2005PA001152, **2006.**

Lu, J., Chen, G., and Frierson, D. M. W.: The Position of Midlatitude Storm Track and Eddy-Driven Westerlies in Aquaplanet AGCMs, J. Atmos. Sci., 67, 3984-4000, doi: 10.1175/2010JAS3477.1, **2010.**

Markgraf, V.: Paleoenvironmental changes at the northern limit of the subantarctic Nothofagus forest, Lat 37°S. Quat. Res., 28, 119–129, **1987.**

Markgraf, V., Dodson, J.R., Kershaw, P.A., McGlone, M.S., and Nicholls, N.: Evolution of late Pleistocene and Holocene climates in the circum-South Pacific land areas, Clim. Dyn., 6, 193-211, **1992.**

Marsland, S.J., Haak, H., Jungclaus, J.H., Latif, M., and Röske, F.: The Max-Planck-Institute global ocean/sea ice model with orthogonal curvilinear coordinates, Ocean Modelling, 5, 91–127, **2003.**

Masson, V., Vimeux, F., Jouzel, J., Morgan, V., Delmotte, M., Ciais, P., Hammer, C., Johnsen, S., Lipenkov, V,Ya., Thompson, M.E., Petit, J, R., Steig, E. J., Stievenard, M., and **Vaikmae, R.:** Holocene Climate variability in Antarctica Based on 11 Ice-Core Isotopic Records, Quat., Res., 54, 348-358, **2000.**

Menviel, L., Timmermann, A., Mouchet, A., and Timm, O.: Climate and marine carbon cycle response to changes in the strength of the Southern Hemispheric westerlies, Paleoceanography, 23, PA4201, doi:10.1029/2008PA001604, **2008.**

Merkel, U., Prange, M., and Schulz, M.: ENSO variability and teleconnections during glacial climates, Quat. Sci. Rev., 29, 86-100, **2010.**

Milankovitch, M.: Kanon der Erdbestrahlungen und seine Anwendung auf das Eiszeitenproblem, Spec Publ, 132, 633, R. Serb. Acad., Belgrade, **1941.**

Moreno, P. I., Francois, J. P., Moy, C. M., and Villa-Martinez, R.: Covariability of the Southern Westerlies and atmospheric CO_2 during the Holocene, Geology, 38, 727-730, doi:10.1130/G30962.1, **2010.**

Opsteegh, J.D., Haarsma, R. J., and Selten, F. M., ECBILT: A dynamic alternative to mixed boundary conditions in ocean models, Tellus, 50A, 348-367, **1998.**

d'Orgeville, M., Sijp, W.P., England, M.H., and Meissner, K.J.: On the control of glacial-interglacial atmospheric CO_2 variations by the Southern Hemisphere Westerlies, Geophys. Res. Lett., 37, doi:10.1029/2010GL045261, **2010.**

Otto-Bliesner, B., Brady, E., Clauzet, G., Thomas, R., Levis, S., and Kothavala, Z.: Last glacial maximum and Holocene climate in CCSM3, J. Clim., 19, 2526-2544, **2006.**

Petoukhov, V., A. Ganopolski, V. Brovkin, M. Claussen, A. Eliseev, C. Kubatzki, and S. Rahmstorf.: CLIMBER-2: A climate system model of intermediate complexity. Part I: Model description and performance for present climate, Clim. Dyn., 16, 1– 17, **2000.**

Pfeiffer, M., and Lohmann, G.: Interglacial climate evolution: a comparison between the Marine Isotope Stages 1 and 5, Clim. Dyn., in preparation, **2011.**

Raynaud, D., Barnola, J, M., Chappellaz, J., Blunier, T., Indermühle, A., and Stauffer, B.: The ice record of green house gases: a view in the context of future changes, Quat. Sci. Rev., 19, 9-17, **2000.**

Renssen, H., Goosse, H., Fichefet, T., Masson, V., Koc, N.: Holocene climate evolution in the high-latitude Southern Hemisphere simulated by a coupled atmosphere-sea-ice-ocean-vegetation model, The Holocene, 17, 951-964, **2005.**

Renssen, H., Seppä, H., Heiri, O., Roche, D.M., Goosse, H., and Fichefet, T.: The spatial and temporal complexity of the Holocene thermal maximum, Nat. Geo., 2, 411-414, doi:10.1038/ngeo513, **2009.**

Roeckner, E., Arpe, K., Bengtsson, L., Christoph, M., Claussen, M., Dümenil, L., Esch, M., Giorgetta, M., Schlese, U., and Schulzweida, U.: The atmospheric general circulation model ECHAM-4: model description and simulation of the present day climate, Report 218. Max-Planck-Institut fur Meteorologie, **1996.**

Roeckner, E., Bäuml, G., Bonaventura, L., Brokopf, R., Esch, M., Giorgetta, M., Hagemann, S., Kirchner, I., Kornblueh, L., Manzini, E., Rhodin, A., Schlese, U., Schulzweida, U., and Tompkins, A.: The atmospheric general circulation model ECHAM5. Part I: Model

description. Max Planck Institute for Meteorology Rep. 349, 127 pp. [available from MPI for Meteorology, Bundesstr. 53, 20146 Hamburg, Germany], **2003.**

Rojas, M., Moreno, P., Kageyama, M., Crucifix, M., Hewitt, C., Abe-Ouchi, A., Ohgaito, R., Brady, E. C., and Hope, P.: The Southern Westerlies during the last glacial maximum in PMIP2 simulations, Clim. Dyn., 32, 525-548, doi:10.1007/s00382-008-0421-7, **2009.**

Rojas, M., and Moreno, P. I.: Atmospheric circulation changes and neoglacial conditions in the Southern Hemisphere mid-latitudes: insights from PMIP2 simulations at 6 kyr, Clim. Dyn., doi: 10.1007/s00382-010-0866-3, **2010.**

Sen Gupta, A., and England, M. H.: Coupled Ocean–Atmosphere–Ice Response to Variations in the Southern Annular Mode, J. Clim., 19, 4457–4486, doi: 10.1175/JCLI3843.1, **2006.**

Shin, S.I., Lui, Z., Otto-Bliesner, B., Brady, E.C., Kutzback, J.E., and Harrison, S.P.: A simulation of the last glacial maximum climate using NCAR CCSM, Clim. Dyn., 20, 127-151, doi:10.1007/s00382-002-0260-x, **2003.**

Shulmeister, J., Goodwin, I., Renwick, J., Harle, K., Armand, L., McGlone, M.S., Cook, E., Dodson, J., Hesse, P.P., Mayewski, P., and Curran, M.: The Southern Hemisphere westerlies in the Australasian sector over the last glacial cycle: a synthesis, Quat. Int., 118-119, 23-53, **2004.**

Sijp, W.P., and England, M.H.: Southern Hemisphere Westerly Wind Control over the Ocean's Thermohaline Circulation, J. Clim., 22, 1277-1286, **2009.**

Steig, E. J., Hart, C. P., White, J. W. C., Cunningham, W. L., Davis, M. D., and Saltzman, E. S.: Changes in climate, ocean and ice-sheet conditions in the Ross embayment, Antarctica, at 6 ka, Ann. Glaciol., 27, 305-310, **1998.**

Thresher, R.E.: Solar correlates of Southern Hemisphere mid-latitude climate variability, Int. J. Climatol., 22, 901-915, **2002.**

Toggweiler, J.R., and Samuels, B.: Effect of Drake Passage on the global thermohaline circulation, Deep-Sea Res. Pt 1., 42, 477-500, **1995.**

Toggweiler, J.R., Russel, J. L., and Carson, S.R.: Midlatitude westerlies, atmospheric CO_2 and climate change during the ice ages, Paleoceanography, 21, PA2005, doi:10.1029/2005PA001154, **2006.**

Toggweiler, J. R., and Russell, J.: Ocean circulation in a warming climate, Nature, 451, 286-288, doi:10.1038/nature06590, **2008.**

Tschumi, T., Joos, F., and Parekh, P.: How important are Southern Hemisphere wind changes for low glacial carbon dioxide? A model study, Paleoceanography, 23, PA4208, doi:10.1029/2008PA001592, **2008.**

Valdes, P.J.: South American palaeoclimate model simulations: how reliable are the models?, J. Quat. Sci., 15, 357-368, **2000.**

Vallis, G. K.: Atmospheric and Ocean Fluid Dynamics, Cambridge University Press, **2006.**

Varma, V., Prange, M., Lamy, F., Merkel, U., and Schulz, M.: Solar-forced shifts of the Southern Hemisphere Westerlies during the Holocene, Clim. Past, 7, 339-347, doi:10.5194/cp-7-339-2011, **2011.**

Wagner, S., Widmann, M., Jones, J., Haberzettl, T., Lücke, A., Mayr, C., Ohlendorf, C., Schäbitz, F., and Zolitschka, B.: Transient simulations, empirical constructions and forcing mechanisms for the Mid-holocene hydrological climate in southern Patagonia, Clim. Dyn., doi 10.1007/s00382-007-0229-x, **2007.**

Wyroll, K-H., Dong, B., and Valdes, P.J.: On the position of southern westerlies at the last glacial maximum: an outline of AGCM simulation results and evaluation of their implications, Quat. Sci. Rev., 19, 881-898, **2000.**

Yeager, S.G., Shields, C.A., Larger, W.G., and Hack, J.J.: The low-resolution CCSM3, J. Clim., 19, 2545-2566, **2006.**

Chapter 4

4. Impact of solar-induced stratospheric ozone decline on Southern Hemisphere Westerlies during the Late Maunder Minimum

V. Varma, M. Prange, T. Spangehl, F. Lamy, U. Cubasch and M. Schulz

(Submitted to *Geophysical Research Letters*)

4.1 Abstract

The Southern Hemisphere Westerly Winds (SWW) constitute an important zonal circulation system that dominates the dynamics of the Southern Hemisphere mid-latitudes, influencing large-scale precipitation and temperature patterns in the extratropics. Variations in their intensity and latitudinal position may also affect ocean dynamics through upwelling in the Southern Ocean. In the present study, the response of the SWW to reduced solar forcing during the Late Maunder Minimum (1675-1715 AD) is investigated. We analyze results from two transient simulations (1630-2000 AD) conducted with the coupled atmosphere-ocean model EGMAM (ECHO-G with Middle Atmosphere Model): one simulation with fixed stratospheric ozone concentration, and one with solar-induced variations in stratospheric ozone content. The results suggest that during periods of lower solar activity, the annual-mean SWW tend to get weaker on their poleward side and shift towards the equator. The SWW shift is much more intense and robust for the simulation with varying stratospheric ozone compared to its fixed ozone counterpart, suggesting an important influence of solar-induced stratospheric ozone variations on mid-latitude troposphere dynamics. Amplification of the solar signal in low-latitude lower stratospheric temperature by changes in photochemical ozone production and associated shortwave heating appears to be crucial in this process. Finally, we present proxy evidence from a high-resolution marine sediment core

from the Chilean continental slope (41°S), which strongly supports the model result of an equatorward displacement of the SWW during the Maunder Minimum.

4.2 Introduction

The Southern Hemisphere Westerly Winds (SWW) constitute an important zonal circulation system that dominates the dynamics of Southern Hemisphere (SH) mid-latitude climate influencing large-scale precipitation patterns and atmospheric heat transports (e.g., Shulmeister et al., 2004). Furthermore, they may influence the global ocean circulation (e.g., Toggweiler and Samuels, 1995; Biastoch et al., 2009) as well as the CO_2 budget in the Southern Ocean (Toggweiler et al., 2006; Anderson et al., 2009).

As a prominent forcing that influences climate on decadal to millennial time-scales (e.g., Gray et al., 2010), solar variations - in terms of the total solar irradiance (TSI) - have recently been suggested to be a potential driver for centennial-scale SWW variability (Varma et al., 2011). The general circulation model used by Varma et al. (2011), however, did not include a detailed representation of the stratosphere. Moreover, solar variations can affect the stratospheric ozone concentration through modification of photo-dissociation rates. This may have implications for the climate response to solar forcing, since shortwave heating in the stratosphere depends on both solar irradiance and ozone concentration.

There has been ever growing evidence, from modeling as well as observational studies, that dynamical coupling between the stratosphere and troposphere may substantially influence the surface climate (e.g., Haigh, 1996; Perlwitz and Harnik, 2003; Haigh et al., 2005; Meehl et al., 2009; Gray et al., 2010; Bal et al., 2011). Most of these studies were devoted to the response of the climate system to the 11-year solar cycle. Nevertheless, a period of special interest regarding the influence of solar variability on Earth's climate, is the Maunder Minimum (1645-1715 AD; hereafter MM), which witnessed an unusually low solar output for a relatively long time (Lean et al., 1995). Shindell et al. (2001) discussed the effect of reduced MM solar forcing and stratosphere-troposphere interactions on regional Northern Hemisphere winter climate with a particular eye towards the behaviour of the Arctic Oscillation/North Atlantic Oscillation (AO/NAO). A shift towards the negative phase of the AO/NAO, characterized by weakened Northern Hemisphere westerlies, as suggested by

Shindell et al. (2001) for the MM was also supported by data and other model studies (e.g., Langematz et al., 2005; Gray et al., 2010; Spangehl et al., 2010).

While most studies on the impact of MM solar forcing on climate focussed on the Northern Hemisphere extratropics, the SH climate during MM has received only little attention, even though there is evidence for a solar influence on the SWW and the AAO based on observational data from the past ~50 years (Roscoe and Haigh, 2007) and modeling studies (Haigh, 1996; Bal et al., 2011). In the present study, we examine the response of the SWW to changes in solar activity and the role of stratospheric ozone variations during the period from the Late Maunder Minimum (1675-1715 AD; hereafter LMM) to pre-industrial (1716-1790 AD; hereafter PI) using transient climate simulations from the coupled atmosphere-ocean general circulation model EGMAM (ECHO-G with Middle Atmosphere Model), carried out by Spangehl et al. (2010).

4.3 Method

The coupled climate model EGMAM (Huebner et al., 2007) is based on ECHO-G (Legutke and Voss, 1999). The atmospheric component is ECHAM4 (Roeckner et al., 1996), extended for the middle atmosphere, with a spatial resolution of T30/L39 (~3.75° and 39 levels). The oceanic component is HOPE-G (Hamburg Ocean Primitive Equation Global Model) which includes a dynamic-thermodynamic sea-ice model (Wolff et al., 1997). The ocean model grid has a horizontal resolution of 2.8° and 20 levels in the vertical (with increased meridional resolution of 0.5° in the tropics).

Two transient simulations were performed using EGMAM covering the period 1630-2000 AD, which were driven by time-dependent changes in radiative forcing accounting for solar variability and volcanic activity (Crowley, 2000) as well as changes in greenhouse gas (GHG) concentrations (Blunier et al., 1995; Etheridge et al., 1996). The change in TSI from the MM to the present day is ~0.3 % (scaled after Lean et al., 1995). The first simulation (hereafter EGMAM1) uses fixed prescribed climatological ozone representing annual cycle variations only (Brühl, 1993). The second simulation (hereafter EGMAM2) additionally includes prescribed variations in stratospheric ozone as part of the solar impact. Here, temporal changes in stratospheric ozone concentration and corresponding changes in

stratospheric heating rates due to solar variations are implemented by globally scaling the monthly ozone anomaly fields with TSI variations. The effect of reduced photolytic ozone production on stratospheric ozone concentration during the MM is estimated on the basis of offline calculations (Langematz et al., 2005; Spangehl et al., 2010). We note that the ozone climatology used here as a background has been corrected for anthropogenic influence and thus represents pre-industrial conditions. Both EGMAM1 and EGMAM2 use a simplified radiation scheme, i.e. the solar spectrum is represented by only two intervals, one for ultraviolet (UV)/visible (0.2-0.68 μm) and one for near-infrared (0.68-4.0 μm) (Roeckner et al., 1996).

Here, we will compare climatic averages from two distinct periods prior to the anthropogenic influence from GHG, the LMM (1675-1715 AD) and the PI (1716-1790 AD), characterized by low and high solar activity, respectively. The difference in the solar forcing between the periods of PI and LMM is ~0.33 W/m^2, while that of volcanic forcing is only ~0.12 W/m^2. Therefore, the dominant forcing of the LMM climate, when compared to PI, is solar. The LMM anomaly of annual mean stratospheric ozone concentration relative to PI exhibits a reduction of up to ~2%. Both simulations, EGMAM1 and EGMAM2, are started from the same initial conditions taken from a long pre-industrial control run. A more detailed description of the model setup, initialisation and forcings is given in Spangehl et al. (2010).

4.4 Results

The annual mean zonal wind anomalies along with the vertical velocity anomalies for the period of the LMM (averaged over 1675-1715 AD) relative to the PI (averaged over 1716-1790 AD) are shown in Fig. 1 for both EGMAM1 and EGMAM2. At the surface, an overall weakening of the westerlies in the latitude belt between ~40°S and 60°S is found during the LMM (Figs. 1a and 1d). North of 40°S, at the northern margin of the SWW belt, a strengthening of the westerlies is found during the LMM in the EGMAM2 experiment. This pattern of SWW weakening between ~40°S and 60°S along with positive westerly wind anomalies to the north of it can be interpreted as an equatorward shift of the annual-mean SWW for the period of lower solar activity. The general SWW weakening and equatorward shift during the LMM is also observed in the higher levels of the troposphere (Figs. 1b and 1e). While the weakening observed is statistically significant at the 0.05 level in the

experiment with varying solar-induced stratospheric ozone (EGMAM2), it is not significant in the experiment with constant ozone (EGMAM1). The austral summer season (December/January/February) witnesses the strongest response pattern of equatorward shift of the SWW in both the simulations (not shown). The equatorward shift of the annual mean SWW resembles the negative phase of the AAO (e.g., Thompson and Wallace, 2000). Consistent with the responses in zonal velocity, anomalies in zonally averaged annual mean vertical velocity (omega) are significant at the 0.05 level only in EGMAM2 (Figs. 1c and 1f). For the LMM, EGMAM2 simulates an anomalous ascent around ~40°S and an anomalous descent around ~20°S, indicating a contraction of the Hadley cell.

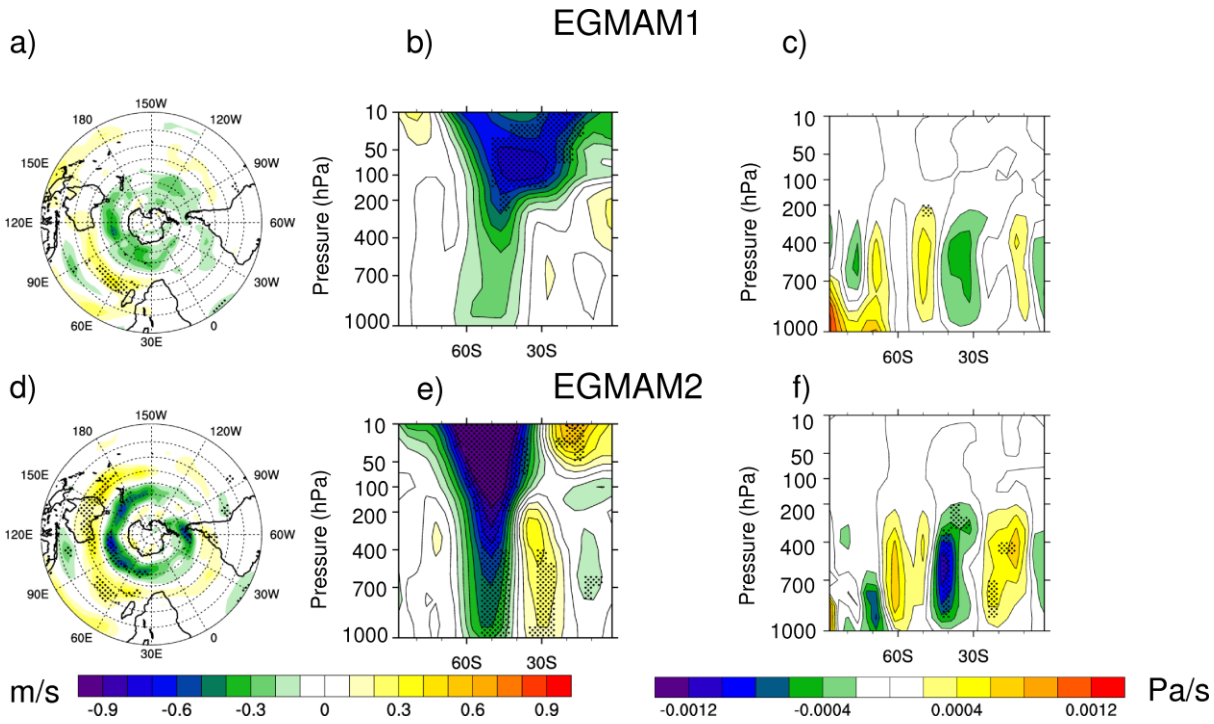

Fig. 1 Annual mean zonal wind and vertical velocity (omega) anomalies (LMM-mean minus PI-mean) in the EGMAM simulations. (a) and (d) Zonal wind anomalies at 1000 hPa in EGMAM1 (fixed ozone) and EGMAM2 (varying ozone), respectively. Latitudes are marked from equator to 90°S and are placed at 10° interval. (b) and (e) Zonally averaged zonal wind anomalies in the Southern Hemisphere in EGMAM1 and EGMAM2, respectively. (c) and (f) Zonally averaged vertical velocity anomalies in the Southern Hemisphere in EGMAM1 and EGMAM2, respectively. Stippling indicates significance of the anomaly at the 0.05 level according to a Student's t-test.

The LMM annual-mean temperature anomalies relative to the PI are shown in Fig. 2. Both simulations, EGMAM1 and EGMAM2, reveal a significant surface cooling in most areas of the SH of similar magnitude. At higher atmospheric levels, the temperature response in EGMAM2 is much more pronounced (and statistically significant) than in EGMAM1 (Figs. 2b and 2d). Here, the dominant feature observed for the LMM temperature anomaly is a general cooling of the lower tropical and subtropical stratosphere that is strongly amplified by the stratospheric ozone loss in EGMAM2 (Fig. 2d).

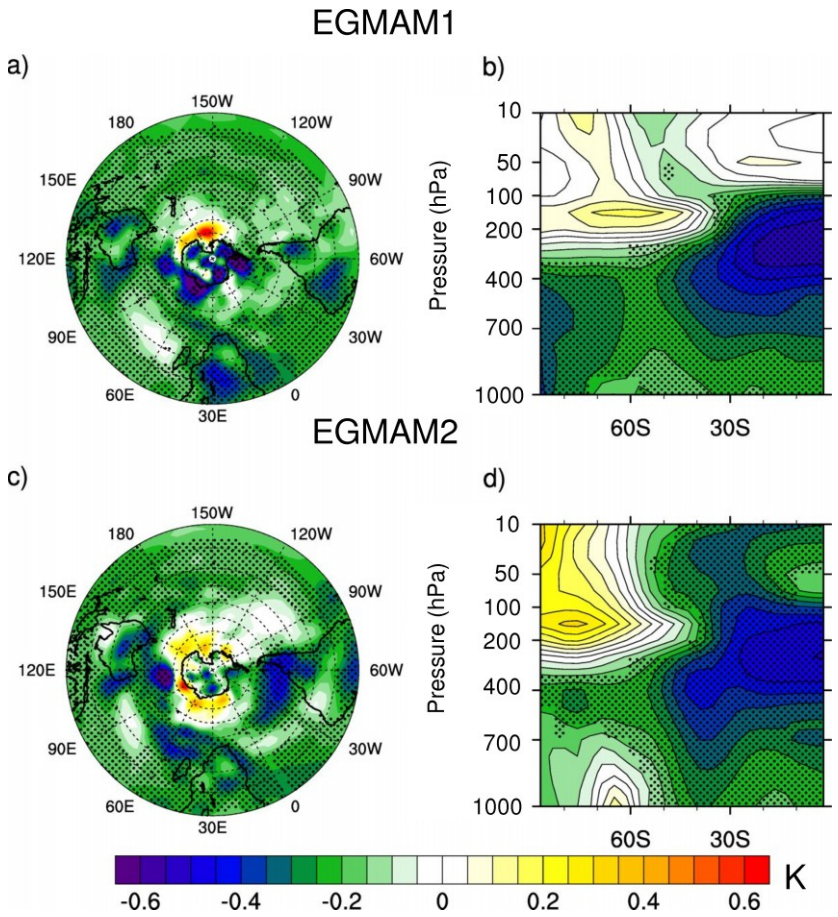

Fig. 2 Annual mean temperature anomalies (LMM-mean minus PI-mean) in the EGMAM simulations. (a) and (c) Surface temperature anomalies in EGMAM1 (fixed ozone) and EGMAM2 (varying ozone), respectively. Latitudes are marked from equator to 90°S and are placed at 10° interval. (b) and (d) Zonally averaged temperature anomalies in the Southern Hemisphere in EGMAM1 and EGMAM2, respectively. Stippling indicates significance of the anomaly at the 0.05 level according to a Student's t-test.

4.5 Discussion

In contrast to EGMAM2, both low-latitude stratospheric temperature and mid-latitude zonal wind signals for the LMM are weak and hardly significant in EGMAM1, suggesting that solar-induced stratospheric ozone variations play a crucial role in governing the SWW response to solar forcing brought about by the dynamical coupling between stratosphere and troposphere. A mechanism of stratosphere-troposphere coupling that can explain our results has been suggested by Haigh et al. (2005). Using a simplified model of the general atmosphere circulation, it was shown that during periods of higher solar activity, a low-latitude heating of the lower stratosphere leads to weakening of the subtropical jets associated with an expansion of the Hadley cells and a poleward shift of the westerlies which is primarily maintained by anomalous eddy momentum flux convergence in the upper troposphere. According to Haigh et al. (2005), low-latitude heating of the lower stratosphere increases the static stability in this region, lowers the tropopause and reduces the wave fluxes there, thus leading to coherent changes through the depth of the troposphere, involving the latitudinal location and width of the mid-latitude jet stream and its associated storm track.

In order to isolate the influence of solar-induced varying ozone on the temperature anomalies, the difference between the annual mean zonally averaged temperature anomalies between EGMAM2 and EGMAM1 is calculated (Fig. 3). The noticeable features of temperature anomalies are the weaker cooling in EGMAM2 compared to EGMAM1 in the SH high-latitude troposphere and lower stratosphere along with a stronger cooling in the SH mid-to-low latitudes lower stratosphere. In both the simulations, the stratospheric warming in the high-latitudes is not statistically significant (from Figs. 2b and 2d) and hence is not further discussed. The relative tropospheric warming in high latitudes is consistent with the negative polarity of the AAO associated with the weaker and equatorward shifted SWW in the EGMAM2 simulation (e.g., Thompson and Wallace, 2000). The pronounced low-latitude lower stratospheric cooling in EGMAM2 indicates that the mechanism suggested by Haigh et al. (2005) can be applied to the LMM. The year-round (not shown) cooling of the low-latitude lower stratosphere during the LMM reduced the static stability over that region and raised the tropopause, leading to the significant equatorward shift of the annual mean SWW, associated with a contraction of the Hadley cell (Fig. 1). In experiments with solar-induced varying stratospheric ozone, the simulated year-round cooling of the low-latitude lower

stratosphere during solar minima is consistent with the stratospheric response to the 11-year Sunspot cycle based on observations and re-analysis data, whereas the observed correlation between solar flux and stratospheric temperatures is ambiguous in high latitudes (Labitzke, 2001).

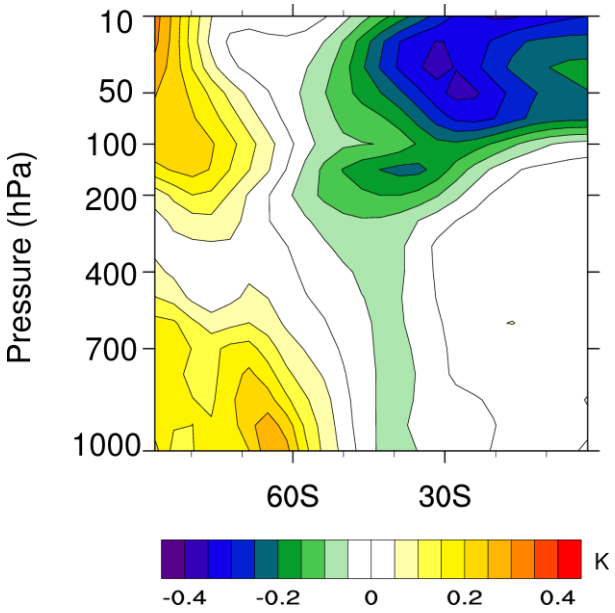

Fig. 3 Difference between the zonally averaged annual mean temperature anomalies (LMM-mean minus PI-mean) in EGMAM2 and EGMAM1 simulations (i.e. Fig. 2d minus 2b) in the Southern Hemisphere.

Our model evidence for a possible relation between solar activity and SWW shifts is supported by proxy data. A high-accumulation rate marine sediment core (GeoB3313-1) from the Chilean continental slope (41°S, 74.45°W) is interpreted as a Holocene record of local rainfall variations through its iron content, which can be interpreted in terms of SWW position (Lamy et al., 2001; Varma et al., 2011). A comparison of this iron record with reconstructions of solar activity based on ^{14}C (Solanki et al., 2004) and ^{10}Be (Steinhilber et al., 2009) for the last 500 years, which include the Dalton Minimum (ca. 1795-1825 AD) and the MM, is shown in Fig. 4. A higher concentration of iron in the sediment core indicates drier conditions probably due to southward shifted SWW, whereas a lower iron concentration is indicative of wetter conditions suggesting northward shifted SWW (Lamy et al., 2001). During the solar minimum periods (e.g. Dalton Minimum and MM), the iron record shows negative anomalies suggesting an enhanced precipitation in the hinterland of the coring site. Pearson correlation coefficients suggest a statistically significant link between solar activity and the SWW, characterized by an equatorward (poleward) shift of the SWW during periods of lower (higher) solar activity, which is especially pronounced during the MM (Fig. 4).

Since a low resolution model has been used in this study, local features and in particular, orographic rainfall at the Andes cannot be fully captured. However, EGMAM still simulates positive precipitation anomalies over the region of enhanced westerlies in Patagonia (in particular during austral summer), but statistically not significant at the 0.05 significance level according to a t-test (not shown).

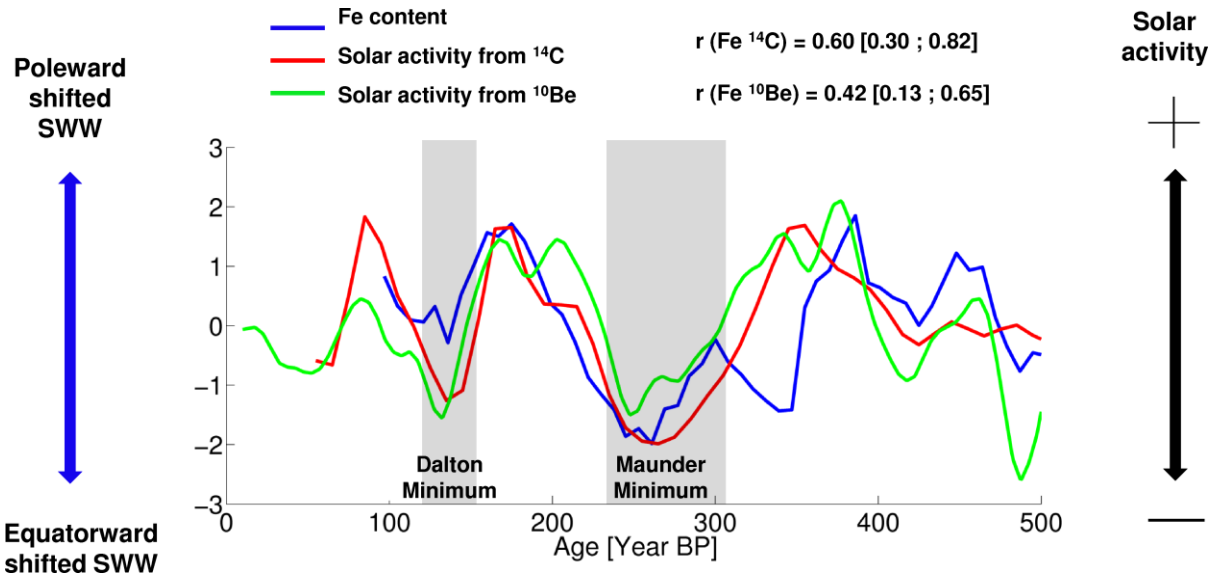

Fig. 4 Reconstruction of the SWW position (based on the GeoB3313-1 iron record, Lamy et al., (2001); blue line) versus solar activity based on ^{10}Be (Steinhilber et al., (2009); green line) and ^{14}C (Solanki et al., (2004); red line), for the last 500 years. Grey bars mark the low solar activity periods of the Dalton Minimum and the Maunder Minimum. Time series are unsmoothed, detrended and standardized. The negative (positive) iron anomalies suggest northward (southward) shifted SWW (Lamy et al., 2001; Varma et al., 2011). 95% confidence intervals (in brackets) for Pearson correlation coefficients (r) were calculated using a bootstrap method, where autocorrelation has been taken into account (Mudelsee, 2003).

4.6 Conclusions

We studied the stratospheric influence on the variability of the SWW during the period from LMM to PI, using results from a coupled atmosphere-ocean model with a detailed representation of the middle atmosphere. The analysis of two transient simulations with fixed

as well as solar-induced varying stratospheric ozone points to an important effect of solar-induced stratospheric ozone variations on the SWW during the MM and possibly also during other multi-decadal to centennial solar minima. The model results support the hypothesis that during periods of lower solar output, the annual mean SWW tend to get weaker on the poleward side and exhibit an equatorward shift. In addition, proxy evidence was presented, which supports the hypothesis of an equatorward SWW shift during solar minima.

While a 'bottom-up' mechanism via shortwave absorption at the surface in combination with feedbacks involving ocean and sea-ice dynamics was suggested by Varma et al. (2011) to explain the SWW response to centennial-scale changes in TSI during the Late Holocene, the present study highlights the significance of the stratosphere along with its ozone content as a potential driver for multi-decadal to centennial-scale extratropical climate variability in the Southern Hemisphere, through a 'top-down' process. Amplification of the solar signal in low-latitude stratospheric temperature by changes in photochemical net ozone production and associated heating rates appears to be crucial in this process. We propose that the 'bottom-up' and 'top-down' mechanisms are not mutually exclusive and that the processes linking solar variability to the SWW in the two different ways may complement each other, thus leading to a stronger total response than given by each individual process alone.

We finally conclude that the role of the Sun in driving SH extratropical climate dynamics has likely been underestimated in previous simulations of past climate change, using models that did not account for solar-induced stratospheric ozone variations. Future studies should further evaluate the uncertainty range of past tropospheric and stratospheric responses to solar forcing by using different reconstructions of total and spectral solar irradiance as well as implementing interactive climate-chemistry feedbacks.

4.7 Acknowledgements

This work is the outcome of a research stay (by Vidya Varma) at the Institut für Meteorologie (Freie Universität Berlin, Germany). The study was funded through the DFG Priority Programme "INTERDYNAMIK". We acknowledge the use of the NCAR Command Language (NCL) in our data analysis and visualization.

4.8 References

Anderson, R. F., Ali, S., Bradtmiller, L. I., Nielsen, S. H. H., Fleisher, M. Q., Anderson, B. E., and Burckle, L. H.: Wind-Driven Upwelling in the Southern Ocean and the Deglacial Rise in Atmospheric CO_2, Science, 323, 1443-1448, doi: 10.1126/science.1167441, **2009.**

Bal, S., Schimanke, S., Spangehl, T., and Cubasch, U.: On the robustness of the solar cycle signal in the Pacific region, Geophys. Res. Lett., 38, L14809, 5pp, doi:10.1029/2011GL047964, **2011.**

Biastoch, A., Böning, W., Schwarzkopf, F. U., and Lutjeharms, J. R. E.: Increase in Agulhas leakage due to poleward shift of Southern Hemisphere westerlies, Nature, 462, 495–498, **2009.**

Blunier, T., Chappellaz, J. A., Stauffer, B., and Raynaud, D.: Variations in atmospheric methane concentration during the Holocene epoch, Nature, 374, 46-49, **1995.**

Brühl, C.: Atmospheric effects of stratospheric aircraft: Report of the 1992 Models and Measurements Workshop, NASA Ref. Publ., 1292II, 240 pp, NASA Goddard Space Flight Cent., Greenbelt, Md, **1993.**

Crowley, T. J.: Causes of climate change over the past 1000 years, Science, 289, 270-277, doi: 10.1126/science.289.5477.270, **2000.**

Etheridge, D., Steele, L. P., Langefelds, L., Francey, R. J., Barnola, J. M., and Morgan, V. I.: Natural and anthropogenic changes in atmospheric CO_2 over the last 1000 years from air in Antarctic ice and firn, J. Geophys. Res., 101, 4115-4128, **1996.**

Gray, L. J., Beer, J., Geller, M., Haigh, J. D., Lockwood, M., Matthes, K., Cubasch, U., Fleitmann, D., Harrison, G., Hood, L., Luterbacher, J., Meehl, G. A., Shindell, D., van Geel, B., and White, W.: Solar influences on climate, Rev. Geophys., 48, 53 pp, doi:10.1029/2009RG000282, **2010.**

Haigh, J. D.: The impact of solar variability on climate, Science, 272, 981-984, doi:10.1126/science.272.5264.981, **1996.**

Haigh, J. D., Blackburn, M., and Day, R.: The response of tropospheric circulation to perturbations in lower-stratospheric temperature, J. Clim., 18, 3672-3685, doi: 10.1175/JCLI3472.1, **2005.**

Huebener, H., Cubasch, U., Langematz, U., Spangehl, T., Niehörster, F., Fast, I., and Kunze, M.: Ensemble climate simulations using a fully coupled ocean-troposphere-stratosphere general circulation model, Philos. Trans. R. Soc. Ser. A., 365, 2089-2101, **2007.**

Labitzke, K.: The global signal of the 11-year Sunspot cycle in the stratosphere: Differences between solar maxima and minima, Meteorol. Z., 10, 83-90, **2001.**

Lamy, F., Hebbeln, D., Rohl, U., and Wefer, G.: Holocene rainfall variability in southern Chile: a marine record of latitudinal shifts of the Southern Westerlies, Earth Planet Sc. Lett., 185, 369-382, **2001.**

Langematz, U., Claussnitzer, A., Matthes, K., and Kunze, M.: The Climate During the Maunder Minimum: A simulation with the Freie Universität Berlin Climate Middle Atmosphere Model (FUB-CMAM), J. Atmos. Solar-Terr. Phys., special issue, 67, 55-69, **2005.**

Lean, J., Beer, J., and Bradley, R.: Reconstruction of solar irradiance since 1610: Implications for climate change, Geophys. Res. Lett., 22, 3195-3198, **1995.**

Legutke, S., and Voss, R.: The Hamburg Atmosphere-Ocean Coupled Circulation Model ECHO-G, Tech. Rep., 18, Dtsch. Klimarechen-zentrum Hamburg Germany, **1999.**

Lu, J., Chen, G., and Frierson, D. M. W.: The position of the midlatitude storm track and eddy-driven westerlies in aquaplanet AGCMs, J. Atmos. Sci., 67, 3984–4000, **2010.**

Meehl, G. A., Arblaster, J. M., Matthes, K., Sassi, F., and van Loon, H.: Amplifying the Pacific climate system response to a small 11 year solar cycle forcing, Science, 325, 1114-1118, doi: 10.1126/science.1172872, **2009.**

Mudelsee, M.: Estimating Pearson's correlation coefficient with bootstrap confidence interval from serially dependent time series, Math. Geol., 35, 651-665, **2003.**

Perlwitz, J., and Harnik, N.: Observational evidence of a stratospheric influence on the troposphere by planetary wave reflection, J. Clim., 16, 3011-3026, **2003.**

Roeckner, E., Arpe, K., Bengtsson, L., Claussen, M., Dümenil, L., Esch, M., Giorgetta, M., Schlese, U., and Schulzweida, U.: The Atmospheric General Circulation Model ECHAM-4: Model description and simulation of present-day climate, MPI Rep., 218, Max-Planck-Inst Für Meteorologie, Hamburg, Germany, **1996.**

Roscoe, H. K., and Haigh, J. D.: Influences of ozone depletion, the solar cycle and the QBO on the Southern Annular Mode, Q. Roy. Meteor. Soc., 133, 1855-1864, **2007.**

Schneider, D. P., Steig, E. J., Van Ommen, T. D., Dixon, D. A., Mayewski, P. A., Jones, J. M., and Bitz, C. M.: Antarctic temperatures over the past two centuries from ice cores, Geophys. Res. Lett., 33, L16707, 5pp, **2009.**

Shindell, D. T., Schmidt, G. A., Mann, M. E., Rind, D., Waple, A.: Solar Forcing of Regional Climate Change During the Maunder Minimum, Science, 294, 2149-2152, **2001.**

Shulmeister, J., Goodwin, I., Renwick, J., Harle, K., Armand, L., McGlone, M. S., Cook, E., Dodson, J., Hesse, P.P., Mayewski, P., and Curran, M.: The Southern Hemisphere westerlies in the Australasian sector over the last glacial cycle: a synthesis, Quatern. Int., 118-119, 23-53, **2004.**

Solanki, S. K., Usoskin, I. G., Kromer, B., Schüssler, M., and Beer, J.: Unusual activity of the Sun during recent decades compared to the previous 11,000 years, Nature, 431, 1084–1087, **2004.**

Spangehl, T., Cubasch, U., Raible, C. C., Schimanke, S., Körper, J., and Hofer, D.: Transient climate simulations from the Maunder Minimum to present day: Role of the Stratosphere, J. Geophys. Res-Atmos., 115, D00I10, doi:10.1029/2009JD012358, **2010.**

Steinhilber, F., Beer, J., and Fröhlich, C.: Total solar irradiance during the Holocene, Geophys. Res. Lett., 36, L19704, doi:10.1029/2009GL040142, **2009.**

Thompson, D. W. J., and Wallace, J. M.: Annular modes in the extratropical circulation. Part I: Month-to-month variability, J. Clim., 13, 1000-1016, **2000.**

Toggweiler, J. R., and Samuels, B.: Effect of Drake Passage on the global thermohaline circulation, Deep-Sea Res. Pt. 1., 42, 477-500, **1995.**

Toggweiler, J. R., Russel, J. L., and Carson, S. R.: Midlatitude westerlies, atmospheric CO_2 and climate change during the ice ages, Paleoceanography, 21, PA2005, 15 pp, **2006.**

Varma, V., Prange, M., Lamy, F., Merkel, U., and Schulz, M.: Solar-forced shifts of the Southern Hemisphere Westerlies during the Holocene, Clim. Past., 7, 339-347, doi:10.5194/cp-7-339-2011, **2011.**

Wolff, J., Maier-Reimer, E., and Legutke, S.: The Hamburg Primitive Equation Model HOPE, Tech. Rep. 18., German Climate Center (DKRZ), **1997.**

Chapter 5

5. Summary and Outlook

5.1 Summary of the results

The main focus of this thesis was to understand the variability of SWW during the Holocene under the influence of solar and orbital forcings. To this end numerical simulations were carried out using the comprehensive coupled climate model CCSM3 with solar and orbital forcings under the Holocene scenario. Along with CCSM3, results from several other models (GCMs as well as EMICs) were also used for inter-comparison. A comparison study with proxy evidence was also provided to test the hypothesis of a possible influence of solar activity on SWW variability.

5.1.1 SWW variability under solar forcing

To investigate the role of TSI on SWW variability, sensitivity experiments were carried out using CCSM3 with a reduced TSI of 1363 W/m^2 and compared with the control simulation with TSI value of 1365 W/m^2 employing the pre-industrial boundary conditions in the low resolution version of the model. Analyses of these model results suggested that for periods of lower (higher) solar activity the annual mean SWW experienced an equatorward/northward (poleward/southward) shift. Another interesting result observed in these simulations was the opposite pattern in the direction of SWW shift for various seasons. Austral summer (DJF) season showed an equatorward shift in SWW for lower solar activity (similar to annual mean pattern) wherein austral winter (JJA) showed a poleward shift for lower solar activity. In addition, to test if the sensitivity of the model is sufficient to detect recurring solar-forced SWW shifts and if the response is dependent on the Holocene background climate, a set of three experiments was carried out with idealized solar forcing where each of the experiments was initialized from an orbitally forced transient Holocene run (9 kyr BP to the present day) by taking the model years having orbital forcing corresponding to 8.5 kyr BP, 5.5 kyr BP and 2.5 kyr BP respectively. A sinusoidally varying solar irradiance forcing with a period of 200 years and amplitude of 1 Wm^{-2} was applied to the model for each time slice (intended to mimic the de Vries solar cycle) and integrated to include 3.5 de Vries solar cycles in each of the three experiments. The TSI forcing along with the position of the SWW (defined in terms

of the difference between the latitudes 55°S and 35°S which represent the southern and northern parts of the SWW belt, respectively) were compared for the early, mid and late Holocene experiments. In each experiment, forcing and response exhibit a strikingly similar temporal pattern, i.e. higher (lower) solar activity resulted in a poleward (equatorward) shift of the SWW, thus supporting the evidence from the first set of sensitivity experiments with high and low TSI values. Also, a high-resolution iron record from the Chilean continental slope (41°S), which is interpreted to reflect changes in the position of the SWW, was shown to be significantly correlated with reconstructed solar activity during the past 3000 years. ***Taken together, the model and proxy results suggest that centennial-scale periods of lower (higher) solar activity caused equatorward (southward) shifts of the annual mean SWW.***

5.1.2 SWW variability under orbital forcing

To study the evolution of the SWW under orbital forcing from the mid-Holocene (7 kyr BP) to pre-industrial modern times (250 yr BP) transient experiments using the comprehensive coupled global climate model CCSM3 were performed using the low resolution version of the model with pre-industrial boundary conditions. In addition to the CCSM3 experiments, a model inter-comparison was also carried out using orbitally forced Holocene transient simulations from four other global climate models namely ECHO-G, COSMOS, ECBilt-CLIO-VECODE and CLIMBER2-LPJ. While ECHO-G and COSMOS are comprehensive coupled GCMs, ECBilt-CLIO-VECODE and CLIMBER2-LPJ belong to the category of EMICs. This study also provided a platform to compare between experiments with accelerated orbital forcing and non-accelerated orbital forcing. The comparison showed that the simulation of the Holocene trends is unaffected by the orbital acceleration technique employed in some of the transient runs. ***Analyses and comparison of the model results consistently suggested that the annual and seasonal mean SWW were subject to an overall strengthening and poleward shifting trend during the course of the mid-to-late Holocene under the influence of orbital forcing, except for the austral spring (SON) season, where the SWW exhibited an opposite trend of shifting towards the equator.***

5.1.3 SWW variability under solar forcing: the role of stratospheric ozone

As mentioned earlier, the solar sensitivity experiments using CCSM3 employed a low resolution version which did not include a detailed stratosphere or ozone chemistry and used

prescribed ozone for simulations. This prevented the understanding of any possible influence of solar activity on SWW variability through the stratosphere and its ozone content. In order to study the response of the SWW to the changes in solar activity in the middle atmosphere, during the period from LMM (1675-1715 AD) to PI (1716-1790 AD), analyses of the simulation results from the AO-GCM, EGMAM, were carried out. The EGMAM model was used by Spangehl et al. (2010) to perform transient simulations using both prescribed as well as solar induced varying stratospheric ozone for the period from MM to present-day (1630-2000 AD). The LMM typically is a period representative of lower solar activity and PI that of a higher solar activity. ***Analyses of the EGMAM results suggested that during periods of lower solar activity, the annual mean SWW tend to get weaker on their poleward side and show an equatorward shift. The response pattern was more intense and robust for the simulations with varying ozone compared to its fixed ozone counterpart.*** A high-resolution iron record from the Chilean continental slope (41°S), interpreted to reflect changes in the position of the SWW, is significantly correlated with reconstructed solar activity during the past 500 years, which also provided the proxy evidence to support the link between solar activity and SWW variability.

5.2 Outlook

5.2.1 'Bottom-up' and 'Top-down' approaches in the Sun-Earth relation

Our results strongly suggest that solar activity is a significant factor affecting the variability in the strength and position of the SWW belt. This has been shown through simulation results from coupled climate models without and with detailed middle atmosphere (CCSM3 and EGMAM respectively). The striking similarity in the response pattern showing an equatorward shift in the annual mean SWW for periods of lower solar activity in both the models suggests that both the 'bottom-up' and 'top-down' approaches of viewing the solar influence on climate (Haigh, 1996; Meehl et al., 2009; Lockwood et al., 2010) are of equal importance. The processes linking solar variability to the SWW in the two different scenarios may complement each other, thus leading to a stronger total response than given by each individual process alone. Hence, it would be important for the future modelling experiments to consider both these aspects in order to get a better assessment of the impact of solar variability on climate.

5.2.2 Palaeo-proxy interpretation

The results from the analyses and comparison of Holocene transient simulations under orbital forcing were controversially escorted by the findings from reconstructed data. While result from Moreno et al. (2010) is in agreement with the model findings, the result from Lamy et al. (2010) is contradicting the model results. However, there was a unanimous agreement by all the models with the result of Lamy et al. (2010) for the austral spring (SON) season. But it should be noted that the model results are only partially comparable with the reconstructions of SWW, especially the ones based on precipitation proxies, since all the models applied in this study belong to the coarse resolution league where capturing the precipitation variabilities in detail remains an issue. The incongruity within the different reconstructed data suggests that for future studies, the interpretation of data with the consideration of any possible seasonal bias should also be cautiously taken into account. Also, it is noteworthy that both the records for SWW show consistent results for the early Holocene period (i.e. ~10 kyr BP to 8 kyr BP). The potential factors that might have caused the inconsistency from the mid-to-late Holocene results are still unclear which also needs to be addressed.

5.2.3 Spectral composition depiction in climate models

Another aspect for a future outlook is the inclusion of solar spectral irradiances in model simulations. It is a known fact that the thermal structure and composition of the atmosphere fundamentally depends on the incoming solar irradiance. While the radiation at the UV wavelengths (0.01-0.4 µm) acts as a major source of heating in the middle atmosphere, the radiation at visible (0.4-0.75 µm) and near-infrared (0.75-4.0 µm) wavelengths are the ones that reach and warm the lower atmosphere including the Earth's surface (Brasseur and Solomon, 2005). This makes the spectral composition of solar radiation a crucial factor in determining the atmospheric structure along with the surface temperature and asserts that the response of the atmosphere to variations in solar irradiance depends significantly on the spectrum (Haigh, 1994). In a recent study by Haigh et al. (2010), it has been shown using the Spectral Irradiance Monitor (SIM) measurements that even though the changes in TSI observed in conventional studies (e.g. Lean, 2000) and SIM data sets were similar, their difference in spectral compositions and the resulting impacts on the stratosphere, produced quite different pictures of the transmission of radiation to the tropopause, modulating a different radiative forcing. Most of the current simulations which study the effect of solar

variability on tropospheric climate (e.g. those assessed in the Intergovernmental Panel on Climate Change assessments; Solomon et al., 2007) are forced mainly by the variations in TSI alone not resolving the full details of the solar spectrum. The study by Haigh et al. (2010) points towards the uncertainty in our understanding about the mechanisms through which the solar activity influences the climate system and suggests the importance of the changes in the solar spectral irradiance that is mostly underestimated. Thus, inclusion of the effects of solar spectral irradiances in the model simulations needs to be addressed which will also provide more or even a different insight into the past climate in the context of Sun-Earth relation.

5.2.4 Influence of GHGs on SWW variability

This thesis aimed to understand the Holocene response of the SWW to natural forcings like solar and orbital. Simulations to this point were also carried out within the context of pre-industrial boundary conditions. The influence of GHGs (especially CO_2) and other anthropogenic forcings on the SH atmospheric circulation is also gaining importance in the light of recent studies (e.g. Kushner et al., 2001; Miller et al., 2006; Arblaster and Meehl, 2006; Arblaster et al., 2011). Model experiments along with the reconstructed data extending to earlier time periods provide the opportunity to study the contribution of GHGs as well, along with natural forcings on climate. However, the uncertainties in GHG forcing scenarios still remain an issue. For instance, the middle Pliocene (ca. 3-5 Ma) was a period that witnessed high warming of up to 3-4°C in the low latitudes and up to 10°C near the poles (e.g. Dekens et al., 2007; Dowsett et al., 2009). Atmospheric CO_2 concentrations of up to 500-600 ppmv (which is roughly twice that of the pre-industrial level) will be required to recreate the Pliocene climate in the model simulations following the generally used GHG forcing scenarios (cf. Schneider and Schneider, 2009). However studies based on proxy as well as model simulations have shown a much less value of about 360-420 ppmv, for atmospheric CO_2 concentration during that period (e.g. Pagani et al., 2010; Lunt et al., 2010). This demonstrates the uncertainty in the GHG forcing generally applied in the models. The modelled response of SWW under the influence of different GHG scenarios during earlier time periods such as Pliocene could contribute in minimising the forcing-scenario related uncertainty provided there are high resolution proxy records extending to the earlier periods to validate the model depiction of SWW during that time.

5.2.5 SWW during early interglacials

Analyses of the SWW variability during the periods prior to that of the Holocene will assist significantly in the understanding of the SH climate during those times. For instance, the Eemian is an interglacial period (~ 130-115 kyr BP) where the eccentricity of the Earth's orbit around the Sun was much larger compared to that of the Holocene and hence the insolation induced changes on climate would also be more pronounced during Eemian than during the Holocene. This definitely must have reflected in the SWW response as well. This points to the need of further model simulations representing early interglacials, focussing on SWW and SH climate. It also demands the requirement of more proxy records from the SH covering those periods, to validate the model performance.

5.3 References

Arblaster, J. M., and Meehl, G. A.: Contributions of external forcings to southern annular mode trends, J. Clim., 19(12), 2896-2905, **2006.**

Arblaster, J. M., Meehl, G. A., and Karoly, D. J.: Future climate change in the Southern Hemisphere: Competing effects of ozone and greenhouse gases, Geophys. Res. Lett., 38, L02701, **2011.**

Brasseur, G., and Solomon, S.: Aeronomy of the Middle Atmosphere: Chemistry and Physics of the Stratosphere, Springer, **2005.**

Dekens, P. S., Ravelo, A. C., McCarthy, M. D.: Warm upwelling regions in the Pliocene warm period, Paleoceanography, 22, doi:10.1029/2006PA001394, **2007.**

Dowsett, H. J., Chandler, M. A., and Robinson, M. M.: Surface temperatures of the Mid-Pliocene North Atlantic Ocean: implications for future climate, Phil. Trans. R. Soc. A , 367, 69–84, **2009.**

Haigh, J. D.: The role of stratospheric ozone in modulating the solar radiative forcing of climate. Nature, 370, 544-546, doi:10.1038/370544a0, **1994.**

Haigh, J.D.: The impact of solar variability on Climate, Science, 272, 981 – 984, **1996.**

Haigh, J. D., Winning, A. R., Toumi, R., and Harder, J. W.: An influence of solar spectral variations on radiative forcing of climate, Nature, 467, 696–699, **2010.**

Kushner, P. J., Held, I. M., and Delworth, T. L.: Southern Hemisphere Atmospheric Circulation Response to Global Warming, J Clim., 14, **2001.**

Lamy, F., Kilian, R., Arz, H.W., Francois, J.P., Kaiser, J., Prange, M., and Steinke, T.: Holocene changes in the position and intensity of the southern westerly wind belt, Nat. Geosci., 3, 695-699, **2010.**

Lean, J.: Evolution of the Sun's spectral irradiance since the Maunder Minimum, Geophys. Res. Lett., 27, 2425-2428, **2000.**

Lockwood, M., Bell, C., Woollings, T., Harrison, R. G., Gray, L. J., and Haigh, J. D.: Top-down solar modulation of climate: evidence for centennial-scale change, Environ. Res. Lett., 5, 034008, **2010.**

Lunt, D. J., Haywood, A. M., Schimdt, G. A., Salzmann, U., Valdes, P. J., and Dowsett, P. J.: Earth system sensitivity inferred from Pliocene modelling and data, Nat., Geo., 3, 60–64, **2010.**

Meehl, G.A., Arblaster, J.M., Matthes, K., Sassi, F., and van Loon, H.: Amplifying the Pacific Climate System Response to a Small 11-Year Solar Cycle Forcing, Science, 325, 1114–1118, **2009.**

Moreno, P. I., Francois, J. P., Moy, C. M., and Villa-Martinez, R.: Covariability of the Southern Westerlies and atmospheric CO_2 during the Holocene, Geology, 38, 727-730, doi:10.1130/G30962.1, **2010.**

Pagani, M., Liu, Z., LaRiviere, J., and Ravelo, A. C.: High Earth-system climate sensitivity determined from Pliocene carbon dioxide concentrations, Nat. Geo., 3, 27–30, **2010.**

Schneider, B., and Schneider, R.: Palaeoclimate: Global warmth with little extra CO_2, Nat. Geo., 3, 6-7, **2010.**

Solomon, S., Qin, D., Manning, M., Chen, Z., Marquis, M., Averyt, K. B., Tignor, M., and Miller, H. L. (eds.) : Contribution of Working Group I to the Fourth Assessment Report of the Intergovernmental Panel on Climate Change, Cambridge University Press, **2007.**

Son, S. W., Gerber, E. P., Perlwitz, J., Polvani, L. M., Gillett, N. P., Seo, K. H., Eyring, V., Shepherd, T. G., Waugh, D., Akiyoshi, H., Austin, J., Baumgaertner, A., Bekki, S., Braesicke, P., Brühl, C., Butchart, N., Chipperfield, M. P., Cugnet, D., Dameris, M., Dhomse, S., Frith, S., Garny, H., Garcia, R., Hardiman, S. C., Jöckel, P., Lamarque, J. F., Mancini, E., Marchand, M., Michou, M., Nakamura, T., Morgenstern, O., Pitari, G., Plummer, D. A., Pyle, J., Rozanov, E., Scinocca, J. F., Shibata, K., Smale, D., Teyssedre, H., Tian, W., and Yamashita, Y.: Impact of stratospheric ozone on Southern Hemisphere circulation change: A multimodel assessment, J Geophys. Res., 115, D00M07, **2010.**

Spangehl, T., Cubasch, U., Raible, C. C., Schimanke, S., Körper, J., and Hofer, D.: Transient climate simulations from the Maunder Minimum to present day: Role of the Stratosphere, J. Geophys. Res-Atmos., 115, D00I10, doi:10.1029/2009JD012358, **2010.**

Appendix 1

Supplementary material for Chapter 3

Here, the spatial distribution of annual mean SWW (Fig. 1) is presented along with trends in the seasonal mean low-level zonal wind (Figs. 2-5) and surface temperature (Figs. 6-9) for the period 7 kyr BP to 250 yr BP for all models. The zonal winds are plotted at 850 hPa for CCSM3, ECHO-G (I and II) and COSMOS, and at the lowermost model level for ECBilt-CLIO-VECODE (800 hPa) and CLIMBER2-LPJ. All polar stereographic plots represent the Southern Hemisphere, with latitudes starting from equator to 90°S, placed at 10° interval.

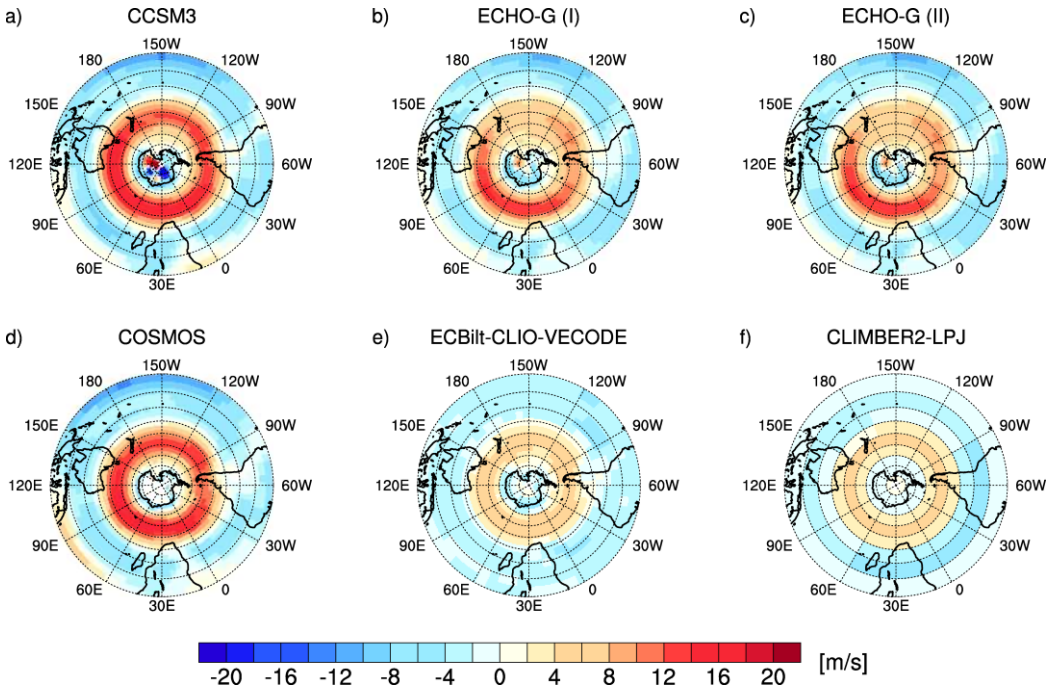

Fig. 1 Annual mean low-level zonal wind in a) CCSM3, b) ECHO-G (I), c) ECHO-G (II), d) COSMOS, e) ECBilt-CLIO-VECODE, and f) CLIMBER2-LPJ, temporally averaged over the period 7 kyr BP to 250 yr BP.

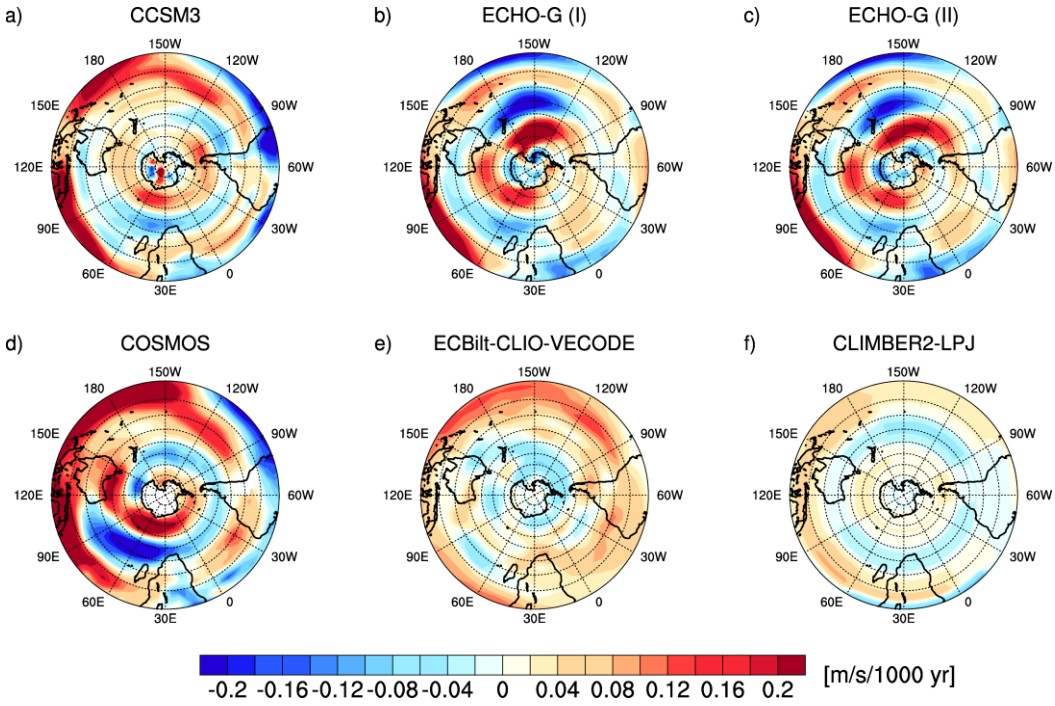

Fig. 2 Trend in the low-level zonal wind for the JJA season in a) CCSM3, b) ECHO-G (I), c) ECHO-G (II), d) COSMOS, e) ECBilt-CLIO-VECODE, and f) CLIMBER2-LPJ.

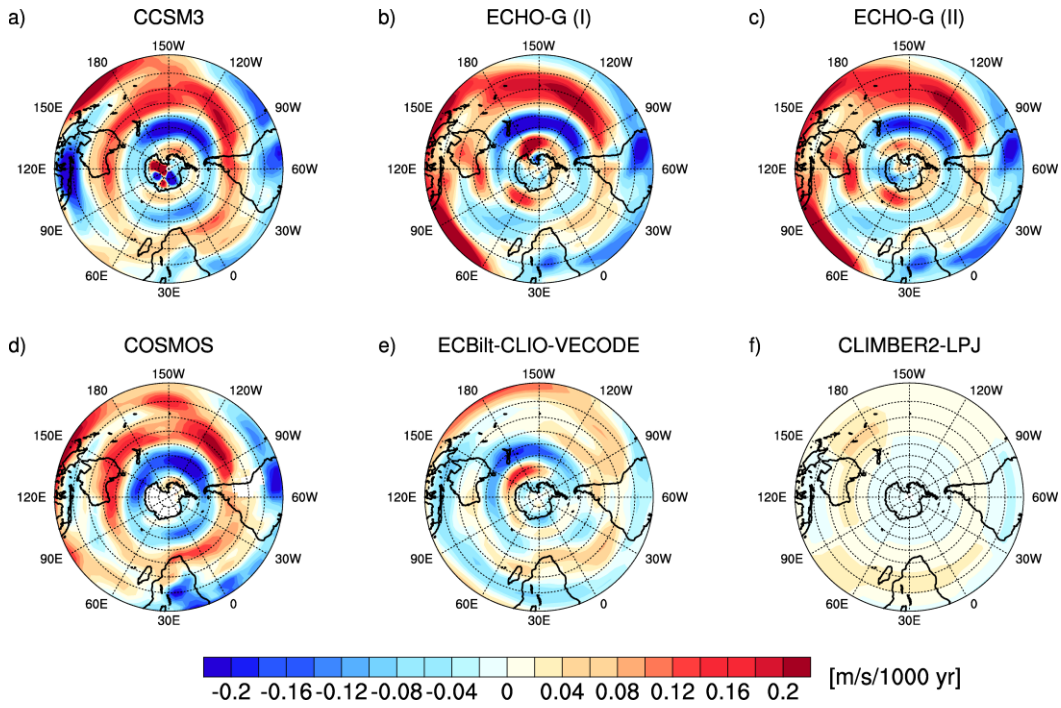

Fig. 3 Same as Fig. 2 but for the SON season.

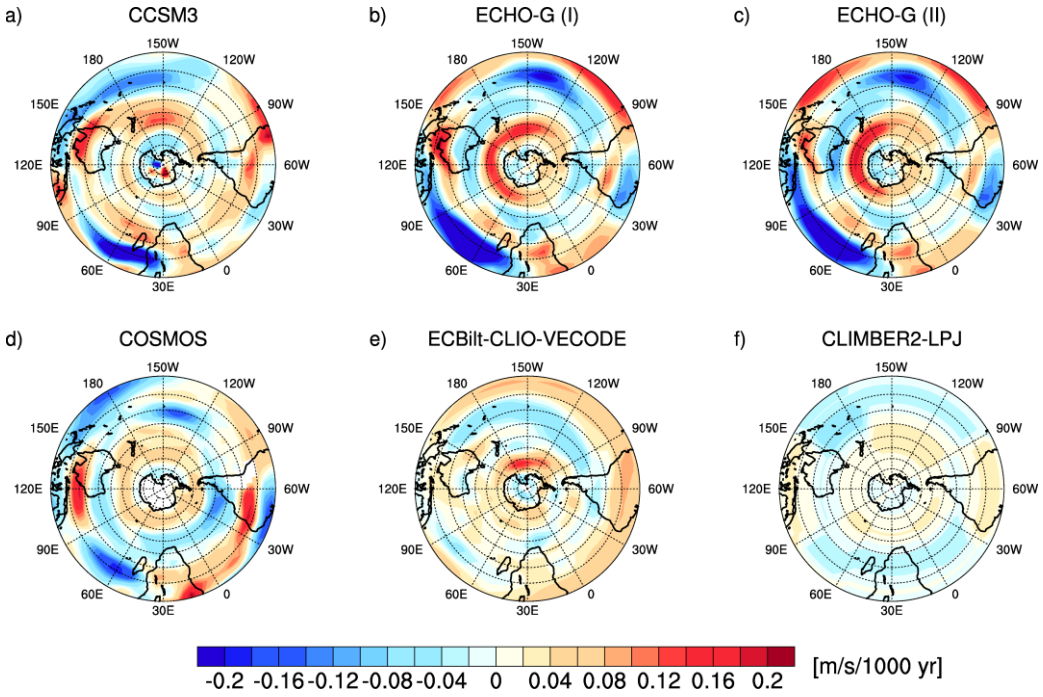

Fig. 4 Same as Fig. 2 but for the DJF season.

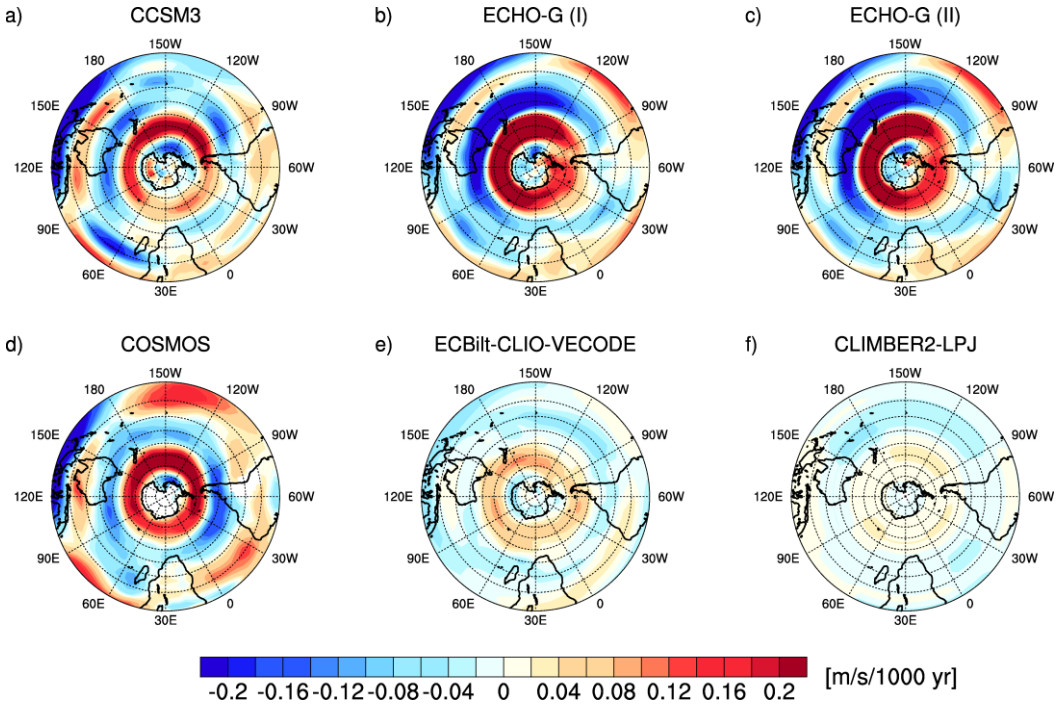

Fig. 5 Same as Fig. 2 but for the MAM season.

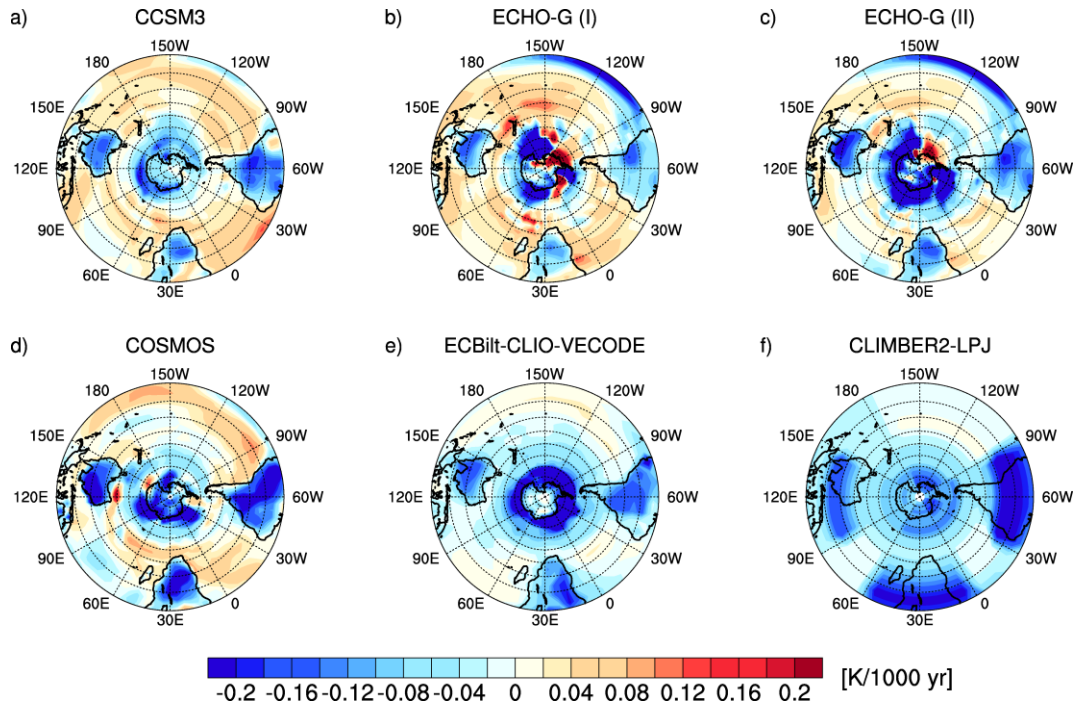

Fig. 6 Trend in the surface temperature for the JJA season in a) CCSM3, b) ECHO-G (I), c) ECHO-G (II), d) COSMOS, e) ECBilt-CLIO-VECODE, and f) CLIMBER2-LPJ.

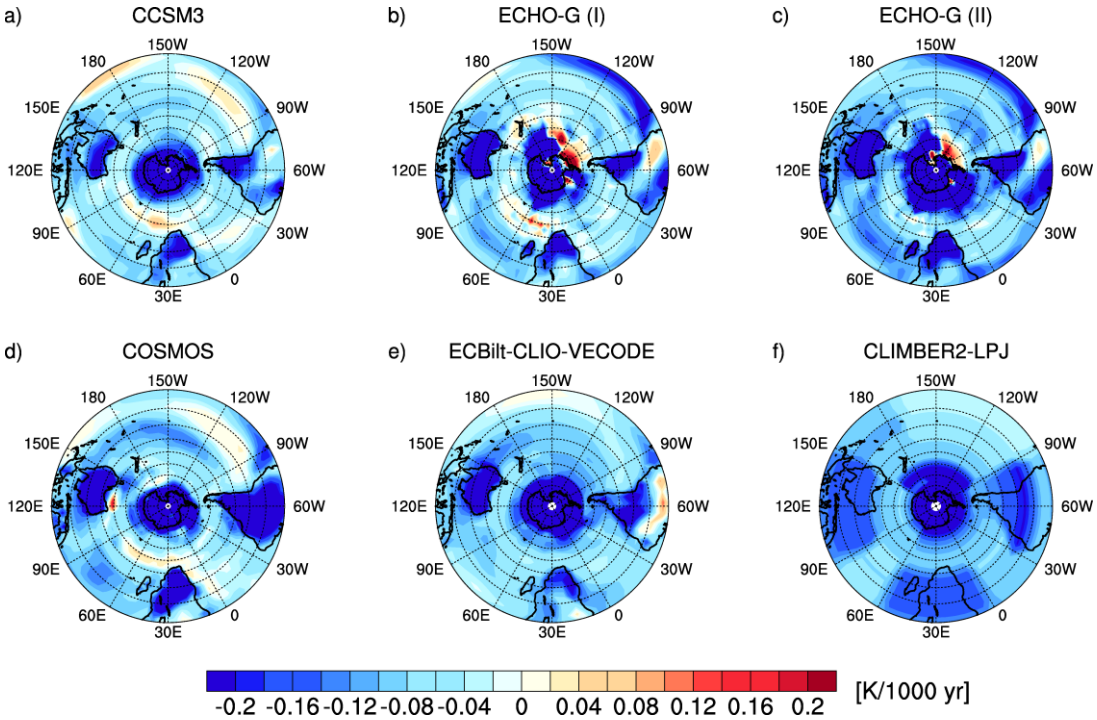

Fig. 7 Same as Fig. 6 but for the SON season.

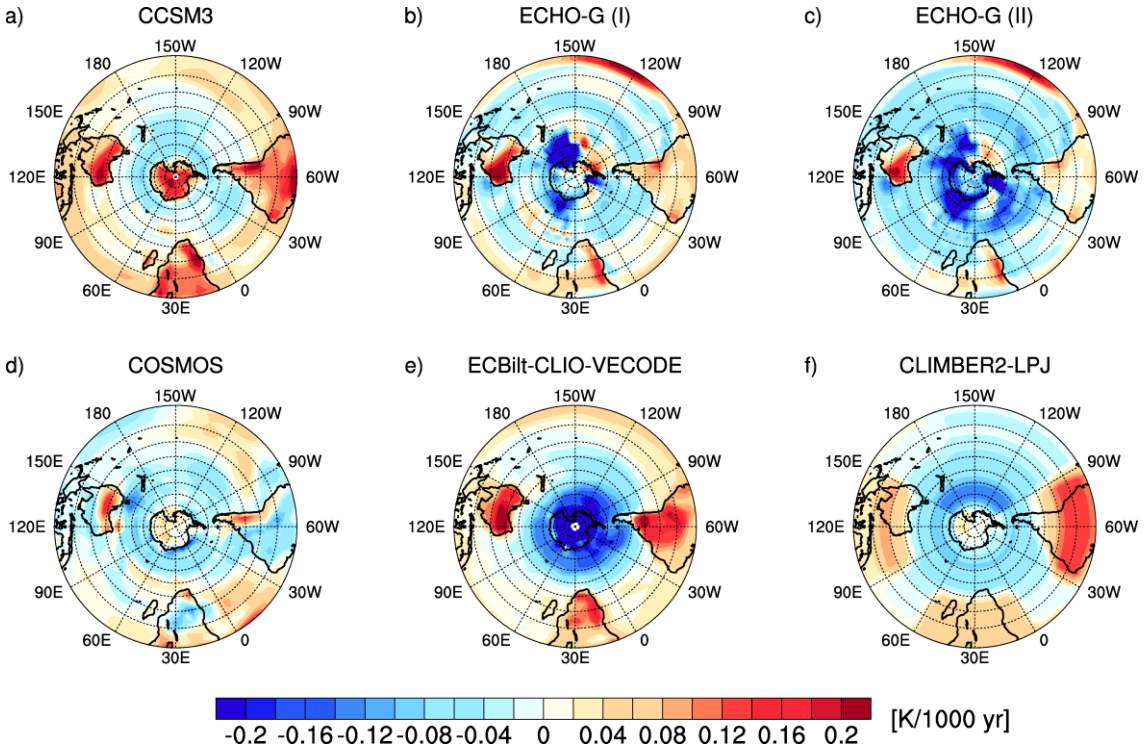

Fig. 8 Same as Fig. 6 but for the DJF season.

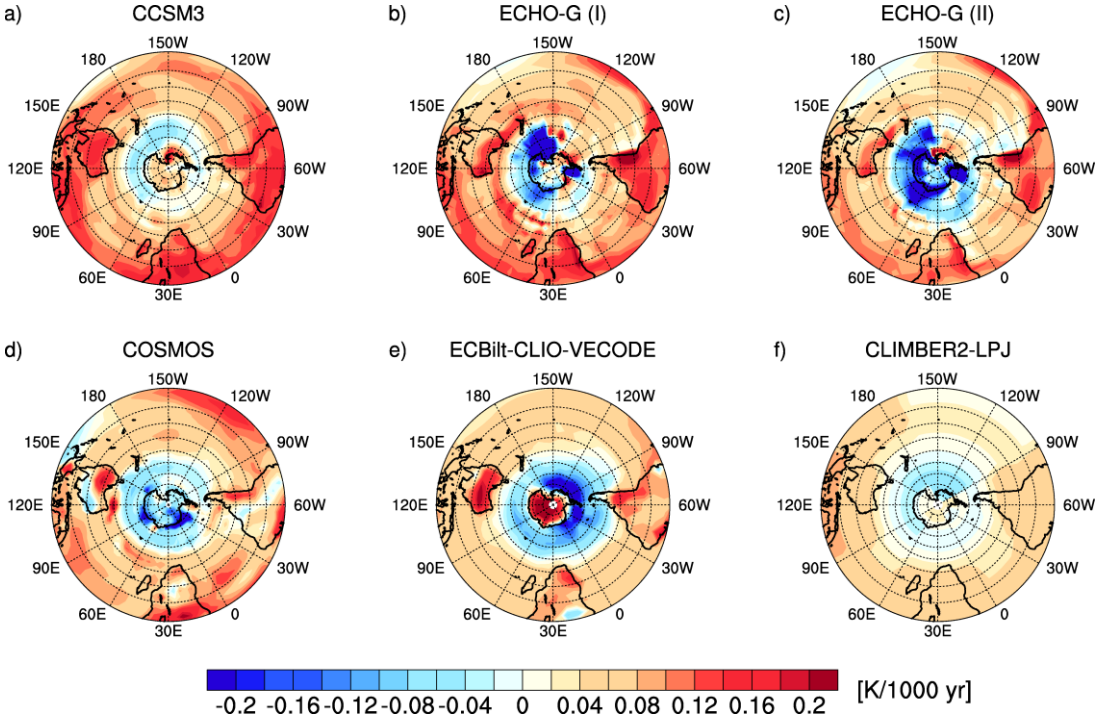

Fig. 9 Same as Fig. 6 but for the MAM season.

Appendix 2

Data distribution

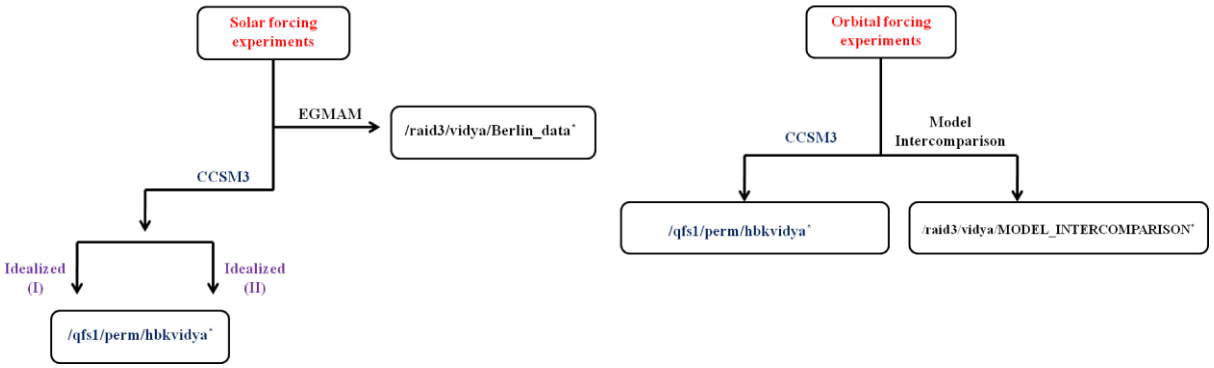

***CCSM3 data for both solar and orbital experiments are stored in the PERM directory of the HLRN machine, Hannover.**

***EGMAM data along with the Holocene transient data used for multi-model inter-comparison are stored in the /raid3/ machine of the Geosystem Modelling working group, Dept. of Geosciences, University of Bremen.**

Idealized (I) represents experiments with low and high TSI values.

Idealized (II) represents experiments with sinusoidally varying TSI values.

In addition, an orbitally forced non-accelerated Holocene transient run was also carried out using CCSM3, the data for which are stored in the MARUM fileserver **(/mnt/marumfs/vidya)**.

The CCSM3 simulation results will be made available on the PANGAEA database (http://www.pangaea.de/).